AN ABSTRACT OF THE DISSERTATION OF

Matthew Buckley Alkire for the degree of
Doctor of Philosophy in
Oceanography presented
on March 19, 2010
Title: Differentiating Freshwater Contributions and their Variability to the Surface and Halocline Layers of Arctic and Subarctic Seas

Abstract approved:

_____
Kelly Falkner

Dramatic and ongoing changes pervading the Arctic and subarctic seas over recent decades have motivated this effort to track and better understand hydrographic variability using chemical tracers. Particular emphasis has been paid to differentiating freshwater contributions to upper layers: namely Pacific water, meteoric water, and sea-ice melt/formation.

Data collected in spring from stations occupied via aircraft in the central Arctic indicate that Pacific origin water partly returned to the mixed and upper halocline layers between 2003 and 2005. The Pacific influence became absent once again from the Makarov Basin between 2006 and 2008. Pacific water appears to be variably entrained into the Transpolar Drift Stream on timescales not clearly linked to Arctic Oscillation indexed atmospheric forcing.

An in-situ ultraviolet spectrophotometer was used to profile nitrate concentrations for the first time in the central Arctic Ocean during 2007-2008 field seasons. Sensor-based nitrate and dissolved oxygen were combined to calculate the NO parameter ($NO = 9xNO_3 + O_2$), a quasi-conservative tracer that has been used to define lower halocline water in the literature. The NO minima in the Makarov Basin occurred above lower halocline water and were concomitant with larger Eurasian river runoff fractions. These features suggest respiratory imprinting of East Siberian Sea shelf waters prior to their offshore advection. Vertical, NO profiles in the

southern Canada Basin implicate multiple influences on the lower halocline, including Eurasian Basin convective processes, diapycnal mixing near the shelf break and ventilation via brine production associated with recurrent coastal polynyas.

Salinity-$\delta^{18}O$ relationships in the Canadian Archipelago and Baffin Bay in late summer in 1997 and 2003 show that a net sea-ice formation signal is inherited from the Arctic Ocean. Local, seasonal sea-ice melt contributions can be estimated by taking this into account. Distributions of freshwater sources are similar to those previously reported using other methods. However, differences in their relative proportions are apparent and suggest variations over time.

Geochemical tracers augment understanding of variability in the formation and circulation of both surface and halocline waters of the Arctic Ocean via quantitative separation of its freshwater components.

Differentiating Freshwater Contributions and their Variability to the Surface and Halocline Layers of the Arctic and Subarctic Seas

by
Matthew Buckley Alkire

A DISSERTATION

submitted to

Oregon State University

in partial fulfillment of
the requirements for the
degree of

Doctor of Philosophy

Presented March 19, 2010
Commencement June 2010

Doctor of Philosophy dissertation of Matthew Buckley Alkire
presented on March 19, 2010

APPROVED:

_____
Major Professor, representing Oceanography

_____
Dean of the College of Oceanic and Atmospheric Sciences

_____
Dean of the Graduate School

I understand that my dissertation will become a part of the permanent collection of Oregon State university libraries. My signature below authorizes release of my dissertation to any reader upon request.

_____
Matthew Buckley Alkire, Author

ACKNOWLEDGEMENTS

I would first and foremost like to thank my major professor, Dr. Kelly Falkner, for giving me the opportunity to conduct this exciting research and the guidance, support, and patience she has shown me over the course of my graduate career at Oregon State University. I would also like to thank Dr. Robert Collier for his generous fulfillment of the role of major professor during Kelly's term at the National Science Foundation. Both Kelly and Bob have always been extremely helpful in all aspects of my work at Oregon State University, whether chemical measurements, field preparations, presentations, papers, or brainstorming are involved, they have always been willing to lend a hand or a thought. I would especially like to thank Dr. James Morison (principle investigator, North Pole Environmental Observatory) for his great contribution and insight, both in the field and during the preparation of presentations and papers related to this dissertation.

Substantial thanks are due to the other members of my committee, Dr. Zanna Chase and Dr. Michael Steele (University of Washington) for their valuable advice and insight during the preparation of this dissertation as well as during my oral examination and dissertation defense. I'd also like to thank my Graduate Council Representative, Dr. Jerry Heidel, for his participation and dedication during my oral and final examinations.

Thanks are also very much deserved the following Oregon State University colleagues: Russell Desiderio for his great work, guidance, and teaching in regards to the processing of dissolved oxygen and in-situ ultraviolet spectrophotometer data; Andy Ungerer for his help and guidance in running barium samples; Andy Ross for his tutelage in the analysis of stable oxygen isotopes; Joe Jennings for his work on nutrient analyses and preparing both reagents and glassware for dissolved oxygen sample collection; and Julie Arrington for her work on total organic carbon analyses (not reported in this dissertation).

I would also like to thank colleagues from the University of Washington: Dr. Ignatius Rigor for International Arctic Buoy back-trajectories he has continuously made available for support of data interpretations; Roger Andersen for his great work in processing CTD data as well as his dedication in organizing and preparing field missions; Dean Stewart for his valuable help in the field; and Andy Heiberg for his organization and planning which make the field work possible. I also gratefully acknowledge Dr. Robert Williams from Scripps Institute of Oceanography and Dr. William Smethie of Lamont Doherty Earth Observatory for their great work on salinity and dissolved oxygen measurements. I also thank Dr. Ken Johnson from Monterey Bay Aquarium Research Institute for invaluable help and support in post-processing and troubleshooting data collected from the in-situ ultraviolet spectrophotometer.

The Kenn Borek Air, Ltd. crew contributed well above and beyond the call of duty to the sampling effort. They did this despite challenging living conditions and fuel availability issues at Borneo.

My research would not have been possible without the great help, guidance, and teaching from all of these fine people.

This research was supported by grants from the National Science Foundation, Office of Polar Programs under grant numbers OPP-9910335 and OPP-0352984.

CONTRIBUTION OF AUTHORS

I wrote all original drafts of the manuscripts/chapters included in this dissertation and revised them according to suggestions and comments subsequently provided to me by co-authors.

Dr. Kelly Falkner is the co-principle investigator on the North Pole Environmental Observatory missions as well as the principle investigator on the Canadian Arctic Throughflow Study. She was directly involved in collecting the data used throughout this dissertation. Dr. Falkner also painstakingly reviewed each revision of every manuscript/chapter included in this dissertation. These revisions included invaluable comments regarding data interpretation and presentation as well as corrections and advice regarding scientific writing style.

Dr. Robert Collier served as the co-principle investigator on the North Pole Environmental Observatory missions during spring 2007-2008, data of which was reported in Chapter 3. Dr. Collier provided guidance and support in organizing, preparing, and carrying out field work as well as subsequent chemical analyses in the laboratory.

Dr. James Morison is the principle investigator of the North Pole Environmental Observatory. He was directly involved in both the field collection of the data reported in Chapters 2 and 3, constructively reviewed the associated manuscripts, and provided helpful comments and suggestions.

Ignatius Rigor provided back-trajectories for sea-ice motion in support of data interpretations in Chapters 2 and 3.

Michael Steele provided comments and suggestions in the preparation of Chapter 2.

Russell Desiderio provided invaluable guidance and support in the post-processing of sensor-based measurements of nitrate collected using the in-situ ultraviolet spectrophotometer. He also diligently commented on the explanations of this processing in Chapter 3 and associated appendices.

Dr. Timothy Boyd provided MATLAB code for interpreting data utilized in the writing of Chapter 4. Dr. Boyd also provided valuable comments and suggestions in the revision of the manuscript.

Dr. Christopher Guay was the co-principle investigator of the Beaufort Gyre Exploration Program spring 2008 field study for which we collected bottle chemistry data and sensor-based measurements of dissolved oxygen and nitrate. Data collected during this program was utilized in the writing of Chapter 3.

Dr. Miles McPhee provided valuable field support during the spring 2008 field program of the North Pole Environmental Observatory. Data collected during this program was utilized in the writing of Chapter 3.

TABLE OF CONTENTS

TABLE OF CONTENTS (Continued)

TABLE OF CONTENTS (Continued)

LIST OF FIGURES

LIST OF FIGURES (Continued)

LIST OF FIGURES (Continued)

LIST OF TABLES

LIST OF APPENDIX FIGURES

DEDICATION

The problem with scientific and technical writing is a lack of passion. As necessary as it may be to convey complex and important points of experimentation, exploration, and discovery, it appears downright criminal that those who dedicate so much of their lives and love on the study of natural processes that it is near impossible to ever translate such fascination and admiration onto the written page. I therefore feel it necessary to take hold of such an opportunity to publish my own thoughts, holding no scientific merit or scrupulous revision, in this space.

I hereby dedicate this dissertation to all of those that told me I couldn't and those who said I could. I dedicate this work to the parents whom gave me life and nurtured and supported that life such that I could work hard to achieve my goals despite any such obstacles that might stand in my way. I devote this effort to those who might come after me with the belief they might not be up to the challenge, but do it anyway, either to prove themselves or just because they don't have anything better to do. I offer this exertion to the family and friends that stood by me and remained ever patient in times of stress and reveled with me in times of jubilation. I dedicate this thesis to a sense of accomplishment and the promise of so much more work to come.

I would like to take this opportunity to thank all those people who provided much needed support, without which graduate study is simply not possible.

DIFFERENTIATING FRESHWATER CONTRIBUTIONS AND THEIR VARIABILITY TO THE SURFACE AND HALOCLINE LAYERS OF ARCTIC AND SUBARCTIC SEAS

1. INTRODUCTION

Relative to its small area (~3%) and volume (~1%) compared to the global ocean, the Arctic Ocean receives and stores a disproportionately large volume of freshwater (~84,000 km^3, liquid and solid) from multiple sources (Serreze et al., 2006). For example, 10% of global river runoff enters the Arctic from both Eurasian and North American continents each year, accounting for approximately 3200 km^3 yr^{-1} or 38% of the total annual freshwater input (Serreze et al., 2006). In addition, Pacific seawater, freshened relative to Atlantic water by a combination of river runoff and direct precipitation, flows northward through Bering Strait providing a freshwater flux (2500 km^3 yr^{-1} relative to a reference salinity of 34.8 or 30% of the total) second only to that of river runoff (Serreze et al., 2006). Direct, net precipitation is considered the third largest freshwater source, contributing ~2000 km^3 yr^{-1} or 24% of the total annual inflow. The formation and melting of sea-ice further adds or removes freshwater to the system seasonally and net effects of these processes are significant terms in both the storage and export of freshwater from the Arctic system.

There are multiple scientific motivations for identifying and quantifying these different freshwater contributions. Pacific waters supply essential nutrients utilized by phytoplankton to fix carbon in the highly-productive Arctic shelves (Cooper et al., 1997; Grebmeier et al., 2006). River runoff can mobilize sizeable stores of terrestrial carbon (Guay et al., 2001; Benner et al., 2005; Raymond et al., 2007), including those from melting permafrost (Camill, 2005) as well as certain contaminants (Macdonald et al., 2005). Sea-ice meltwater can promote undersaturation with respect to calcium carbonate minerals that are important to marine ecology and carbon dioxide fluxes from the ocean to the atmosphere in specific regions of the Arctic and subarctic seas

can be affected differently by the different freshwater components (Yamamoto-Kawaii et al., 2009).

In addition, the fate of this freshwater is important to global climate studies. Export of only a fraction of the stored freshwater volume in the Arctic to the North Atlantic has the potential to slow or even inhibit deep water formation and convection in the Labrador and Greenland Seas, thus impacting meridional overturning circulation and oceanic heat transport (Aagaard and Carmack, 1989). Furthermore, Eurasian river runoff and Pacific water play integral roles in the formation and ventilation of the halocline layer (Jones and Anderson, 1986; Rudels et al., 1996; Steele et al., 2004), which acts as a barrier to upward diffusion of heat from the deep Atlantic layer to the overlying sea ice (Steele et al., 1995).

As the climate warms, the inputs and distributions of Pacific water, meteoric water, and sea-ice processes are expected to respond in different and perhaps divergent ways (Carmack et al., 2008). It is therefore important to be able to quantify the contributions of these freshwater sources in the Arctic and subarctic seas so that temporal and spatial variability in their distributions and circulation can be successfully tracked. It was the focus of this PhD research to apply a range of tracers and state-of-the-art in-situ sensing toward this aim.

Prior to the early 1990s, the hydrography and circulation of the Arctic Ocean was assumed to be relatively predictable. However, beginning in 1990, an anomalously warm pulse of Atlantic water was detected north of the Kara Sea (Quadfasel et al., 1991). Subsequent studies traced this warm pulse, up to 2ºC greater than ocean climatology extending to the 1930s, over the next ten years as it traveled cyclonically around the Arctic periphery and into the deeper basins (McLaughlin et al., 1996; Carmack et al., 1997; Morison et al., 1998; McLaughlin et al., 2002; McLaughlin et al., 2004). In addition to the warming of the Atlantic layer, an intrusion of Atlantic waters into the Makarov Basin displaced Pacific waters from the central Arctic, resulting in the migration of the front between Atlantic and Pacific

derived waters from an approximate position over the Lomonosov Ridge to the Menedeleev-Alpha Ridge system (Morison et al., 1998).

Simultaneously, a retreat of the cold halocline layer from the Amundsen Basin was linked to the displacement of Eurasian river runoff from the Laptev Sea shelf eastward toward the East Siberian Sea (Steele and Boyd, 1998). Thus, a general salinization of the Eurasian Basin and concomitant freshening of the Canadian Basin took place during the early to mid 1990s. These changes have been accompanied by an unmistakable declining trend both in extent and thickness of the Arctic sea ice cover (Comiso, 2002; Rigor et al., 2004).

As evidence linked such changes to warming, the public's attention has been turned toward the polar regions. This has helped to enable the science community to intensify research efforts in the region and particularly during the 2007-2008 International Polar Year. The North Pole Environmental Observatory (NPEO), spearheaded by Dr. James Morison of the Applied Physics Laboratory, University of Washington, was borne in 2000 out of scientific concern about the unprecedented changes. The NPEO has a goal of establishing a continuous monitoring platform used to gather data for the understanding of variability in the central Arctic Ocean subsequent to observations confirming a shift in the hydrographic regime in the early 1990s. This thesis research took advantage of NPEO sampling opportunities provided by aerial hydrographic surveys in spring in regions where oceanic fronts are being observed to vary. Annual surveys have taken place during spring 2000-2008 and will resume in 2010-2013.

Several possible low-salinity sources, combined with prevailing low temperatures, demand use of a number of chemical tracers to identify and quantify freshwater contributions. A range of geochemical tracers can be applied because biological influences, physical processes, and chemical fingerprints serve to differentiate them in different water sources. These include stable oxygen isotopes (Redfield and Friedman, 1969; Tan and Strain, 1980; Ostlund and Hut, 1984; Kipphut, 1990; Tan and Strain, 1996; Cooper et al., 1997), silicic acid (Bauch et al.,

1995), phosphate (Ekwurzel et al., 2001), dissolved inorganic nitrogen to phosphate relationships (Jones et al., 1998; Jones et al., 2003; Taylor et al., 2003; Alkire et al., 2007; Yamamoto-Kawai et al., 2008), barium (Guay and Falkner, 1997; Taylor et al., 2003; Guay et al., 2009), dissolved organic carbon (Guay et al., 1999) and total alkalinity (Anderson et al., 2004; Yamamoto-Kawai et al., 2005). The chapters in this thesis constitute three projects involving tracer hydrography to resolve water type distributions and circulation patterns in the Arctic and neighboring seas.

In Chapter 2, salinity, $\delta^{18}O$, nutrients, and barium are applied to differentiate contributions of Pacific water, meteoric water, and sea-ice meltwater to seawater samples collected from the central Arctic Ocean during spring 2000-2006 by Dr. Kelly Falkner as part of the NPEO program. The distributions of these water types over the upper 0-150 meters, combined with back-trajectories of sea-ice motion derived from data collected through the International Arctic Buoy Program (IABP), are interpreted to result from partial relaxation of hydrographic conditions back toward pre-1990s conditions in accordance with atmospheric forcing partially reverting to pre-1990's patterns. The material presented in Chapter 2 was published in *Deep-Sea Research I* in July 2007.

In Chapter 3, results are presented from the first vertical in-situ, optical sensor-based profiles of nitrate from the central Arctic and Canada Basin that were obtained as part of an International Polar Year program during spring 2007 and 2008 field seasons of the NPEO and Beaufort Gyre Exploration Program (BGEP). The chemical tracer sampling was conducted with Dr. Robert Collier and the author of this thesis, Matthew Alkire, in 2007 and by Matthew Alkire in 2008. These nitrate data were combined with in-situ sensor-based profiles of dissolved oxygen to derive the first high-resolution vertical profiles of the derived "NO" parameter to be reported for the Arctic Ocean. The NO parameter is defined as $NO = 9 \times NO_3^- + O_2$ and is quasi-conservative assuming simple Redfield type nutrient cycling once waters are isolated from gas exchange and no nitrogen fixation or denitrification occurs (Broecker, 1974).

These high-resolution tracer data were combined with bottle-based geochemical tracers to investigate variability in the formation and ventilation of different halocline waters in the central Arctic and southern Canada Basin. These data demonstrate the utility of continuous sensor data for generating fresh insights into water mass tracing in the Arctic. The material presented in Chapter 3 was submitted for publication in *Deep-Sea Research I* during January 2010.

In Chapter 4, mapping of freshwater types in channels of the Canadian Arctic Archipelago (CAA) and Baffin Bay was carried out building on insights gained from geochemical tracers in the Arctic interior. Samples were collected as part of two field missions led by Dr. Falkner: (1) Legs 1-3 of the US-Canadian Joint Ice Ocean Studies (JOIS) conducted during summer 1997 and (2) the Canadian Archipelago Throughflow Study (CATS) conducted during summer 2003. Specifically, salinity-$\delta^{18}O$ relationships are exploited to calculate local, seasonal sea-ice melt contributions which can be under-estimated when using a conservation-equation approach to a water component analysis with endmembers appropriate to the Arctic interior. An inherited, net ice formation signal from the Arctic interior is taken into account in observed salinity-$\delta^{18}O$ relationships in the CAA and Baffin Bay and a linear mixing line between an average, high-latitude meteoric water source and a brine-enriched halocline water is used as a reference to which local sea-ice meltwater contributions can be calculated. The resulting distributions of local sea-ice meltwater and meteoric water are contrasted with previous studies in the region in order to better constrain different freshwater contributions. The material presented in Chapter 4 will be revised and supplemented prior to submission for publication in the *Journal of Marine Systems* in April 2010.

Finally, some general conclusions are provided in Chapter 5.

2. THE RETURN OF PACIFIC WATERS TO THE UPPER LAYERS OF THE CENTRAL ARCTIC OCEAN

Matthew B. Alkire[1*], Kelly K. Falkner[1], Ignatius Rigor[2], and Michael Steele[2], James Morison[2]

[1] College of Oceanic and Atmospheric Sciences, Oregon State University, Corvallis, Oregon, USA
[2] Polar Science Center, Applied Physics Laboratory, University of Washington, Seattle, Washington, USA

Published in *Deep-Sea Research I*, Volume 54, Pages 1509-1529, July 1, 2007.

2.1 Abstract

Temperature, salinity, and chemical measurements, including the nutrients silicic acid (Si), nitrate (NO_3), nitrite (NO_2), ammonium (NH_4), and phosphate (PO_4 or P), the oxygen isotopic composition of seawater ($\delta^{18}O$) and barium (Ba) concentrations were obtained from the central Arctic Ocean along transects radiating from the North Pole in early spring, 2000-2006. Stations that were reoccupied over this time period were grouped into five regions: from Ellesmere Island, (1) north along 70ºW and (2) northwest along 90ºW; near the North Pole, (3) on the Amundsen Basin flank and (4) directly over the Lomonosov Ridge; (5) through the Makarov Basin along 170-180ºW. These regions had been shown by others to have undergone marked changes in water-mass assemblies in the early 1990s, but our time series tracer hydrographic data indicate a partial return of Pacific origin water within the mixed layer and the upper halocline layers beginning in 2003-2004. Back-trajectories derived from satellite-tracked ice buoys for these stations indicate that the upper levels of Pacific water in the central Arctic in 2004-2006 transited westward from Bering Strait along the Siberian continental slope into the East Siberian Sea before entering the Transpolar Drift Stream (TPD). By 2004, the TPD shifted back from alignment over the Alpha-Mendeleev Ridge toward the Lomonosov Ridge, as was characteristic prior to the early 1990s. At most stations occupied in 2006, a decrease in the Pacific influence was observed, both in the mixed layer and in the upper halocline, which suggests the Canadian branch of the TPD was shifting back toward North America. Clearly the system is more variable than has been previously appreciated.

2.2 Introduction

During the 1990s, the Arctic Ocean exhibited considerable changes. Substantial warming (up to 2ºC greater than ocean climatology extending to the 1930s) of the core of inflowing Atlantic water (~300-400 m) coincided with a counter-clockwise shift in the front in the central Arctic separating Atlantic and Pacific waters from their alignment with the Lomonosov Ridge to the Mendeleev-Alpha Ridge system (McLaughlin *et al.*, 1996; Morison *et al.*, 1998). At the same time, the cold halocline layer, formed by a combination of advective and convective processes that alter incoming Atlantic water on and north of the Barents Sea shelf, retreated from a large area of the Eurasian Basin (Steele *et al*., 1995; Rudels *et al*., 1996; Steele and Boyd, 1998). This may have been the result of or accentuated by the displacement of Eurasian River water further east along the shelf before it crossed into the interior. The Makarov Basin underwent significant alteration in its water-mass structure with displacement of Pacific-origin water, including nutrient-rich upper halocline water (S~33.1), by relatively nutrient impoverished Atlantic-influenced upper-layer and halocline water (McLaughlin *et al*., 1996; Swift *et al*., 1997; McLaughlin *et al.*, 2002; McLaughlin *et al.*, 2004). Swift *et al.* (2005) report the absence of Pacific-influenced upper halocline water as early as 1984-1985.

The ocean changes have been linked to alteration of the atmospheric pressure fields over the Arctic (Proshutinsky and Johnson, 1997; Thompson and Wallace, 1998; Morison *et al.*, 1998; Steele and Boyd, 1998; McLaughlin *et al*., 2002; Rigor *et al.*, 2002; Karcher *et al.*, 2003; Polyakov *et al.*, 2004; Polyakov *et al.*, 2005). High-resolution ocean models driven by realistic wind fields lend particular insight into the nature of the linkages. For example, Karcher *et al.* (2003) used a 0.25 x 0.25º horizontal resolution ocean model coupled to a dynamic-thermodynamic sea-ice model over a domain including the northern North Atlantic, the Nordic Seas and the Arctic Ocean. The model was forced by realistic winds from the ECMWF reanalysis for 1979-1993, and, after a 20-year spin-up, warmer Atlantic water fluxes were delivered in pulses over the study period, with the largest occurring in 1989-1994**.**

Consistent with observations, the model shows a topographically-steered boundary current that moves these anomalously warmer waters across the Kara and Laptev Seas and into the Makarov Basin toward the North Pole and over the Lomonosov Ridge into the Canadian Basin (Karcher *et al.*, 2003). McLaughlin *et al.* (2004) observed anomalously warm Atlantic waters in the upstream regions of the Canadian Basin in 1997-1998, signaling the continuing propagation of the 1989-1994 warm event cyclonically around the periphery of the Arctic.

Karcher *et al.* (2003) further reported that their model showed a decrease in the temperature and inflow of Atlantic water during the second half of the 1990s coinciding with a shift in the atmospheric pressure back toward more anti-cyclonic patterns. Therefore, the circulation and water mass structure of the Arctic Ocean might be expected to return toward conditions more typical prior to the regime shifts observed in the early 1990s. Observations appear to bear this out. For example, Boyd *et al.* (2002) report a partial recovery of the cold halocline layer in the Eurasian Basin beginning in 1999-2000. Morison *et al.* (2006) found that the North Pole Environmental Observatory (NPEO) temperature and salinity fields from the central Arctic Ocean, particularly in the Atlantic layers, returned largely toward climatology by 2004, indicating a 3-7 year lag from the atmospheric pressure shift. In addition, Morison *et al.* (2007) attributed a decreasing trend in bottom pressure in the central Arctic to a decrease in salinity resulting from a relaxation of atmospheric forcing toward climatological conditions.

The NPEO program was launched in April 2000 in order to provide publicly available data in an attempt to gain insight on the annual variations in hydrographic properties of the central Arctic Ocean subsequent to the dramatic changes observed in the early 1990s. The data can be accessed at the NPEO home page, http://psc.apl.washington.edu/northpole/, or from the National Snow and Ice Data Center, where it is archived (Morison *et al*., 2002). Here we discuss in further detail variability in the NPEO temperature, salinity, and geochemical bottle data (Si, NO_3,

NO_2, NH_4, PO_4, Ba, and $\delta^{18}O$) for the upper few hundred meters of the water column over the last six years.

2.3 Methods

As part of the NPEO program, a ski-equipped De Havilland DHC-6 aircraft was used to occupy hydrographic stations in early spring starting in 2000 (Fig. 2.1b). After some minor sample-freezing problems during the initial sampling year of the project (more detail below), a gas-powered generator was run in the aft storage compartment of the aircraft (in 2005 the generator was placed on the ice to decrease the fire hazard) with its exhaust venting out the slightly ajar compartment door. A Hermann Nelson heater was plugged into the generator and set on the ice adjacent to the pilot's side of the aircraft with its ducting routed into the aircraft via the pilot's window. After a hole was drilled through the ice for water sampling, a nylon shelter was suspended from the cargo doors and a gantry for a small hydrographic winch was set into place. The combined generator and heater warmed the space in the aircraft-shelter and prevented freezing of samples and equipment.

Figure 2.1 a) General map of the Arctic Ocean. BS=Bering Sea, CS=Chukchi Sea, ESS=East Siberian Sea, CB=Canada Basin, MR=Mendeleev Ridge, AR=Alpha Ridge, EI=Ellesmere Island, MB=Makarov Basin, AB=Amundsen Basin, LR=Lomonosov Ridge, LS=Laptev Sea, KS=Kara Sea, and FS=Fram Strait. The study area is outlined in red for reference. b) Stations reoccupied during NPEO program from 2000-2006 (excluding 2002). Stations names are different from those listed in the NPEO archive. Stations are marked according to the five groups identified in the text: from Ellesmere Island (1) north along 70ºW (stars) and (2) northwest along 90ºW (squares); near the North Pole (3) on the Amundsen Basin flank and (4) directly over the Lomonosov Ridge (both diamonds), and (5) through the Makarov Basin along 170-180ºW (pluses). For details of station coordinates and year of occupation, see Table 2.2.

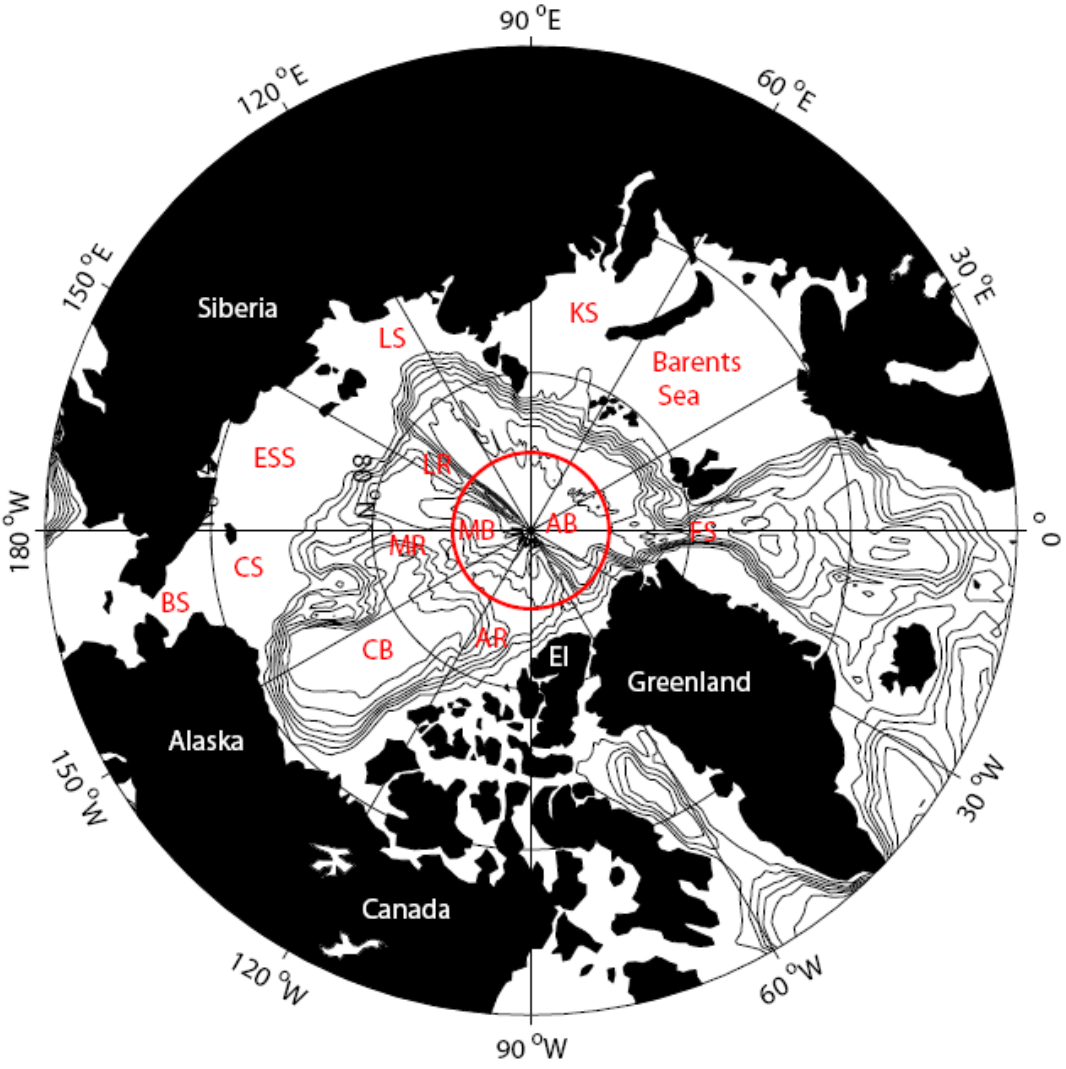
90 °E
120 °E
60 °E
150 °E
30 °E
180 °W
0 °
150 °W
30 °W
120 °W
60 °W
90 °W
80 °N
Siberia
LS
KS
Barents
Sea
ESS
LR
MB
AB
ES
MR
CS
BS
CB
AR
EI
Greenland
Alaska
Canada

Fig. 2.1a

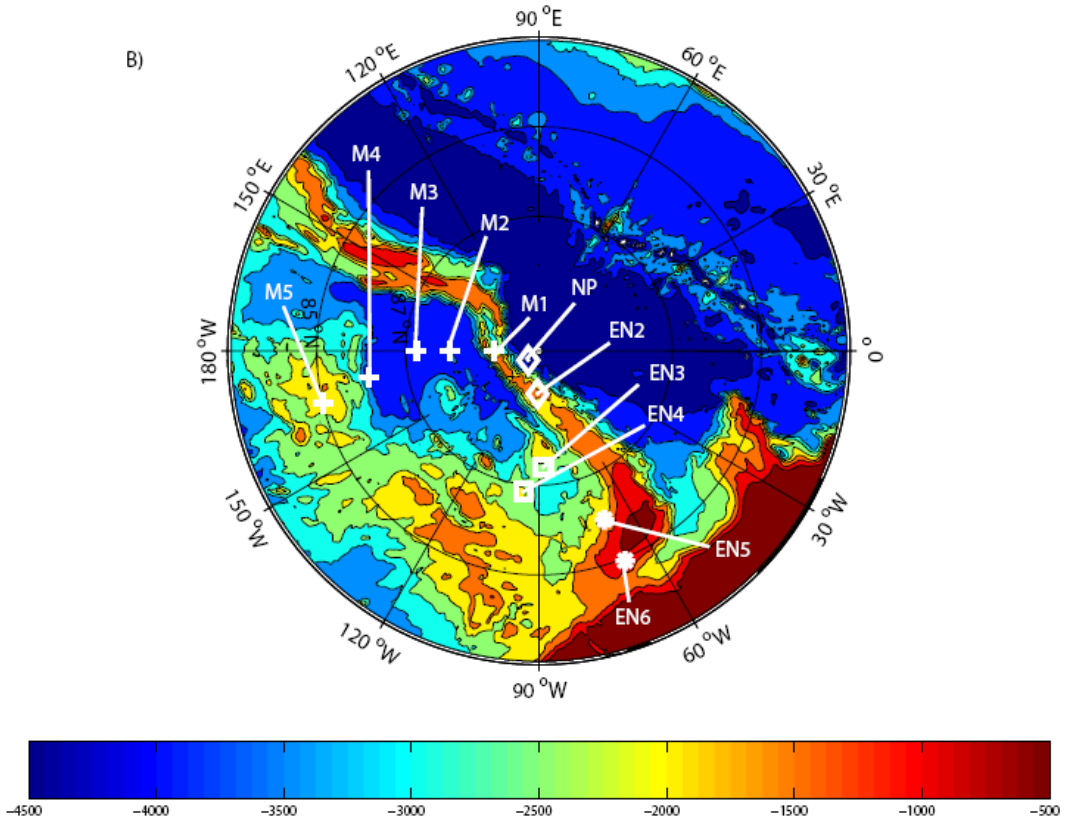
B)
90 °E
120 °E
60 °E
150 °E
30 °E
180 °W
0 °
150 °W
30 °W
120 °W
60 °W
90 °W
M4
M3
M2
M5
M1
NP
EN2
EN3
EN4
EN5
EN6
85 °N
−4500
−4000
−3500
−3000
−2500
−2000
−1500
−1000
−500

Fig. 2.1b

2.3.1 Water Sampling Procedure

Seawater samples were obtained by drilling 10-inch holes in the ice and using an electric-powered portable winch to lower 1.5-L custom-constructed Niskin bottles (General Oceanics model 1010 with 8-inch extension) mounted on a small-diameter Kevlar line. An internally recording Seacat SBE19 CTD was simultaneously hung from the bottom of the line. Bottles were lowered to target depths as indicated on the winch meter wheel and tripped by messenger after the shallowest bottle was in place for a flushing time of 3-5 minutes (no delay in messenger drop prior to 2004). Upon retrieval, each Niskin bottle was placed on a rack in the aircraft, where samples were immediately drawn. Salinity samples were collected in 125-mL glass bottles, the caps of which were fitted with conical polyethylene inserts. Oxygen isotope samples were collected in 20-mL glass bottles with similarly outfitted caps. Nutrient samples were collected in 60-mL high-density polyethylene (HDPE) bottles and stored frozen until analysis. The bottles were pre-cleaned by soaking in pH 1.5 HCl overnight followed by copious rinsing with reverse osmosis deionized water (RODW). Barium samples were collected in 30-mL HDPE bottles that were pre-cleaned by soaking overnight at 60ºC in pH 1.5 HCl and rinsing with RODW.

2.3.2 Analytical procedures

Bottle salinities were analyzed using a model 8400A Guideline Autosal salinometer standardized with IAPSO standard seawater. Precision on the practical salinity scale for these determinations was 0.001-0.002 ($\leq$ 0.004 in 2004). Analyses for the frozen nutrients were performed back in the laboratory immediately after thawing using a hybrid Alpkem RFA 300 and Technicon AA-II (AutoAnalyzer II)-based system and the JGOFS/WOCE suggested nutrient protocols (Gordon *et al.*, 1994). The Si and NO_3 + NO_2 and NO_2 channels were RFA-based, whereas PO_4 and NH_4 channels were AA-II based. After standing overnight in the dark, the samples were reanalyzed for Si to avoid polymerization effects (Gordon *et al.*, 1994). Inter-cruise reproducibility achieved during the WOCE Hydrographic Program, Pacific

One-Time Survey, was ~1, 2, and 1% for Si, PO_4 (hereafter referred to as P), and NO_3, respectively, and uncertainties are estimated to be ± 0.02 μM for NO_2 and 0.03 μM for NH_4. Barium was determined by isotope-dilution using a VG Thermo Excel inductively-coupled quadrupole mass spectrometer as previously described with minor modifications (Falkner *et al.,* 1994). Precision was estimated to be 3% for all sample years. Oxygen isotopes were analyzed by the CO_2 equilibration method on the COAS Finnegan Mat 251 mass spectrometer. Results are reported in del units relative to VSMOW. Precision (1σ) was estimated to be ± 0.05‰ for years 2000-2002 and ± 0.03‰ for years 2003-2005.

The CTD depths and temperatures were assigned to individual bottles by matching the bottle salinities to a linearly interpolated downcast CTD salinity nearest the target depth. Generally, salinities bracketing or equal to measured bottle values were observed in both the up and down CTD casts near the target bottle depths. This lends confidence that the Niskin bottles were tripped correctly and did not leak or experience freezing problems. Some uncertainty is introduced using this method, however. The Niskin bottles integrate 1 m of water during sampling, which can encompass steep property gradients especially prevalent near the surface. Furthermore, the deeper the Niskin bottles were cast, the larger was the discrepancy between actual and target depths as would be expected from a non-zero wire angle. Meter wheel error or multiple intrusions in the deeper layers may have also contributed some uncertainty in temperature assignments although these are typically ≤ 0.01ºC.

Some other minor logistical problems were encountered throughout these NPEO missions. During the 2000 sampling year, some Niskin bottles experienced freezing of up to 5% of their contents, and so bottle salinities exceeded CTD salinities by ≤ 5%. The analytical data were corrected for this small factor under the assumption that dissolved constituents are excluded during the ice formation. Oxygen isotope data were not corrected for this effect, since the fractionation factor between sea ice and seawater is quite small, and the impact on the fluid should be less

than measurement error, given the small amount of ice formed. Modifications in water sampling techniques during subsequent years (described previously) prevented this from recurring. During the 2004 sampling year, bottle salinities (15 m) exceeded CTD salinities in the top 20 m. It is believed this resulted from entrainment of water from the drill hole (where water refreezes and increases salinity locally). Less than 10% entrainment occurred, and so the effect on chemical measurements was small. During the 2005 sampling year, the wait time before releasing the messenger was extended to five minutes, resulting in bottle salinities matching CTD values at ± 1 m of the target depth or the CTD salinities exceeding bottle salinities by only 0.004-0.022, which is negligible with respect to errors in other chemical measurements. This wait time was also utilized in 2006. However, the 2006 samples ≤ 20 m had CTD salinities that exceeded bottle salinities by ≤ 0.02. Such deviations exceed the precision of bottle salinities by an order of magnitude; thus, these observations result from some artifact that is difficult to explain at this time. The bottle salinities in the 60-120 m range matched CTD salinities within $\pm$ 2 m of their target depths.

2.3.3 Water type contributions

The contribution of Atlantic and Pacific water can be estimated using N:P relationships (where $N = NO_3 + NO_2$) as first presented by Jones *et al.* (1998). This treatment presumes that Redfield-type behavior generally governs the nutrient relationships, but denitrification in the Bering Sea and over the Chukchi shelf depletes fixed inorganic nitrogen concentrations in Pacific water that passes into the Arctic Ocean via Bering Strait. Within the central Arctic, the N and P composition of a water parcel is presumed to result from a mixture of Pacific and Atlantic water. Limitations of the method include possible contributions by other sources such as river water, sea-ice melt, and precipitation and imprint by non-Redfield type nutrient processes internal to the Arctic Ocean. Since N-processing is so active over the Chukchi shelf, NH_4 can be a significant component of inorganic fixed nitrogen in the Pacific endmember (we ignore organic forms of fixed nitrogen that can be complicated by river inputs and particulate cycling and don't appear to be

numerically important in this context). Thus, it is preferable to apply all forms of dissolved inorganic nitrogen ($NO_3 + NO_2 + NH_4$) for characterizing endmembers and calculating fractional contributions. Here we use the revised Pacific line specified by Yamamoto-Kawaii *et al.* (2006) that includes NH_4: N (mmol m^{-3}) = 13.957 x P – 11.306, with the Atlantic line specified by Jones *et al.* (1998): N (mmol m^{-3}) = 17.499 x P – 3.072. We use the measured values of total inorganic N to determine the possible range of P as defined by the endmember relationships. The measured P is compared to this range to determine the fractional contributions of Atlantic and Pacific water. If the endmember lines were strictly parallel, then this would be a unique solution to the problem. Since they are not quite parallel, we obtain an estimated uncertainty by also starting with measured values of P to determine the possible range of N. In general, the results agree within 2-6% for the central Arctic samples:

$$f_{ATL} = (P_{meas} - P_{PAC}) / (P_{ATL} - P_{PAC})$$

$$= [P_{meas}-((N_{meas}+11.306)/13.957)]/[(N_{meas}+3.072)/17.499-(N_{meas}+11.306)/13.957)]$$

$$f_{PAC} = 1 - f_{ATL}$$

Because of a lack of NH_4 data in 2001, we utilized $N = NO_3 + NO_2$ in the above equations to calculate Pacific and Atlantic fractions. We estimated the uncertainty due to the missing NH_4 by comparing results with and without NH_4 for the samples for which we do have data. Without NH_4, this approach generally overestimated Pacific fractions by $\leq$ 6% (135 samples) although one sample yielded a 15% overestimation. Note that we set any fractions that were found to be > 100% or < 0 to these respective boundary values; deviations were $\leq$ 10% in all cases. The sensitivity of these calculations regarding assumptions about the river, precipitation, and sea-ice melt contributions was explored by Taylor *et al*. (2003), and the effects are included in a total estimated uncertainty of Atlantic and Pacific fractions of ~14% of the total water mass.

Fractional contributions from water types other than Atlantic and Pacific origin waters were initially determined via a mass balance approach utilizing salinity,

Ba, and $\delta^{18}O$ data according to endmembers presented by Taylor *et al*. (2003). Water types included Eurasian river water, North American river water, sea-ice melt (SIM), and general Arctic seawater (ASW, a component that includes both Pacific and Atlantic origin water). Note that negative values of SIM are meaningful and are assumed to represent the removal/addition of water/salt by the formation of sea ice (Ostlund and Hut, 1984).

We found that the North American river water component, which has a very high Ba concentration (138-574 nmol m^{-3}), contributed no significant volume (< 3%, Taylor *et al.*, 2003) to any samples discussed in this paper. The relatively high Ba concentrations (≥ 60 nmol m^{-3}) in the data set result from a combination of Eurasian river water (12-175 nmol m^{-3}) and Pacific seawater (65-73 nmol m^{-3}), influences that are both elevated over Atlantic waters (40-45 nM) (Guay and Falkner, 1997; Taylor *et al*., 2003). Hence, we revised the mass balance calculations by dropping the North American river component. Contributions of Eurasian river runoff, SIM, and ASW were calculated using only salinity and $\delta^{18}O$ data and the endmembers given in Table 2.1. Results are given in Table 2.2. Note that all reported uncertainties in this paper are expressed in absolute terms. Based on Taylor *et al.* (2003), the uncertainties are estimated to be 5% in the Eurasian river water and 6% in the SIM.

Table 2.1 Endmember values and uncertainties for sea-ice meltwater, Eurasian river water, and Arctic seawater components calculated via mass balance.

	Sea-ice meltwater	Eurasian river water	Arctic seawater
Salinity	3	0	34.2
$\delta^{18}O$ (‰)	1	-17.6	-0.13
Estimated uncertainty (%)[a]	5	6	NA[b]

[a]Errors reported are absolute errors.
[b]NA is not applicable.

2.3.4 International Arctic Buoy Program (IABP) back-trajectories

The coastal origin of the samples was estimated by projecting the drift of the sea-ice sampling locations back in time based on the drift of buoys deployed within

the sea-ice as part of the International Arctic Buoy Program (IABP). These buoys recorded (up to 60 times per day) sea-level pressure (SLP), surface air temperature (SAT), and geographic position to within 300 m over an average lifetime of ~2 years. The data recorded by the buoys are transmitted via the Argos satellite system. Data were interpolated to 3-hourly positions, from which both daily and monthly estimates were calculated. Fields of sea-ice motion were calculated from the observed monthly displacements of the buoys following procedures of Rigor *et al*. (2002) and were not supplemented with winds. Back-trajectories of the sea-ice were constructed using a model that projects the drift of our stations back in time through these archived velocity fields until the sample reaches its likely point of origin along the coast. The estimated error in the back trajectory locations is about 100 km yr^{-1} (Pfirman *et al*., 1997). It appears likely that at least major circulation patterns of the very surface mixed layer follow trajectories similar to those of the ice, which are largely wind-driven (Morison *et al*., 1998; Karcher and Oberhuber, 2002; Steele *et al*., 2004).

Table 2.2 Contributions of sea-ice meltwater (SIM), Eurasian river water (ER), and Arctic seawater (ASW) calculated from a mass balance using salinity and $\delta^{18}O$ data according to methods of Taylor *et al*. (2003). Pacific and Atlantic contributions were calculated separately according to methods of Jones *et al*. (1998) and Yamamoto-Kawaii *et al.* (2006).

Station	Year	Latitude	Longitude	Depth (m)	SIM	ER	ASW	Pacific	Atlantic
EN6	2000	84.93	-67.47	4.9	-7	16	92	88	12
EN6	2000	84.93	-67.47	130.6	-6	5	101	40	60
EN6	2003	84.89	-66.5	62.2	-5	13	92	100	0
EN6	2003	84.89	-66.5	125.8	-4	5	99	38	62
EN5	2000	85.96	-68.63	5.8	-5	15	89	86	14
EN5	2003	86	-68.8	67.3	-10	16	93	97	3
EN5	2003	86	-68.8	126.5	-4	5	99	25	75
EN4	2000	86.85	-96.23	5.5	-10	17	93	68	32
EN4	2000	86.85	-96.23	133.3	-3	2	101	16	84
EN4	2004	86.99	-90.49	15	-12	19	93	46	54
EN4	2004	86.99	-90.49	76	-4	8	95	100	0
EN4	2004	86.99	-90.49	126.8	-3	4	100	16	84
EN3	2003	87.41	-87.87	66.9	-9	15	94	100	0
EN3	2003	87.41	-87.87	98.5	-5	7	98	33	67
EN3	2005	87.45	-89.15	20	-8	15	93	98	2
EN3	2005	87.45	-89.15	60.3	-8	16	93	96	4
EN3	2005	87.45	-89.15	102.4	-4	5	98	46	54

Table 2.2 (continued)

Station	Year	Latitude	Longitude	Depth (m)	SIM	ER	ASW	Pacific	Atlantic
EN2	2000	89.04	-92.05	5.2	-15	15	100	17	83
EN2	2000	89.04	-92.05	136	-10	4	106	5	95
EN2	2003	88.98	-88.98	1.8	-12	19	93	79	21
EN2	2003	88.98	-88.98	59.7	-6	9	96	61	39
EN2	2003	88.98	-88.98	125.8	-1	1	100	10	90
EN2	2004	89.07	-87.32	15	-13	20	93	35	65
EN2	2004	89.07	-87.32	100.7	-3	3	100	16	84
EN2	2005	89.03	-88.56	20.3	-10	17	93	89	11
EN2	2005	89.03	-88.56	62.7	-11	17	94	72	28
EN2	2005	89.03	-88.56	101.2	-2	3	100	10	90
EN2	2006	89.01	-88.41	20.4	-	-	-	100	0
EN2	2006	89.01	-88.41	58.9	-	-	-	21	79
EN2	2006	89.01	-88.41	79.4	-	-	-	35	65
EN2	2006	89.01	-88.41	98.7	-	-	-	1	99
EN2	2006	89.01	-88.41	119	-	-	-	0	100
NP	2000	89.68	-138.8	12.4	-13	18	95	24	76
NP	2000	89.68	-138.8	134.3	-2	1	100	1	99
NP	2001	89.57	73.06	9.9	-10	15	95	8	92
NP	2001	89.57	73.06	101	-2	2	100	7	93
NP	2003	89.82	-113	61.5	-6	7	98	9	91
NP	2003	89.82	-113	126.1	-1	1	100	4	96
NP	2004	89.96	-113.2	15	-12	16	96	24	76
NP	2004	89.96	-113.2	64.8	-10	14	96	22	78

Table 2.2 (continued)

Station	Year	Latitude	Longitude	Depth (m)	SIM	ER	ASW	Pacific	Atlantic
NP	2005	89.79	151.52	20.3	-9	16	93	93	7
NP	2005	89.79	151.52	62.6	-8	12	96	22	78
NP	2005	89.79	151.52	100.1	-1	2	99	5	95
NP	2006	89.98	-170.2	20.1	-	-	-	49	51
NP	2006	89.98	-170.2	59.1	-	-	-	9	91
NP	2006	89.98	-170.2	78.7	-	-	-	15	85
NP	2006	89.98	-170.2	99.5	-	-	-	11	89
NP	2006	89.98	-170.2	118.3	-	-	-	3	97
M5	2001	85.02	-166.5	75	-5	7	98	22	78
M5	2004	85.01	-166.6	15	-11	19	92	77	23
M5	2004	85.01	-166.6	64.5	-5	10	95	47	53
M5	2004	85.01	-166.6	149.3	-1	0	101	7	93
M5	2006	84.98	-169.8	20.4	-	-	-	56	44
M5	2006	84.98	-169.8	59.9	-	-	-	49	51
M5	2006	84.98	-169.8	80.3	-	-	-	27	73
M5	2006	84.98	-169.8	100.2	-	-	-	13	87

Table 2.2 (continued)

Station	Year	Latitude	Longitude	Depth (m)	SIM	ER	ASW	Pacific	Atlantic
M4	2001	86.14	-171	11	-12	19	93	28	72
M4	2001	86.14	-171	75	-3	6	98	16	84
M4	2001	86.14	-171	99	-3	3	99	6	94
M4	2004	86.15	-171.3	15	-10	19	91	-	-
M4	2004	86.15	-171.3	64.5	-7	11	96	27	73
M4	2004	86.15	-171.3	149.6	-1	0	101	5	95
M4	2006	85.97	-169.9	20.3	-	-	-	44	56
M4	2006	85.97	-169.9	60.3	-	-	-	16	84
M4	2006	85.97	-169.9	80.5	-	-	-	30	70
M4	2006	85.97	-169.9	99.6	-	-	-	12	88
M4	2006	85.97	-169.9	118	-	-	-	4	96
M3	2001	87.25	179.81	104	-2	2	100	6	94
M3	2004	87.27	-178.9	15	-13	19	94	46	54
M3	2004	87.27	-178.9	64	-10	15	95	34	66
M3	2004	87.27	-178.9	148.8	-1	0	101	13	87
M3	2006	86.93	-179.7	20.3	-	-	-	25	75
M3	2006	86.93	-179.7	59.4	-	-	-	28	72
M3	2006	86.93	-179.7	78.9	-	-	-	19	81
M3	2006	86.93	-179.7	99.5	-	-	-	7	93
M3	2006	86.93	-179.7	118.4	-	-	-	2	98

Table 2.2 (continued)

Station	Year	Latitude	Longitude	Depth (m)	SIM	ER	ASW	Pacific	Atlantic
M2	2004	88	-179.9	15	-13	19	94	18	82
M2	2004	88	-179.9	66	-8	12	96	18	88
M2	2006	87.99	-179.9	58.8	-	-	-	14	86
M2	2006	87.99	-179.9	78.3	-	-	-	15	85
M2	2006	87.99	-179.9	99.4	-	-	-	11	89
M2	2006	87.99	-179.9	117	-	-	-	0	100
M1	2001	88.99	-179.7	13.5	-12	18	94	18	82
M1	2001	88.99	-179.7	99	-3	4	99	11	89
M1	2004	88.69	-179.6	15	-14	20	94	25	75
M1	2004	88.69	-179.6	65.9	-7	11	96	37	63
M1	2004	88.69	-179.6	150	-1	0	101	12	88
M1	2006	88.85	168.67	19.8	-	-	-	15	85
M1	2006	88.85	168.87	55.5	-	-	-	14	86
M1	2006	88.85	168.87	76.6	-	-	-	10	90
M1	2006	88.85	168.87	91.1	-	-	-	4	96
M1	2006	88.85	168.87	104.4	-	-	-	2	98

2.4 Results and Discussion

The stations that were reoccupied over the study period were grouped into five regions and their tracer hydrographic properties in the upper 150 m compared in time and space. This depth range encompasses the surface mixed layer and upper halocline layer as well as part of the lower halocline layer. The surface mixed layer, as defined here, extends to the depth at which salinity changes by 0.1 from the surface. Note that the CTD experienced artifacts from the drill hole ranging from 2-6 m in the upper water column; therefore, these data as well as any bottle samples collected at the affected depths have not been considered in the analysis. The locations of the stations representing each region are illustrated in Fig. 2.1b and are grouped as follows: from Ellesmere Island, (1) north along 70ºW in 2000, 2003, and 2004, and (2) northwest along 90ºW in 2000 and 2003-2005; near the North Pole, (3) on the Amundsen Basin flank in 2000-2001 and 2003-2006 and (4) directly over the Lomonosov Ridge in 2000 and 2003-2006; (5) through the Makarov Basin along 170-180ºW in 2001, 2004, and 2006.

Note that the observations presented here may not represent an entirely synoptic view of the hydrography of the central Arctic during each year of observation. Unfortunately, because of the difficulty of working in this region, few data from late winter months are available for comparison. The mixed layer is likely to be most spatially and temporally variable as it is subject to sea ice melting/freezing, winter mixing, the opening of leads, river influence, and biological influence during the summer months. Below the mixed layer, features in the central Arctic originate from advection, and their source regions can certainly exhibit both spatial and temporal variability not necessarily captured by an array of single casts taken annually. Moreover, it remains possible that our stations inadvertently sampled eddies known to exist throughout the Arctic. We do sample consistently during mid-April in an attempt to capture the end of winter conditions each year. In the

following treatment, we shall take the simplest approach and assume the data are a reasonable first approximation of the synoptic picture.

2.4.1 North of Ellesmere Island

Two stations north of Ellesmere Island, designated EN6 and EN5 (Fig. 2.1b), were the only places sampled in this study to display the very fresh (S<31) surface mixed layer (Fig. 2.2) that is purported to define a western Arctic-type assembly (McLaughlin *et al*., 1996), and they did so only during the 2000 occupation. The mixed layer became progressively thicker (> 60 m), saltier (S > 31.5), and cooler (θ < -1.6ºC) in subsequent occupations. We note that the Freshwater Switchyard Program (FWSYD) has occupied additional stations between Ellesmere Island and the North Pole, including locations closer to Alert. All available CTD data for 2003-2005 indicate that these stations do not exhibit the fresh (S<31) mixed layer observed at EN6 and EN5 in 2000. These data are to be presented in more detail in a future publication. However, we include the FWSYD occupations of EN6 and EN5 in 2004 in Fig. 2.2 for comparison.

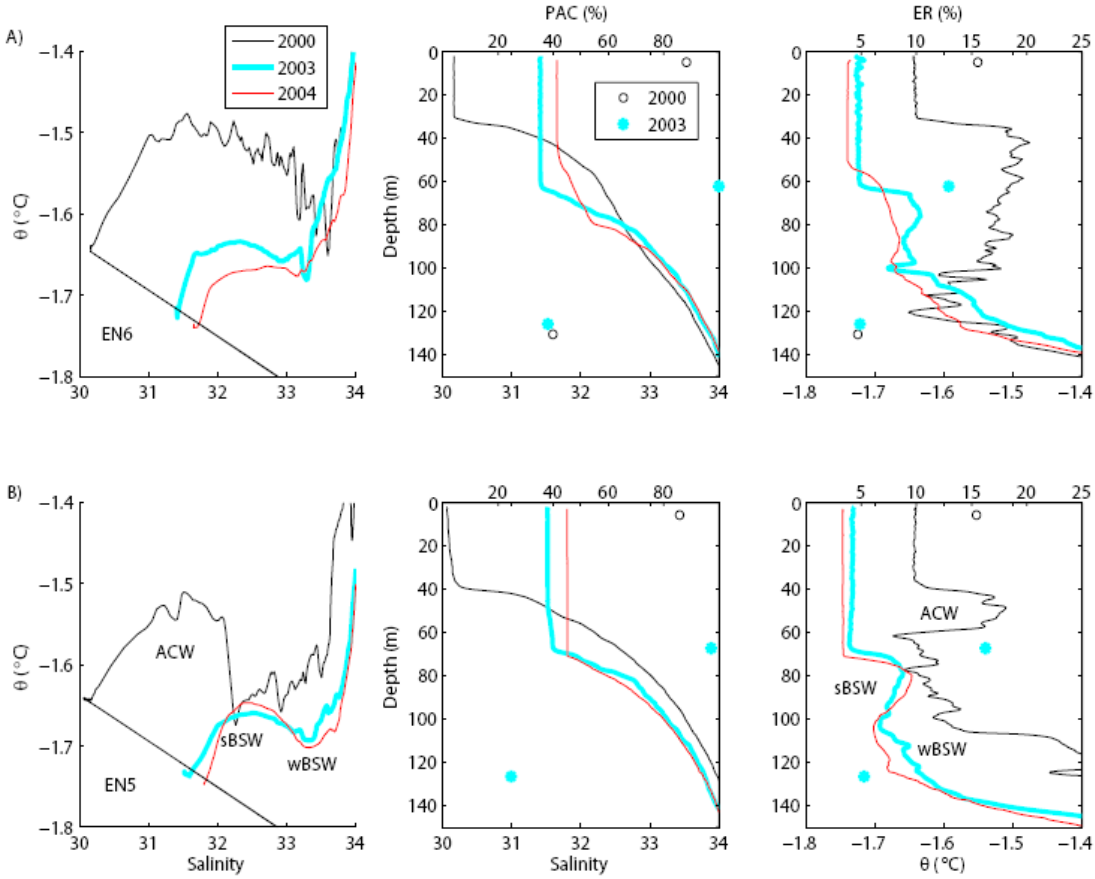

Figure 2.2 θ-S plots (left), salinity and percent Pacific water profiles (middle), and θ and percent Eurasian river water (ER) profiles (right) at stations (A) EN6 and (B) EN5. Thin black lines in θ-S space represent the freezing temperatures.

Available tracer data indicate that both EN6 and EN5 stations exhibited a slightly lower Pacific influence in the mixed layer in 2000, whereas in 2003, it was entirely Pacific-derived (Fig. 2.2). Below the mixed layer at each station in 2000 were potential temperature maxima ($-1.65 \leq \theta_{max} \leq -1.5$ºC) between salinities of 31 and 33 (Fig. 2.2). These properties are within the temperature and salinity characteristics of Alaskan Coastal Water (ACW, $31 \leq S \leq 32$) and summer Bering seawater (sBSW, $32 \leq S \leq 33$) as defined by Steele *et al.* (2004). Alaskan Coastal Water was probably present at both stations in 2000, although best defined at EN5 (Fig. 2.2B), but extensive interleaving structures make it difficult to unambiguously

identify sBSW. In 2003 and 2004, there was no ACW at either station, but sBSW was identifiable and located between 70 and 80 m depth. No bottle samples were obtained within the sBSW core.

The potential temperature minimum (θ_{min}) typically found between salinities of 32.9-33.2, characteristic of winter Bering seawater (wBSW) (Steele *et al*., 2004), was also difficult to define confidently at these stations in 2000 because of the presence of interleaving structures; however, we do note local θ_{min}'s within the correct salinity range for wBSW at depths of 100 and 80 m at stations EN6 (Fig. 2.2A) and EN5 (Fig. 2.2B), respectively. No water samples were obtained at salinities characteristic of wBSW in 2000 or 2003; therefore we cannot be certain that the nutrient maximum layer was present. However, relatively high (> 10 μmol m^{-3}) Si concentrations (not shown), measured below the θ_{min} and associated with salinities $\geq$ 33.9, imply that the 25-40% contribution of Pacific water probably bore the high-nutrient wBSW signature. In contrast to observations in 2000, the presence of the θ_{min} was evident and 0.1-0.2ºC cooler in 2003 and 2004, particularly at station EN5 (Fig. 2.2B).

The decreased influence of summer Pacific halocline waters, signified by the lack of ACW and decrease in the θ_{max} associated with sBSW, contrasted with the apparent increase in the contribution of wBSW. This suggests the circulation of ACW, sBSW and wBSW may be decoupled at least part of the time in this region (presuming that the source properties of these water types remain roughly constant and no local effects were responsible for the observed changes). Also note that the Pacific influence to the ASW component at ~125 m was less at station EN5 than EN6 in 2003 (the only year for which bottle data were available for both stations at this depth). This may result from the closer

proximity of station EN5 to lower halocline waters that can be topographically steered along the Mendeleev and Alpha Ridges (Karcher and Oberhuber, 2002). The larger Pacific influence at EN6 might be attributed to the boundary undercurrent observed by Newton and Sotirin (1997); however, that would require a sizeable

displacement of that current since station EN6 is located ~100 km north of the line occupied in their study.

2.4.2 Northwest of Ellesmere Island

Two additional stations, located further northwest of Ellesmere Island, EN4 and EN3 (Fig. 2.1b), were occupied in 2000 and 2004 and 2003 and 2005, respectively. During the 2000 and 2003 occupations, the mixed layer was relatively fresh (S~31.5) and shallow (≤ 30 m). The mixed layer was thicker (~60 m) and slightly saltier in 2004 and 2005 (Fig. 2.3). The Pacific component of the mixed layer increased from ~70% in 2000 (EN4, Fig. 2.3A) to 100% in 2003 (EN3, Fig. 2.3B), a trend similar to stations EN6 and EN5 to the southeast (Fig. 2.2). However, the contribution of Pacific water to the ASW component of the mixed layer declined to ~50% in 2004 (Fig. 2.3A), and rebounded to dominate the mixed layer the following year (Fig. 2.3B).

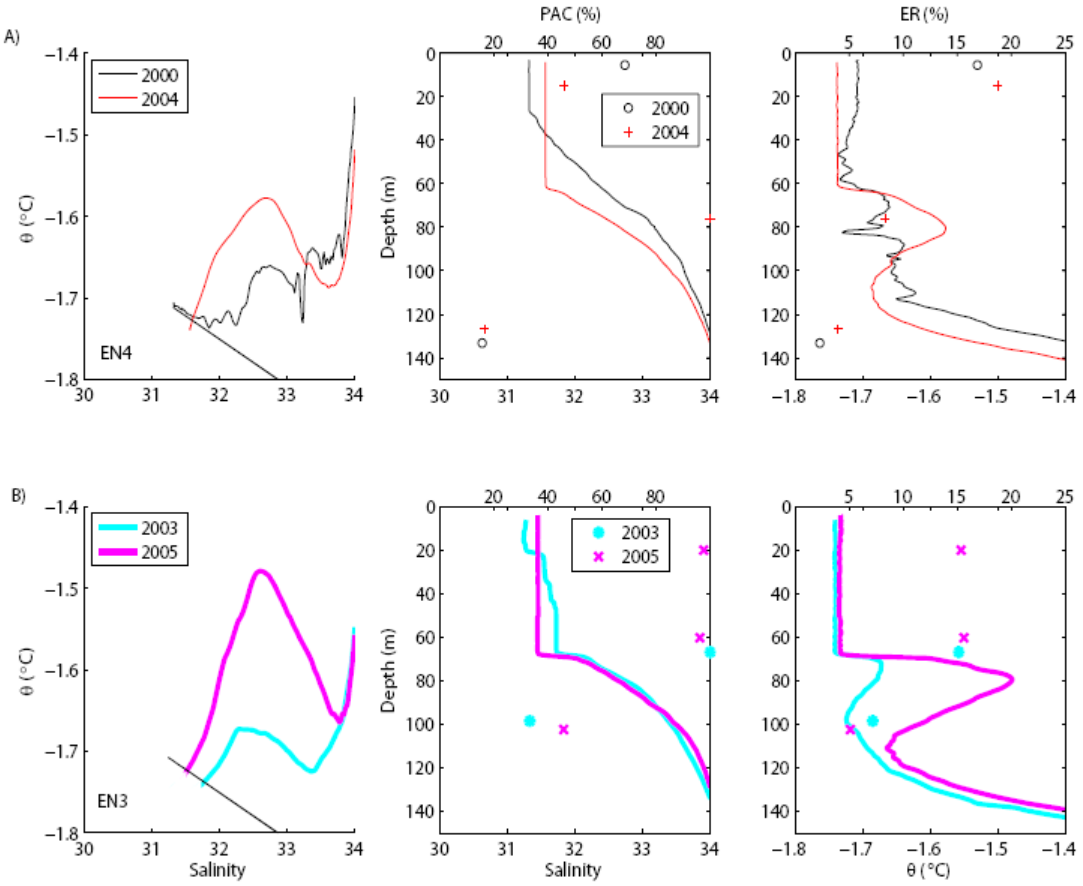

Figure 2.3 θ-S plots (left), salinity and percent Pacific water profiles (middle), and θ and percent Eurasian river water (ER) profiles (right) at stations (A) EN4 and (B) EN3. Thin black lines in θ-S space represent the freezing temperatures.

The low Pacific contribution to the mixed layer in 2004 was coincident with a deeper and saltier mixed layer and a slightly larger influence from Eurasian river water and negative SIM relative to previous occupations. Recall that negative values of SIM imply the net removal/input of water/brine due to the formation of sea ice. This contribution of brine to the mixed layer in the central Arctic might be derived from surrounding shelves or locally produced via the re-freezing of open leads during winter months (Ostlund and Hut, 1984; Yamamoto-Kawaii *et al.*, 2005). Significant contributions of brine below the mixed layer and within the upper halocline are most likely derived from shelf sources where the most intensive ice formation takes place

(Martin and Cavalieri, 1989; Cavalieri and Martin, 1995). This brine is likely of Siberian shelf origin since highly negative SIM fractions were typically coincident with higher Eurasian river contributions. Because of the similarities of the contributions of both river runoff and brine, observed differences in salinity, $\delta^{18}O$, and nutrients can be attributed to differences in contributions of Pacific versus Atlantic water. For simplicity, we refer to the combined Eurasian river water and brine contributions as Siberian shelf influence.

The presence of sBSW or wBSW at EN4 (Fig. 2.3A) was difficult to discern in 2000 because of multiple θ_{max}'s between salinities 32 and 34 (60-100 m). The signatures of Pacific-influenced upper halocline waters were clearer in subsequent occupations, indicating an increasing influence, at least in the case of sBSW, in this region during the time of sampling. For example, sBSW was unambiguously evident at station EN3 in 2003 (Fig. 2.3B) and the θ_{max} appeared sharper (centered at S~32.75), thicker, and warmer in 2004 and 2005. In addition, the bottle sample collected within the core of the sBSW signature (~75 m) at station EN4 in 2004 (Fig. 2.3A) displayed an entirely Pacific-derived ASW component. Deeper samples ($\geq$ 100 m) were somewhat less (20-46%) Pacific-influenced and had salinities > 33.5 and $\theta \geq$ -1.72ºC. However, the 2003 and 2005 samples, collected near the θ_{min}'s, had relatively high Si concentrations (12-20 μM), suggesting the Pacific contribution was from wBSW.

2.4.3 North Pole

The North Pole station was occupied each year (although without water sampling in 2002) during the seven-year period and was located on the Amundsen Basin flank of the Lomonosov Ridge at latitudes > 89.57ºN (Fig 2.1b). In 2000, 2001, 2004, and 2006, the mixed layer (Fig. 2.4A) was saline (S>32) and cold ($\theta \leq$ -1.76˚C), reflective of an eastern Arctic-type assembly (McLaughlin *et al*., 1996). During occupations in 2003 and 2005, however, the mixed layer was markedly fresher ($S \leq 31.6$) and somewhat warmer ($\theta \geq$ -1.74˚C). The influence of Pacific water in the mixed layer was low ($\leq$ 24%) during occupations in 2000, 2001, and

2004 and markedly higher in 2005 (90:10) and 2006 (50:50, Fig. 2.4A). Overall, these data suggest that although the influence of Pacific water was higher in the mixed layer in 2005-2006 (relative to years 2000-2004), there is significant interannual variability.

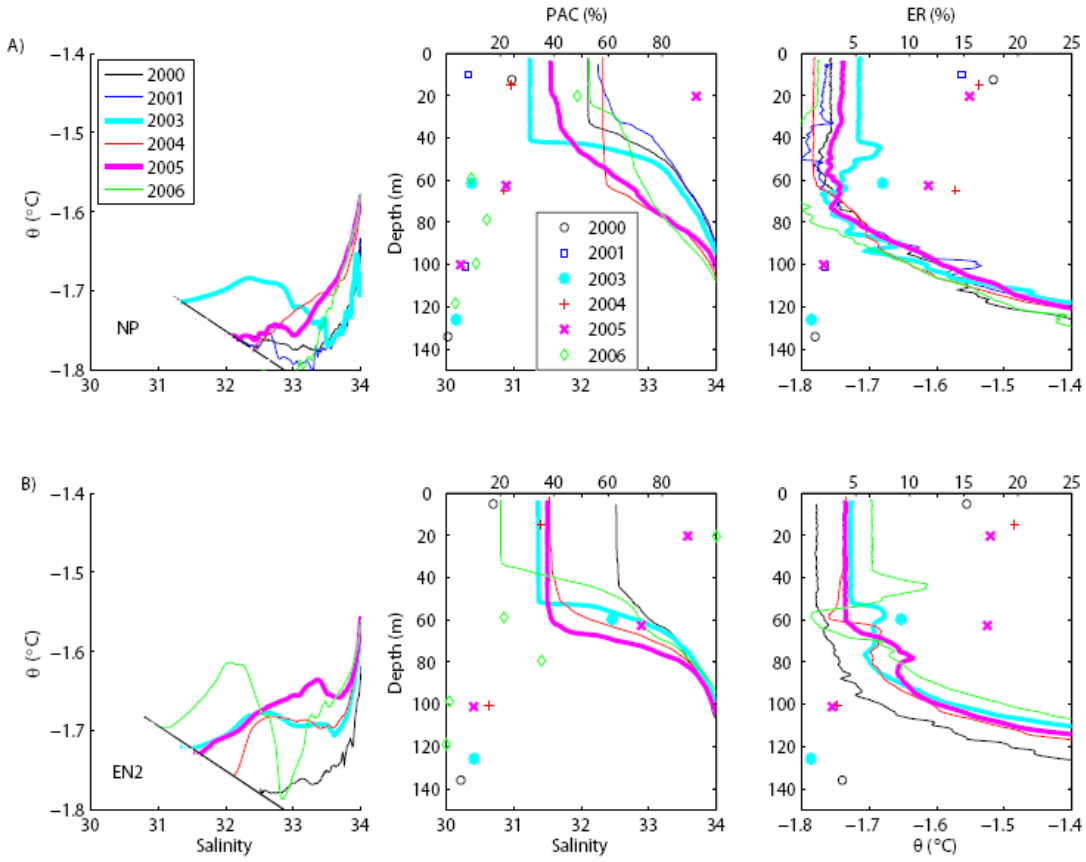

Figure 2.4 θ-S plots (left), salinity and percent Pacific water profiles (middle), and θ and percent Eurasian river water (ER) profiles (right) at stations (A) NP and (B) EN2. Thin black lines in θ-S space represent the freezing temperatures.

The North Pole station did not exhibit a clearly-defined θ_{max} typical of sBSW except in 2003 (Fig. 2.4A). However, the Pacific contribution to the ASW component within the upper halocline (~60 m) was somewhat higher in 2004-2005 relative to 2003 and 2006 (Fig. 2.4A). A θ_{min} associated with a salinity of ~33.5 (65-70 m) in 2003 was embedded within a series of complex interleaving structures

associated with ~90% Atlantic water in the ASW and so was most likely a remnant winter mixed layer feature rather than wBSW. The presence of a weak θ_{min} at the salinity typically associated with wBSW (S~33.1) in 2005 suggested an influence of wBSW; however, since bottle samples did not capture this feature, its presence cannot be confirmed with nutrient data.

2.4.4 Over the Lomonosov Ridge near the North Pole

Another region that was reoccupied several times (but not in 2001 or 2002) during the NPEO study was located at EN2 southeast of the pole over the Lomonosov Ridge (Fig. 2.1b). In 2000, the mixed layer was very saline (S>33) and cold (θ < -1.75ºC) (Fig. 2.4b), indicative of predominately eastern Arctic assembly characteristics (McLaughlin *et al*., 1996). In 2003-2006, however, the stations displayed a relatively fresh upper mixed layer ($S \leq 31.75$). Similar to the North Pole, the salinity of the mixed layer was fresher in 2003 (S~31.3) and somewhat saltier in 2004 (S~31.6) and 2005 (S~31.5). However, in marked contrast to the North Pole observations, the mixed layer was very fresh (S<31) in 2006. The Pacific water contribution to the ASW was also very high (>90%) in the mixed layer in 2005 and 2006.

We suggest two possibilities for the observed differences in the mixed layer between stations NP and EN2 during the 2006 occupation. First, station EN2 may have been within the river water freshened TPD in 2006 while the North Pole was not. Only modest meandering of the TPD could generate high variability in the upper layers in this region. Alternatively, the break in the bathymetry of the Lomonosov Ridge in this region or upstream at the shelf may help promote eddy formation. Eddies sampled in the vicinity of the North Pole would lend apparent variability that isn't necessarily representative of a shift in circulation. Support for the latter comes from a closely spaced helicopter-based CTD survey across the Lomonosov Ridge that was conducted as part of NPEO in April 2002 and appeared to sample an eddy that extended from the surface through the mixed layer (see archived NPEO data at NSIDC).

There was no θ_{max} or θ_{min} that would signal sBSW or wBSW contributions in 2000 (Fig. 2.4B). However, in contrast to the observations at the North Pole, all subsequent occupations displayed a θ_{max} ($-1.7 \leq \theta \leq -1.6$ºC) between 50 and 80 m depth (Fig. 2.4B). The 2003-2004 features appear to have the right salinity characteristics for sBSW; however, that observed in 2005 was anomalously salty ($S>33$). The 2006 θ_{max} was located slightly shallower (~45 m) and at a somewhat lesser salinity, indicating the presence of ACW. The bottle data indicate a similar Pacific:Atlantic ratio in the ASW component nearest the θ_{max}'s (~60 m) in 2003 (~60:40) and 2005 (~70:30), followed by a drastic decrease to ~ 20:80 in 2006 (Fig. 2.4B).

Relatively warm θ_{min}'s were consistently observed at salinities between 33.6 and 33.7 in 2003-2005. In 2006, however, the θ_{min} was colder (near the freezing point, $\theta < -1.78$ºC), shallower (55-60 m), and fresher ($S \leq 33.0$) than previously observed (Fig. 2.4b). The Pacific influence associated with this θ_{min} was low (21%), indicating low nutrient water that might have originated in the Eurasian Basin and mixed with waters from Siberian shelves, where seasonal ice formation can produce waters of the observed salinity and temperature (McLaughlin *et al.*, 2004; Falkner *et al*., 2005; Woodgate *et al*., 2005).

2.4.5 Makarov Basin

Stations extending northward from the Mendeleev Ridge through the Makarov Basin along 170-180ºW were sampled in 2001, 2004, and 2006. Note that stations M5, M4, M3, and M1 were occupied in all years whereas station M2 was sampled in 2004 and 2006 only. Station M5 was located over a high in the Mendeleev Ridge. Nearby, M4 was positioned at the base of that ridge where it grades into the Makarov Basin. Both M3 and M2 were located over the deep Makarov Basin. Station M1 was situated over the Lomonosov Ridge where the bathymetry takes a turn (Fig. 2.1b).

In general, a northward decline in the Pacific influence to the mixed layer from a maximum at station M5 was marked by an increase in salinity and a decrease in the Pacific:Atlantic ratio of the ASW component (Figs. 2.5-2.7). At each

individual station, the salinity of the mixed layer did not change much over time, with the exception of stations M5 (Fig. 2.5A) and M1 (Fig. 2.7), which had markedly fresher and saltier mixed layers in 2006, respectively. The Pacific:Atlantic ratio of the ASW component in the mixed layer decreased at stations M5, M3, and M1 between 2004 and 2006.

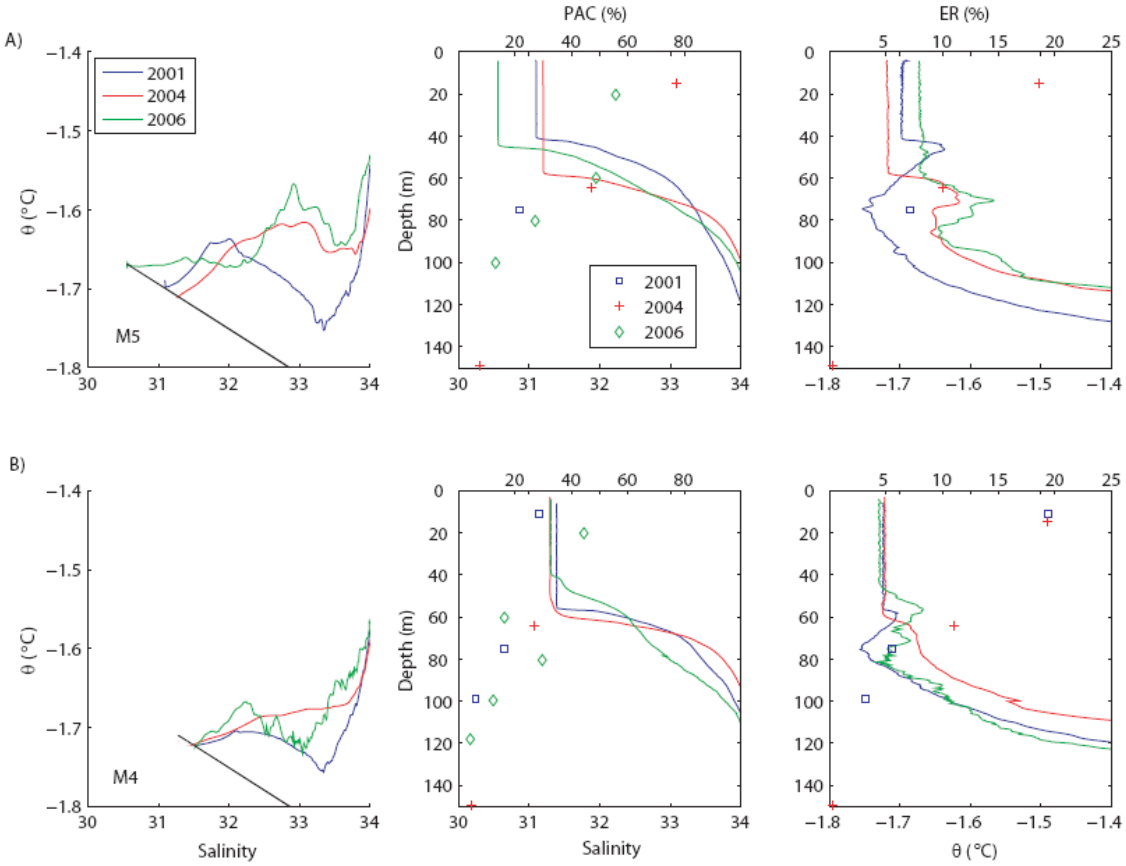

Figure 2.5 θ-S plots (left), salinity and percent Pacific water profiles (middle), and θ and percent Eurasian river water (ER) profiles (right) at stations (A) M5 and (B) M4. Thin black lines in θ-S space represent the freezing temperatures.

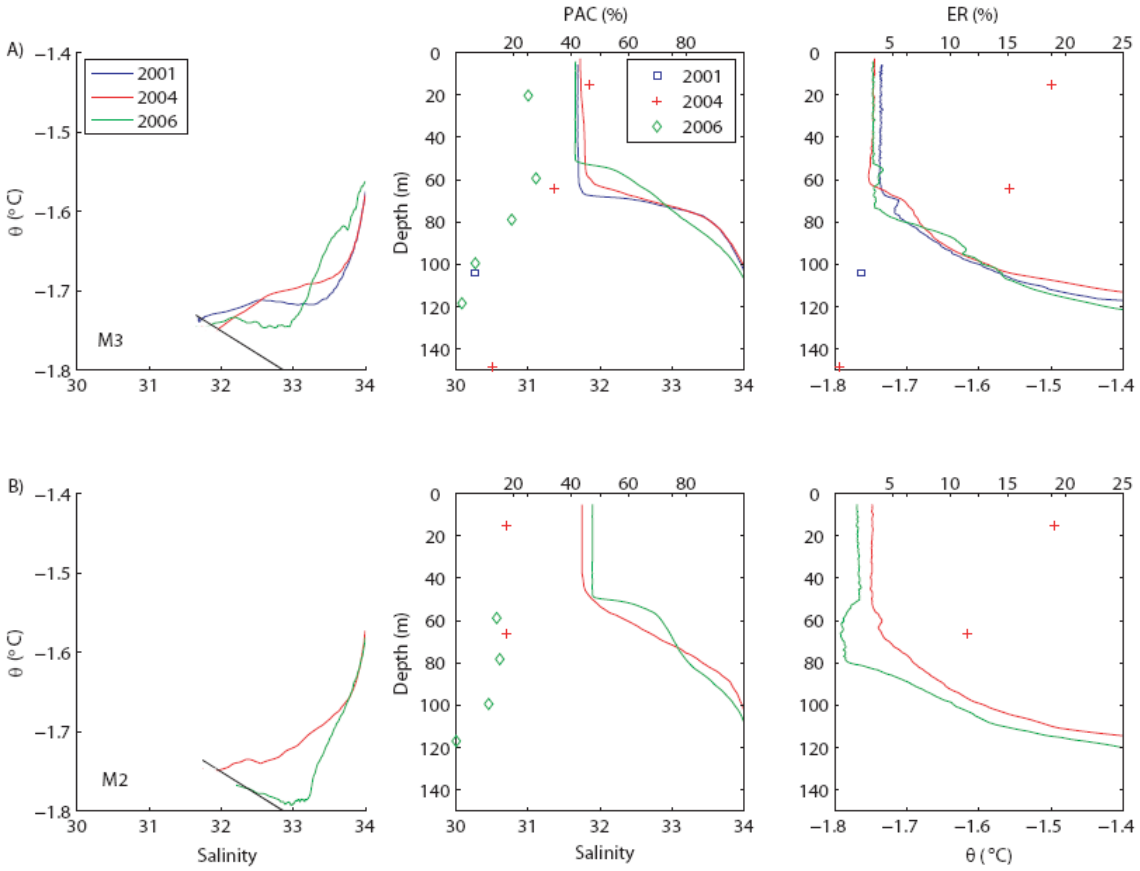

Figure 2.6 θ-S plots (left), salinity and percent Pacific water profiles (middle), and θ and percent Eurasian river water (ER) profiles (right) at stations (A) M3 and (B) M2. Thin black lines in θ-S space represent the freezing temperatures.

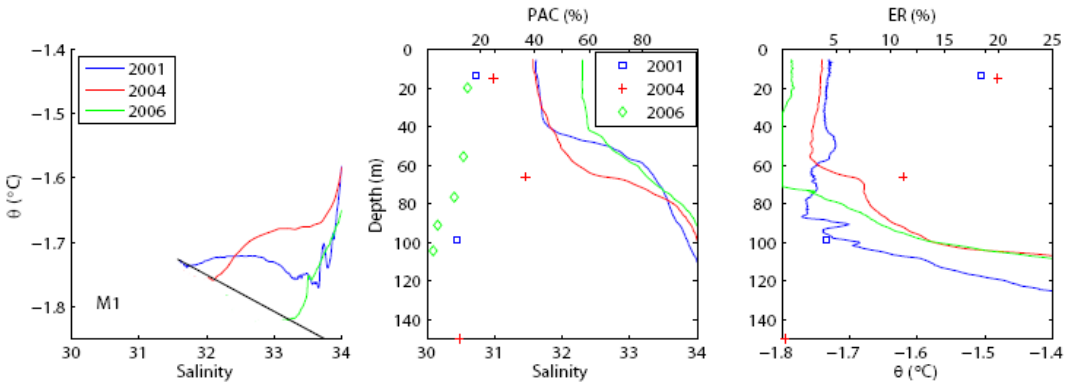

Figure 2.7 θ-S plots (left), salinity and percent Pacific water profiles (middle), and θ and percent Eurasian river water (ER) profiles (right) at station M1. Thin black lines in θ-S space represent the freezing temperatures.

The presence of sBSW and wBSW was evidenced by θ_{max}'s and θ_{min}'s, respectively, in the appropriate salinity range at stations M5 and M4 in 2001 and 2006 (Fig 2.5). Note, however, that the potential temperature profile of station M1 (Fig. 2.7) suggested the presence of weak θ_{max} and θ_{min} signatures in 2001. In 2004, M5 (Fig. 2.5A) was the only station with clearly evident sBSW and wBSW signatures. Stations M3 (Fig. 2.6A) and M2 (Fig. 2.6B) exhibited very limited presence of Pacific halocline waters during all occupation years, and thus seem to represent more quiescent conditions in the basin interior. In 2001, bottle samples collected between 75 and 100 m depth had Pacific influences ≤ 20% at all stations (Figs. 2.5-2.7), despite the correspondence to θ_{min} signatures at stations M5 and M4 (Fig. 2.5). Samples collected at ~60 m depth in 2004, however, exhibited more pronounced (20-50%) Pacific contributions, particularly at stations M5 (~50%) and M1 (40%), close to the Mendeleev and Lomonosov Ridges, respectively. Pacific:Atlantic ratios at ~60 m did not change significantly at stations M5-M2 between 2004 and 2006; however, the Pacific influence at station M1 decreased substantially.

During all three occupation years, temperature signatures defining the Pacific halocline waters diminish northward from M5 to M2 (Figs. 2.5-2.6). Such a trend is

consistent with mixing across the branches of the TPD with the Canadian basin influence most pronounced at the southern end of the transect. However, an anomalously high (~40%) Pacific influence and slight θ_{max} at station M1 (~60 m) during the 2004 occupation as well as the hint of potential temperature maxima and minima in 2001 were manifest. This may be indicating that there are alternate pathways for the transport of Pacific halocline waters within the TPD. We note that a similar θ_{max} was also evident at station EN2 in 2004 (Fig. 2.4B).

Karcher and Oberhuber (2002) reported from model runs that the circulation of the lower halocline was bathymetrically aligned similar to that of the Atlantic layer and that this water exits the cyclonic gyre by crossing the Lomonosov Ridge between the North Pole and Greenland. It is not clear that the bathymetric effects should extend to the relatively shallow depths ($\leq$70 m) and low salinities ($S \leq 32.7$) associated with the anomalies discussed in the previous paragraph. However the complex bathymetry in the vicinity of station M1 (Fig. 2.1B) may promote eddy generation and so play an indirect role in accounting for our observations.

2.4.6 Back-trajectories and Pacific Water Circulation

McLaughlin *et al.* (2002) noted that a displacement of Pacific-origin waters upward in the water column and out of the Makarov Basin in 1993 was coincident with both the freshening of Pacific water entering via Bering Strait and increased penetration of warmer Atlantic water into the Canadian Basin. Steele *et al*. (2004) and Morison *et al*. (2006) have attributed the anomalously fresh mixed layer observed north of Ellesmere Island in 2000 (see section 2.3.1) to displaced Pacific waters. It has been argued that the area north of Ellesmere Island is highly susceptible to fluctuations in the surface circulation regime of the Arctic since it is positioned near the downstream end of the Transpolar Drift (TPD) (Steele *et al*., 2004). The highly cyclonic atmospheric circulation corresponding to a high Arctic Oscillation index (AO) in the 1990s (Thompson and Wallace, 1998) shifted the origin of the TPD from the New Siberian Islands toward the East Siberian Sea, which is in closer contact with Pacific waters entering through the Bering Strait (Jones *et al*., 1998; Steele *et al*.,

2004). As a consequence, the region north of Ellesmere Island might be subject to a more pronounced Pacific influence under a high AO. Under this scenario, the influence of Pacific water north of Ellesmere Island might then be expected to decline as the TPD shifts its origins back toward the New Siberian Islands under lower AO conditions. How do other locations in the central Arctic respond to such shifts in the circulation pattern? Here, we provide evidence for the interaction of two branches, the Canadian and Siberian branches (Karcher and Oberhuber, 2002), of the TPD and their influence on the Pacific water distribution within the central Arctic.

Figure 2.8 illustrates three pathways that sea ice (and presumably surface water) followed through the Arctic during the NPEO program. Back-trajectories for all stations occupied during NPEO generally follow one of these three pathways. Trajectories for individual stations are presented in three additional figures provided in Appendix A. Path #1, which is characteristic for stations NP and EN2 in 2000, illustrates what we interpret to be the Siberian branch of the TPD. Along this trajectory, stations receive ice (and surface waters) from the Laptev Sea shelf that flow along a pathway aligned roughly over the Lomonosov Ridge. Path #2, which is characteristic for stations EN6 and EN5 in 2000, illustrates the movement of ice within the recirculation of the anti-cyclonic Beaufort Gyre prior to incorporation into what we interpret to be the Canadian branch of the TPD, which is roughly aligned over the Mendeleev-Alpha Ridge. Path #3 involves a change in the circulation pattern that was first observed in 2004 as all occupied stations received ice and surface waters from a westward-flowing branch of the Bering Strait outflow that moved along the Siberian coastline into the East Siberian Sea prior to turning northward. We interpret this change to be a consequence of a possible shift of the Canadian branch of the TPD clockwise toward Siberia and an expansion of the Beaufort Gyre (discussed in more detail below).

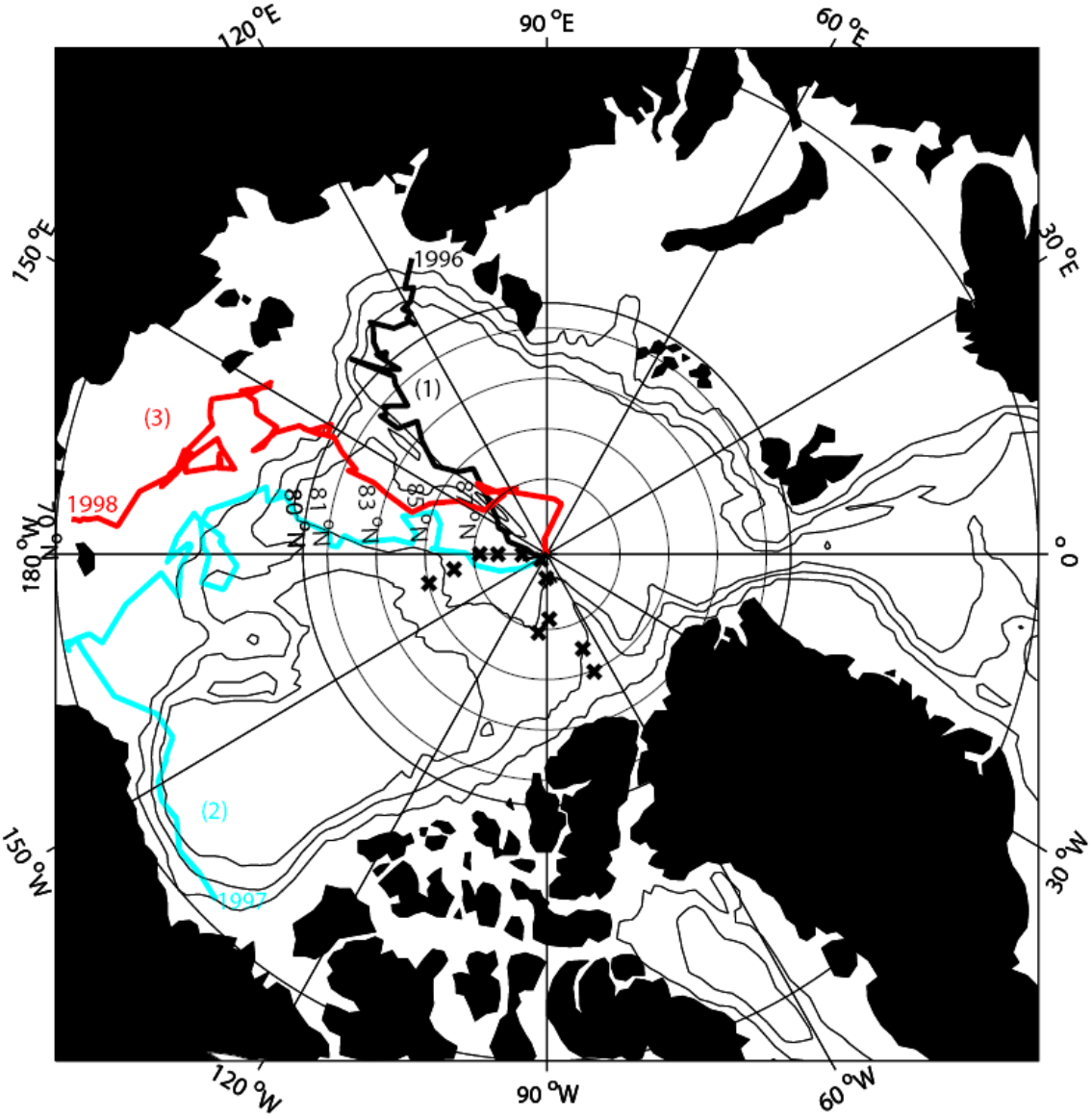

Figure 2.8 Sample International Arctic Buoy Program (IABP) back-trajectories for station NP during occupations in 2000 (black), 2003 (cyan), and 2004 (red). Years annotated on map mark the year of origin calculated for the ice at the beginning of the trajectory. These trajectories are analogous to all other occupied stations and represent the three main pathways by which ice traveled to occupied stations: Path #1 illustrated by the 2000 trajectory; Path #2 illustrated by the 2003 trajectory; and Path #3 illustrated by the 2004 trajectory.

During the 2000 occupation, stations north and northwest of Ellesmere, which had trajectories analogous to Path#2/Canadian branch, had a markedly higher Pacific influence in the mixed layer and the upper halocline (Figs. 2.2-2.3) relative to NP (Fig. 2.4A) and EN2 (Fig. 2.4B), which had trajectories analogous to Path #1/Siberian branch (Fig. 2.8). Therefore, these trajectories suggest that the two branches of the TPD carry waters of different Atlantic and Pacific composition to the central Arctic; and Atlantic waters had a larger contribution to the Makarov Basin side of the Mendeleev Ridge in 2000.

Stations NP and M4-M1 had back-trajectories similar to Path #1 (Fig. 2.8) and displayed equally low (≤ 30%) contributions from Pacific water during the 2001 occupation (see Figs. 2.4-2.7). Thus, the Siberian branch of the TPD extended (at least in 2001) from the Amundsen Basin side of the Lomonosov Ridge well into the Makarov Basin. Note also that at stations that were supposedly affected by the Siberian branch of the TPD in 2000 and 2001, in addition to a low Pacific influence in the mixed layer, there was also no clearly defined sBSW signal (Figs. 2.4-2.7). In contrast, stations northwest of Ellesmere Island (Fig. 2.3) and station M5 (Fig. 2.5A) displayed a clearly defined sBSW signal during years 2000 and 2001, respectively. Therefore, the Canadian branch of the TPD, which we assume to carry waters representative of the northern Beaufort Gyre (see Fig. 14 of Steele *et al.*, 2004), also contributes to the distribution of sBSW in the central Arctic.

In contrast to the 2000 and 2001 occupations, all stations occupied in 2003 received ice from the Canadian branch of the TPD/recirculation from the Beaufort Gyre (Path #2 in Fig. 2.8). Coincidentally, these stations had a higher Pacific influence relative to stations occupied in 2000 and 2001. Stations north and northwest of Ellesmere Island (EN3-EN6) had high contributions (>85%) from Pacific water (Figs. 2.2-2.3), whereas, closer to the North Pole (NP and EN2, Fig. 2.4), stations displayed progressively lower contributions, suggesting an increased input from Atlantic-influenced surface water westward/clockwise from the Mendeleev Ridge. The larger contributions of Pacific water relative to 2000,

especially at stations NP and EN2, could indicate an expansion or shift of either of the Canadian branch/Beaufort Gyre or the Pacific influence within this flow between 2000 and 2003. Assuming the Canadian branch of the TPD was responsible for the northeastward motion roughly along the Mendeleev Ridge, the trajectories indicate a similar surface circulation regime in 2000 and 2003 for stations north and northwest of Ellesmere Island. However, assuming that source properties of Pacific-influence upper halocline waters remain relatively constant, the lack of ACW and the apparent decrease in sBSW north of Ellesmere Island (stations EN6 and EN5) between 2000 and 2003, as well as the increase in sBSW at stations EN2 and NP, are in general agreement with a transition to a less positive AO state (Steele *et al.*, 2004).

The circulation pattern appeared to change in 2004, as the occupied stations received ice via trajectories similar to Path #3 (Fig. 2.8). This suggests a possible shift of the Canadian branch of the TPD clockwise toward Siberia and an expansion of the Beaufort Gyre; this is similar to the circulation scheme depicted in Steele *et al*. (2004) for a negative AO state. Despite the apparent incorporation of Pacific waters from the Bering Strait into the TPD and/or expansion of the Beaufort Gyre, all stations occupied (with the exception of station M5) displayed a low (< 30%) Pacific influence to the mixed layer (Fig. 2.2-2.7); however, the presence of sBSW at stations EN4, M5, and EN2 was more pronounced than observed in previous occupations.

In 2005, stations received ice from trajectories similar to either Path #3 (EN3) or Path #1 (NP and EN2). However, in contrast to observations in 2004, the Pacific influence to the mixed layer was high (>85%) at these stations, indicating that dilution with Atlantic waters along this pathway subsided between 2004 and 2005. The similar pathways by which ice reached stations NP and EN2 in 2000 and 2005 indicate a larger influence of Pacific water in the East Siberian and Laptev Seas to account for the higher fractions of Pacific water observed at these stations. Therefore, we infer the Canadian branch of the TPD has spread and/or shifted clockwise toward Siberia. We note, however, that although the mixed layer had a much larger Pacific contribution at stations EN2 and NP in 2005, the influence of

sBSW only slightly increased at EN2 and was weak (relative to 2003) at NP. In contrast, the sBSW signature at station EN3 (Fig. 2.3B), where there was a much lower Atlantic influence at depth relative to stations EN2 and NP (Fig. 2.4), was very strong. However, station EN3 may have had a more direct influence from the northern Beaufort Gyre due to its location. This would suggest a lateral gradient in Pacific influence across the Canadian branch of the TPD and significant mixing between Pacific-influenced and Atlantic-influenced halocline waters contributing to the Siberian flank.

The Pacific influence decreased at all stations except EN2 and M4 in 2006. Stations NP, EN2, and M3-M1 had trajectories reflective of Path #1, whereas station M4 had a trajectory comparable to Path #3, and that for M5 was analogous to Path #2. These observations may be a result either of an increased mixing of Atlantic and Pacific waters prior to incorporation into the TPD or of a reversion of the Canadian branch of the TPD counter-clockwise back toward the Mendeleev Ridge.

We also briefly note the important implications suggested by the absence of North American river water (NAR) throughout the study (see Section 2.3.3). Taylor *et al*. (2003) found that NAR was replaced by Eurasian river water in the upper water column of Fram Strait in 1998 and suggested NAR must be stored within the Beaufort Gyre and/or exit the Arctic through the Canadian Archipelago. Their findings are consistent with a counter-clockwise shift of the TPD resulting in the displacement of Beaufort Gyre surface waters that were shown to carry an NAR signature in 1993-94 (Guay and Falkner, 1997). However, the relaxation of the Canadian branch of the TPD and expansion of the Beaufort Gyre (suggested by the back-trajectories) did not result in the return of NAR to the central Arctic (at least through 2005, no data yet available for 2006) despite the observed return of Pacific waters. We suggest the NAR might have resided within the inner circulation of the Beaufort Gyre or passed directly through the Canadian Archipelago, and as a result, did not contribute to the stations occupied despite the gyre's apparent expansion. If associated with the inner

gyre, the presence of NAR might be correlated with ACW, which also may be restricted to the inner portion of the Beaufort Gyre (see Fig. 14 of Steele *et al*., 2004).

2.5 Summary and Conclusions

At stations north of Ellesmere Island, the Pacific influence to the mixed layer was slightly greater in 2003 relative to 2000, whereas data from θ-S properties supported a decreased influence of ACW and sBSW in the upper halocline layer in 2003 and 2004 relative to 2000 (Fig. 2.9A). Further northwest of Ellesmere Island, the influence of Pacific water increased significantly in both the mixed layer and the upper halocline (sBSW) during later occupations (2004-2005, Fig. 2.9B). Pacific water returned to the mixed layer of the North Pole in 2003-2006 (highest influence in 2005); however, sBSW was clearly evident only in 2003 (Fig. 2.9C).

Near the pole over the Lomonosov Ridge, station EN2 displayed a high Pacific influence in the mixed layer and the upper halocline (sBSW and/or ACW) in 2003-2006. The section extending northward through the Makarov Basin generally displayed a northward decrease in Pacific influence, both in the mixed layer and the upper halocline, from a maximum at station M5 closest to the Bering Strait. Station M5 exhibited evidence of Pacific influence to the mixed layer as well as the upper halocline during all three occupations (Fig. 2.9D). An anomalously high Pacific:Atlantic ratio coincident with a weak θ_{max} at station M1 in 2004 suggested an additional pathway for the transport of Pacific-influenced halocline waters, possibly via eddy generation in the vicinity of the complex bathymetry of the Lomonosov Ridge.

Overall, these patterns support a partial return of Pacific-origin waters to the mixed layer and upper halocline of the central Arctic beginning in 2003-2004. This return is marked by the expansion of the Beaufort Gyre in 2003 and the movement of Pacific waters (as indicated by back-trajectories) westward from the Bering Strait into the East Siberian Sea in 2004 (Fig. 2.8). These waters then encounter and mix with waters of Atlantic-origin and propagate northward into the central Arctic within the TPD. Prior to this return, the Canadian and Siberian branches of the TPD appeared to

carry waters of predominately Pacific and Atlantic origin, respectively, to the central Arctic (at least during relatively neutral AO states). Interannual variability in the Pacific influence to the mixed layer and upper halocline suggests that the alignment and interaction of the Canadian and Siberian branches of the TPD are subject to changes on much shorter timescales than for the core Atlantic layer.

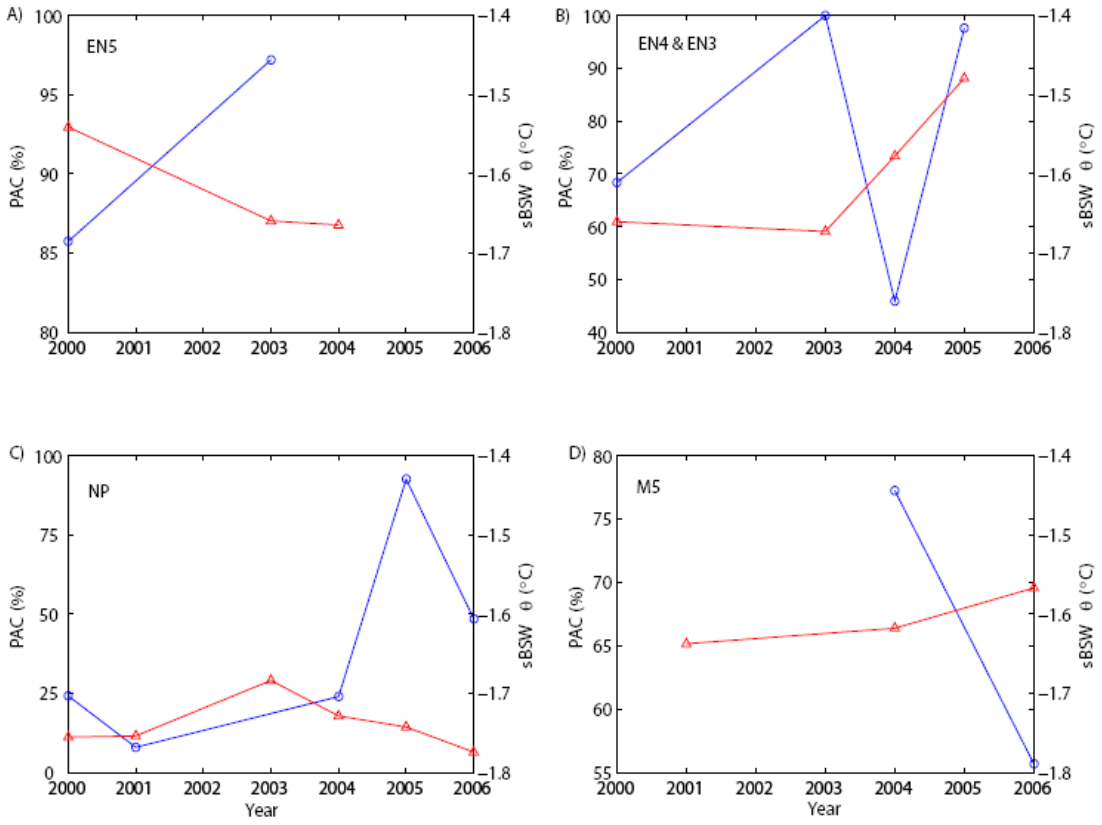

Figure 2.9 Time series of the contribution of Pacific water to the mixed layer (blue circles) and the θ_{max} associated with sBSW (red triangles), taken as the maximum potential temperature for salinities $32 \leq S \leq 33$ for stations (A) EN5, (B) EN4 (2000 and 2004), and EN3 (2003 and 2005), (C) NP, and (D) M5. Note the different scales of the Pacific fraction (%).

The return of Pacific waters, both in the mixed layer and in the upper halocline, to the central Arctic in 2004 did not seem to mark a lasting condition. The

decrease in Pacific influence observed in the mixed layer and upper halocline at most stations occupied in 2006 could signal movement of the Canadian branch of the TPD back toward North America, which could diminish the Pacific influence to the central Arctic in subsequent years.

Is the AO primarily responsible for the observations? In general, the increased influence of sBSW and/or ACW to the central Arctic is in agreement with that expected due to a relaxation of the AO based on the circulation scheme proposed by Steele *et al*. (2004) as well as the 3-7 year lag time between the decline of the AO in the mid-1990s and the return of Pacific waters to the central Arctic in 2003-2005 argued by Morison *et al*. (2006). However, the Pacific contribution to the mixed layer appears much more variable on interannual timescales not clearly linked to the AO. Deeper in the water column, wBSW was not always coincident with either the mixed layer or sBSW/ACW, suggesting that circulation of these layers can also be decoupled and are responding on a different timescale than typical of the AO.

2.6 References

Boyd, T.J., M. Steele, R.D. Muench, J.T. Gunn (2002), Partial recovery of the Arctic Ocean halocline, *Geophysical Research Letters 29*: doi:10.1029/2001GL014047.

Carmack, E.C., K. Aagaard, J.H. Swift, R.W. Macdonald, F.A. McLaughlin, E.P. Jones, R.G. Perkin, J.N. Smith, K.M. Ellis, L.R. Kilius (1997), Changes in the temperature and tracer distributions within the Arctic Ocean Section, *Deep-Sea Research II 44*: 1487-1502.

Martin, S., D.J. Cavalieri (1989), Contributions of the Siberian shelf polynyas to the Arctic Ocean intermediate and deep water, *Journal of Geophysical Research 94*: 12,725-12,738.

Cavalieri, D., S. Martin (1995), The contribution of Alaska, Siberian, and Canadian coastal polynyas to the cold halocline of the Arctic Ocean, *Journal of Geophysical Research 99*: 18343-18362.

Cooper, L.W., T.E. Whitledge, J.M. Grebmeier (1997), The nutrient, salinity, and stable oxygen isotope composition of Bering and Chukchi Seas waters in and near the Bering Strait, *Journal of Geophysical Research 102*: 12563-12573.

Falkner, K.K., R.W. Macdonald, E.C. Carmack, T.J. Weingartner (1994), The potential of barium as a tracer of Arctic water masses, in *The Polar Oceans and Their Role in Shaping the Global Environment: The Nansen Centennial Volume, AGU Geophys. Monograph Series*, edited by O.M. Johannessen, R.D. Muench, and J.E. Overland, pp. 63-76, AGU Books, Washington DC.

Falkner, K.K., M. Steele, R.A. Woodgate, J.H. Swfit, K. Aagaard, J. Morison (2005), Dissolved oxygen extrema in the Arctic Ocean halocline from the North Pole to the Lincoln Sea, *Deep-Sea Research I 52*: 1138-1154.

Gordon, L.I., J.J.C. Jr., A.A. Ross, J.M. Krest (1994), A suggested protocol for continuous flow automated analysis of seawater nutrients (phosphate, nitrate, nitrite and silicic acid) in the WOCE Hydrographic Program and the Joint Global Ocean Fluxes Study, WOCE Operations Manual, Vol. 3: The Observational Program, Section 3.1: WOCE Hydrographic Program, Part 3.1.3: WHP Operations and Methods., pp. 52 loose-leaf, Woods Hole, MA.

Guay, C.K., K.K. Falkner (1997), Barium as a tracer of Arctic halocline and river waters, *Deep-Sea Research II 44*: 1543-1569.

Guay, C.K., K.K. Falkner (1998), A survey of dissolved barium in the estuaries of major Arctic rivers and adjacent seas, *Continental Shelf Research 18*: 859-882.

Guay, C.K., K.K. Falkner, R.D Muench, M. Mensch, M. Frank, R. Bayer (2001), Wind-driven transport pathways for Eurasian Arctic river discharge, *Journal of Geophysical Research 106*: 11469-11480.

Jones, E.P., L.G. Anderson, J.H. Swift (1998), Distribution of Atlantic and Pacific waters in the upper Arctic Ocean: Implications for circulation, *Geophysical Research Letters 25*: 765-768.

Jones, E.P., J.H. Swift, L.G. Anderson, M. Lipizer, G. Civitarese, K.K. Falkner, G. Kattner, F. McLaughlin (2003), Tracing Pacific water in the North Atlantic Ocean, *Journal of Geophysical Research 108*: doi:10.1029/2001JC001141.

Karcher, M.J., J.M. Oberhuber (2002), Pathways and modification of the upper and intermediate waters of the Arctic Ocean, *Journal of Geophysical Research 107*: doi:10.1029/2000JC000530.

Karcher, M.J., R. Gerdes, F. Kauker, C. Koberle (2003), Arctic warming: Evolution and spreading of the 1990s warm event in the Nordic seas and the Arctic Ocean, *Journal of Geophysical Research 108*: doi:10.1029/2001JC001265.

Macdonald, R.W., D.W. Paton, E.C. Carmack (1995), The freshwater budget and under-
ice spreading of Mackenzie River water in the Canadian Beaufort Sea based on salinity and $^{18}O/^{16}O$ measurements in water and ice, *Journal of Geophysical. Research 100*: 895-919.

McLaughlin, F.A., E. Carmack, R. Macdonald (1996), Physical and geochemical properties across the Atlantic/Pacific water mass front in the southern Canadian Basin, *Journal of Geophysical Research 101*: 1183-1197.

McLaughlin, F.A., E. Carmack, R. Macdonald (2002), The Canada Basin, 1989-1995: Upstream events and far-field effects of the Barents Sea, *Journal of Geophysical Research 107*: doi:10.1029/2001JC000904.

McLaughlin, F.A., E.C. Carmack, R.W. Macdonald, H. Melling, J.H. Swift, P.A. Wheeler, B.F. Sherr, E.B. Sherr, E.B (2004), The joint roles of Pacific and Atlantic-origin waters in the Canada Basin, 1997-1998, *Deep-Sea Research I 51*: 107-128.

Morison, J., M. Steele, R. Andersen (1998), Hydrography of the upper Arctic Ocean measured from the nuclear submarine U.S.S. *Pargo*, *Deep-Sea Research I 45*: 15-38.

Morison, J., M. Steele, K. Falkner (2002, updated 2006), *North Pole Environmental Observatory aerial CTD survey.* Boulder, Colorado USA: National Snow and Ice Data Center. Digital media.

Morison, J., M. Steele, T. Kikuchi, K. Falkner, W. Smethie (2006), Relaxation of central Arctic Ocean hydrography to pre-1990s climatology, *Geophysical Research Letters 33*: doi:10.1029/2006GL026826.

Morison, J., J. Wahr, R. Kwok, C. Peralta-Ferriz (2007), Recent trends in Arctic Ocean mass distribution revealed by GRACE, *Geophysical Research Letters 34*: doi:10.1029/GL029016.

Ostlund, H.G., G. Hut (1984), Arctic Ocean Water Mass Balance From Isotope Data, *Journal of Geophysical Research 89*: 6373-6381.

Pfirman, S.L., R. Colony, D. Nurnberg, H. Eicken, I.G. Rigor (1997), Reconstructing the origin and trajectory of drifting sea ice, *Journal of Geophysical Research 102*: 12575-12586.

Polyakov, I.V., G.V. Alekseev, L.A. Timokhov, U.S. Bhatt, R.L. Colony, H.L. Simmons, D. Walsh, J.E. Walsh, V.F. Zakharov (2004), Variability of the Intermediate Atlantic Water of the Arctic Ocean over the Last 100 Years, *Journal of Climate 17*: 4485-4497.

Polyakov, I.V., A. Beszczynska, E.C. Carmack, I.A. Dmitrenko, E. Fahrbach, I.E. Frolov, R. Gerdes, E. Hansen, J. Holfort, V.V. Ivanov, M.A. Johnson, M. Karcher, F. Kauker, J. Morison, K.A. Orvik, U. Schauer, H.L. Simmons, O. Skagseth, V.T. Sokolov, M. Steele, L.A. Timokhov, D. Walsh, J.E. Walsh (2005), One more step toward a warmer Arctic, *Geophysical Research Letters 32*: doi:10.1029/2005GL023740.

Proshutinsky, A.Y., M.A. Johnson (1997), Two circulation regimes of the wind-driven Arctic Ocean, *Journal of Geophysical Research 102*: 12493-12514.

Rigor, I.G., J.M Wallace, R.L. Colony (2002), Response of Sea Ice to the Arctic Oscillation, *Journal of Climate 15*: 2648 – 2668.

Rigor, I.G., J.M. Wallace (2004), Variations in the age of Arctic sea-ice and summer sea-ice extent, *Geophysical Research Letters 31*: doi:10.1029/2004GL019492.

Rudels, B., L.G. Anderson, E.P. Jones (1996), Formation and evolution of the surface mixed layer and halocline of the Arctic Ocean, *Journal of Geophysical Research 101*: 8807-8821.

Steele, M., T. Boyd (1998), Retreat of the cold halocline layer in the Arctic Ocean, *Journal of Geophysical Research 103:* 10419-10435.

Steele, M., J. Morison, W. Ermold, I. Rigor, M. Ortmeyer (2004), Circulation of summer Pacific halocline water in the Arctic Ocean, *Journal of Geophysical Research 109*: doi:10.1029/2003JC002009.

Swift, J.H., E.P. Jones, K. Aagaard, E.C. Carmack, M. Hingston, R.W. Macdonald, F.A. McLaughlin, R.G. Perkin (1997), Waters of the Makarov and Canada basins, *Deep-Sea Research II 44*: 1503-1529.

Swift, J.H., K. Aagaard, L. Timokhov, E.G. Nikiforov (2005), Long-Term Variability of Arctic Ocean Waters: Evidence From A Reanalysis of the EWG Data Set, *Journal of Geophysical Research 110*: doi:10.1029/2004JC002312.

Taylor, J.R., K.K. Falkner (2003), Quantitative considerations of dissolved barium as a tracer in the Arctic Ocean, *Journal of Geophysical Research 108*: doi:10.1029/2002JC001635.

Thompson, D.W.J., J.M. Wallace (1998), The Arctic Oscillation signature in the wintertime geopotential height and temperature fields, *Geophysical Research Letters 25*: 1297-1300.

Weingartner, T., K. Aagaard, R. Woodgate, S. Danielson, Y. Sasaki, D. Cavalieri (2005), Circulation on the north central Chukchi Sea shelf, *Deep-Sea Research II 52*: 3150-3174.

Woodgate, R.W., K. Aagaard, T.J. Weingartner (2005), A year in the physical oceanography of the Chukchi Sea: Moored measurements from autumn 1990-1991, *Deep Sea-Research II 52*: 3116-3149.

Woodgate, R.W., K. Aagaard, J.H. Swift, K.K. Falkner, W.M. Smethie (2005), Pacific ventilation of the Arctic Ocean's lower halocline by upwelling and diapycnal mixing over the continental margin, *Geophysical Research Letters 32*: doi:10.1029/2005GL023999.

Yamamoto-Kawai, M., N. Tanaka (2005), Freshwater and brine behaviors in the Arctic Ocean deduced from historical data of $\delta^{18}O$ and alkalinity (1929-2002 A.D.), *Journal of Geophysical Research 110*: doi:10.1029/2004JC002793.

Yamamoto-Kawaii, M., F.A. McLaughlin, E.C. Carmack, S. Nishino, K. Shimada (2008), Freshwater budget of the Canada Basin, Arctic Ocean from salinity, $\delta^{18}O$, and nutrients, *Journal of Geophysical Research 113*: doi:10.1029/2006JC003858.

3. THE FIRST SENSOR-BASED PROFILES OF THE NO PARAMETER IN THE CENTRAL ARCTIC AND SOUTHERN CANADA BASIN: NEW INSIGHTS REGARDING THE COLD HALOCLINE

Matthew B. Alkire (malkire@coas.oregonstate.edu)[1], Kelly K. Falkner[1], James Morison[2], Robert W. Collier[1], Christopher K. Guay[3], Russell A. Desiderio[1], Ignatius G. Rigor[2], Miles McPhee[4]

[1]College of Oceanic and Atmospheric Sciences, Oregon State University, Corvallis, Oregon, USA
[2]Polar Science Center, Applied Physics Laboratory, University of Washington, Seattle, Washington, USA
[3]Pacific Marine Sciences and Technology LLC, Oakland, California, USA
[4]McPhee Research Co., Naches, Washington, USA

Submitted to the journal *Deep-Sea Research I* for publication in January 2010

3.1 Abstract

Here we report the first vertical in-situ, optical sensor-based profiles of nitrate from the central Arctic and Canada Basin that were obtained as part of an International Polar Year program during spring 2007 and 2008 field seasons of the North Pole Environmental Observatory (NPEO) and Beaufort Gyre Exploration Program (BGEP). These nitrate data were combined with in-situ sensor-based profiles of dissolved oxygen to derive the first high-resolution vertical NO profiles to be reported for the Arctic Ocean. Previous reports based on bottle data have identified a distinct lower halocline layer based on an NO minimum at about S = 34.2 that was proposed to be formed initially in the Nansen Basin and then advected elsewhere in the Arctic. Greater resolution afforded by our data reveal an even more pronounced NO minimum within the upper cold halocline of stations located within the Makarov Basin. Thus a distinct lower salinity source ventilates the Makarov and not the Amundsen Basin. In addition, a larger Eurasian River Water influence overlies this halocline source in the Makarov during this time frame. Observations in the southern Canada Basin corroborate previous studies confirming multiple lower halocline influences including diapycnal mixing between Pacific winter waters and Atlantic-derived lower halocline waters, ventilation via brine formation induced in persistent openings in the ice or polynyas, and cold, O_2-rich lower halocline waters originating in the Eurasian Basin. Continuous sensing of chemical properties provides a considerable advance for understanding the processes contributing to and circulation of the halocline that insulates the sea ice from Atlantic water heat and is an important source of nutrients for Arctic ecosystems.

3.2 Introduction and Background

The upper (0-350 m) Arctic Ocean is comprised of three main layers: a cold and relatively fresh surface mixed layer, an underlying halocline, and below that warm and salty water of Atlantic origin. The stratified halocline stores a significant amount of freshwater, particularly in the Canada Basin (15-20 meters equivalent height; Carmack et al., 2008), and prevents heat from the Atlantic layer from readily

mixing upward to melt sea-ice (Aagaard et al., 1981; Steele and Boyd, 1998). Halocline properties cannot be produced by simple mixing between surface and deeper waters but instead imply independent origins (Aagaard et al., 1981). Understanding variability and trends in various sources and processes ventilating the halocline is important for projecting the future state of the ice cover and freshwater cycling in the region as Earth's climate warms. It is also important for Arctic ecosystems as the halocline waters are nutrient rich. This study describes a significantly improved observational basis for documenting halocline features and changes.

In the sector defined by 0 to about 90 degrees east longitude, the Arctic Ocean halocline (0-150 m) originates primarily from processes acting on waters of Atlantic origin. Elsewhere generally fresher, Pacific derived contributions (referred to as the upper halocline) can override the denser Atlantic ones (lower halocline). Lower halocline water (LHW, $34.1 \leq S \leq 34.5$) has been identified by a bend or kink in θ-S diagrams close to the freezing point (Aagaard et al., 1981; Steele et al., 1995; Steele and Boyd, 1998; Kikuchi et al., 2004) as well as a minimum in the NO parameter (Jones and Anderson, 1986; Wilson and Wallace, 1990), where $NO = 9 \times [NO_3^-] + [O_2]$ and is quasi-conservative assuming simple Redfield type nutrient cycling once waters are isolated from gas exchange and no nitrogen fixation or denitrification occurs (Broecker, 1974).

It was initially proposed that lower halocline water forms via brine rejection during ice formation over the shelves followed by lateral advection along equal density surfaces (Aagaard et al. 1981). Later it was recognized that convective processes in the basin and interaction of shelf and basin waters were also required to more fully explain observations (Rudels et al., 1996). For this it is envisioned that Atlantic waters undergo cooling and freshening over several summer melt and winter freeze seasons as they propagate eastward along the Siberian continental slope. Each summer season, biological productivity can consume dissolved nutrients from these surface waters. Excess gaseous oxygen produced can then be lost to gas exchange

with the atmosphere aided by wind-driven convection prior to the winter freeze-up. This mechanism should lower the NO of the water. Eventually fresher, more nutrient rich shelf waters can override these waters along their transit pathway, inhibiting convection and preventing further gas exchange and so establishing a vertical minimum in NO.

On the basis of bottle data, it is known that Arctic shelf waters can display similarly low or even lower values of NO (Wilson and Wallance, 1990). This has been shown to result from denitrification in sediments on the Beaufort, Chukchi, and East Siberian shelves (Codispoti et al., 1991; Devol et al., 1997; Nitishinsky et al., 2007). However, these waters generally do not have high enough salinities to ventilate the lower halocline.

During the mid to late 1990s, the cold halocline layer separating the mixed layer and lower halocline layer retreated from the Amundsen Basin (Steele and Boyd, 1998). It was proposed that river runoff from the Laptev Sea moved alongshore toward the East Siberian Sea during summer months as a result of enhanced basin scale cyclonic wind forcing (Steele and Boyd, 1998; Guay et al., 2001; Ekwurzel et al., 2001; Boyd et al., 2002; Dmitrenko et al., 2005; 2008) in contrast to a northward/offshore advection in the vicinity of the Lomonosov Ridge under predominately anti-cyclonic atmospheric forcing. Coincident with the retreat of the cold halocline layer from the Amundsen Basin was a northward extension of convective lower halocline water formation, which does not require the input of shelf waters and produces lower halocline water closer to the freezing point, from the Nansen Basin as far as the Lomonosov Ridge (Kikuchi et al., 2004). During the late 1990s and early 2000s, these trends partially reversed (Boyd et al., 2002) and offshore advection of river runoff from the Laptev Sea shelf was observed to resume (Guay et al., 2001; Boyd et al., 2002).

Numerous investigators have recently described two different types of LHW in the Canada Basin: cold/O_2-rich LHW in the northern area and warm/O_2-poor LHW in the southwestern area (McLaughlin et al., 2004; Rudels et al., 2004; Shimada

et al., 2005; Woodgate et al., 2005; Itoh et al., 2007). Various sources for these LHWs have been proposed. McLaughlin et al. (2004) initially hypothesized the cold and oxygen-replete LHW marked a new source of LHW injected into the Canada Basin from the East Siberian Sea. However, Rudels et al. (2004) and Shimada et al. (2005) argued these waters more likely had origins in the winter mixed layer of the Nansen or Amundsen Basins. Itoh et al. (2007) used potential temperature, potential vorticity, and oxygen saturation to trace the cold and O_2-rich LHW to the Nansen Basin. The relatively warm and O_2-deficient LHW variety was proposed by Woodgate et al. (2005), to be a product of diapycnal mixing between Pacific winter water and Atlantic-origin lower halocline water upwelled onto the northern Chukchi shelf/slope.

Shimada et al. (2005) additionally differentiated between relatively oxygen depleted and enriched upper halocline waters ($33.1 \leq S \leq 34.0$) as Pacific winter waters (PWW) originating from the western and eastern Chukchi Sea, respectively. They identified Western Chukchi Pacific Winter Waters (PWWs) as having an O_2 minimum between salinities 33.1-33.5 overlying O_2-rich LHW. Eastern Chukchi PWWs, overlying the O_2-poor LHW, exhibited relatively higher O_2 and temperatures. Shimada et al. (2005) attributed the higher oxygen in eastern Chukchi PWW to nearby polynyas where oxygen enriched surface waters are made dense by brines produced during ice formation. Woodgate et al. (2005) argued that the warmer temperatures were inconsistent with such a source and so pointed to lower biological activity in the eastern Chukchi Sea as a possible explanation for the higher oxygen concentrations.

This work reports the first sensor-based vertical profiles of nitrate in the central Arctic Ocean and southern Canada Basin. Combined with similar profiles of dissolved oxygen, we produce high-resolution profiles of the NO parameter. These data offer substantial improvement over discrete bottle-based sampling that can alias vertical features. Here we highlight how river-influenced Siberian shelf water trajectories into the central Arctic Ocean are reflected in the distribution of the NO

minima and use the NO parameter to distinguish multiple halocline water influences in the Canada Basin.

3.3 Data and Methods

In 2007 and 2008, the springtime airborne hydrographic surveys of the North Pole Environmental Observatory (NPEO) program were expanded to cover a larger area than in the past and to use a new profiling instrument for water properties. The general approach remained the same, however, and has been described in detail by Alkire et al. (2007). Briefly, seawater samples were collected from a ski-equipped De Havilland DHC-6 aircraft using 1.5 L custom constructed Niskin bottles (General Oceanics model 1010 with 8-inch extension) mounted on a Kevlar line and lowered through the 10-inch hole drilled through the ice. Prior to sampling, a nylon tent was suspended from the cargo doors and a gantry for a small hydrographic winch set into place. A Hermann Nelson heater, powered by a gas-powered generator, was set on the ice adjacent to the pilot's side of the aircraft with its ducting routed into the aircraft via the pilot's window to prevent instruments and samples from freezing.

Bottles were lowered to target depths (20, 60, 80, 100, 120, and 300 meters for central Arctic and 20, 60, 85, 195, 310, and 430 meters for southern Canada Basin stations) using an electric-powered portable winch and tripped by messenger after the shallowest bottle was in place for a flushing time of 5 minutes. Upon retrieval, each Niskin bottle was placed on a rack in the aircraft where samples were immediately drawn. During the 2007 deployment, seawater sample collection was conducted immediately following instrument casts (without bottles) whereas this order was reversed during the 2008 deployment. Niskin bottle deployment required approximately 30 minutes. Instrument casts to ~800 meters demanded a similar amount of time (30-40 minutes).

Starting in 2007, sensor-based vertical profiles were collected by coupling two separate instrument packages in a vertical configuration for deployment through the 10-inch diameter sea ice hole. The nitrate sensor system, the sample stream of which was not pumped, consisted of a V2 Satlantic In-Situ Ultraviolet Spectrophotometer

(ISUS) mounted vertically in-line below its 15-V dc battery pack in a stainless steel frame such that the sample probe was oriented downwards. Attached below this by means of locking carabiners was an actively-pumped Seabird SBE19 *plus* Seacat conductivity, temperature, depth (CTD) sensor system outfitted with an SBE43 dissolved oxygen (O_2) sensor. The SBE43 was plumbed in-line between the temperature and conductivity sensors and a Seabird 2.0K pump. The separation between the ISUS sample probe and the CTD thermistor was open to the ocean and spanned 0.9 meters. To minimize vulnerability to damage on transit through the ice, no connecting cables or plumbing were used between the ISUS and CTD. Time and challenging field conditions dictated a simple approach for these initial deployments; ultimately, it will be preferable to integrate the ISUS sensor in the pumped sample stream and data collection system.

Internally recorded ISUS and CTD data were merged after collection as described in Appendix B. The complete suite of data has been archived at the Cooperative Arctic Data and Information Service site (CADIS) and can be obtained at http://cdp.ucar.edu/browse/browse.htm?uri=http%3a%2f%2fdataportal.ucar.edu%2fmetadata%2fcadis%2fOcean_and_Sea_Ice%2fEnvironmental_Obs%2fEnvironmental_Obs.thredds.xml.

Note that in 2008, nitrate data were successfully acquired from all Canada Basin stations but only a subset of the central Arctic sampling locations (Makarov stations M2, M3, M5-M7 and Amundsen stations A8-A9). However, CTD-O_2 data were acquired at all stations (see Fig. 3.1). As discussed in detail in Appendix B, maximal uncertainties in the nitrate and dissolved oxygen profile data are 1 and 4 mmol m^{-3}, respectively. We propagate these errors to estimate uncertainties in the NO parameter of ~9.8 mmol m^{-3}. Errors for other measurements are within usual bounds (Alkire et al., 2007).

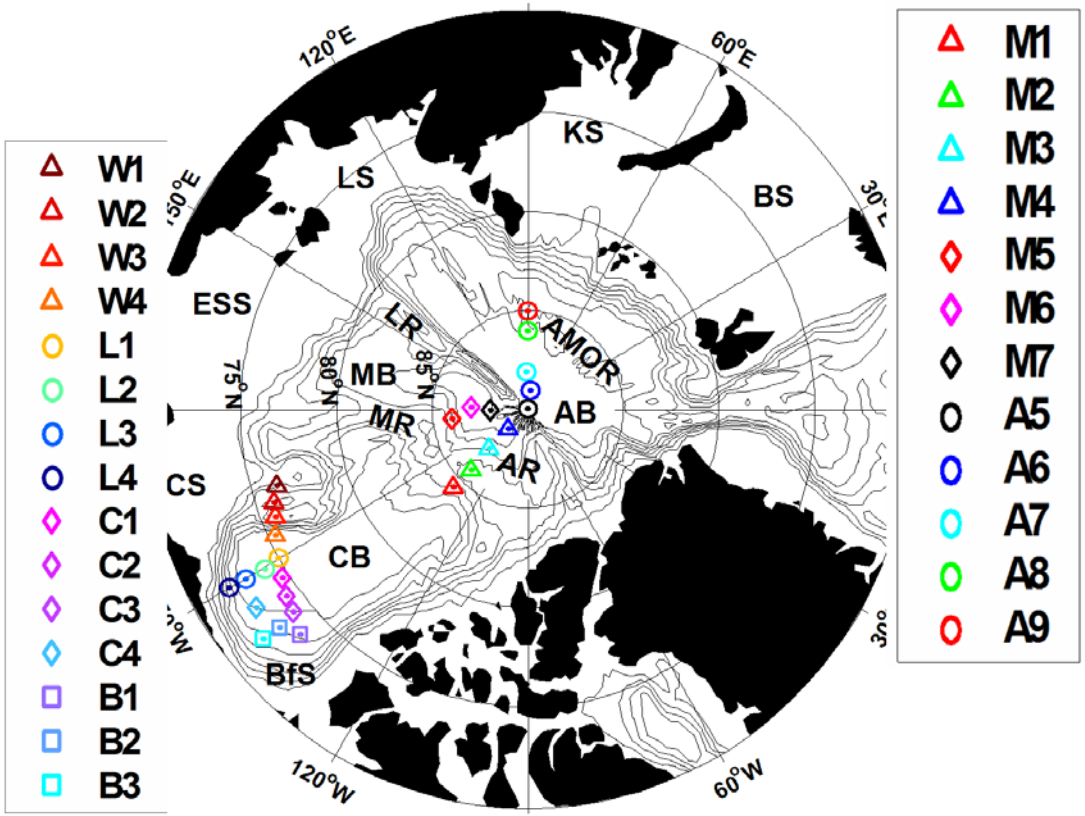

Figure 3.1 Locations of hydrographic stations occupied in the central Arctic during 2007-2008 and southern Canada Basin during 2008. The stations are color-coded to match Figures 3 and 4. Isobaths range from 500 to 3500 meters (500 meter intervals). AB = Amundsen Basin, AMOR = Arctic Mid-Ocean Ridge, AR = Alpha Ridge, BfS = Beaufort Sea, BS = Barents Sea, CB = Canada Basin, CS = Chukchi Sea, ESS = East Siberian Sea, KS = Kara Sea, LR = Lomonosov Ridge, LS = Laptev Sea, MB = Makarov Basin, MR = Mendeleev Ridge.

3.3.1 Water Type Analyses

Contributions of sea-ice meltwater, meteoric water, and Pacific and Atlantic seawater were computed for water samples employing methods described in Yamamoto-Kawai et al. (2008). All endmember characteristics and associated uncertainties were adapted from Yamamoto-Kawai et al. (2008) and are given in Table 3.1. First, the salinity and stable oxygen isotope composition ($\delta^{18}O$) of the seawater endmember are assigned. For Canada Basin samples having salinity ≤ 33, the seawater endmember was assumed to consist entirely of Pacific seawater (Yamamoto-Kawai et al., 2008). This assumption was not applied to the central Arctic samples as both Atlantic and Pacific seawater can contribute to waters with salinities < 33. For Canada Basin samples with salinities > 33 and all central Arctic samples, the salinity and $\delta^{18}O$ of the seawater endmember were calculated via weighted average of Pacific and Atlantic contributions determined by dissolved inorganic nitrogen:phosphate ratios (Alkire et al., 2007).

Table 3.1 End-member values used in water type analyses. See section 2.1 for details.

Water Type	**Salinity**	**$\delta^{18}O$**	**Unc.***
Ice melt	4 ± 1	(-2; 0**) ± 1	0.03
Pacific seawater	32.5 ± 0.2	-0.8 ± 0.1	0.14
Atlantic seawater	34.87 ± 0.03	0.24 ± 0.05	0.14
Meteoric Water	0	-20 ± 2	0.03

*Uncertainty in water type fractions derived from varying endmember definitions within the range of uncertainty expressed in the table (Yamamoto-Kawai et al. , 2008).

**Ice melt $\delta^{18}O$ end-member defined as -2 and 0 for Canada Basin and central Arctic samples, respectively (Pfirman et al., 2004).

Next, conservation equations of mass, salinity, and $\delta^{18}O$ are applied to estimate fractions of sea-ice meltwater, meteoric water, and seawater comprising the sample. Finally, the Pacific and Atlantic water fractions are then iteratively refined

by multiplying the composite seawater fraction by the Pacific and Atlantic contributions estimated from the dissolved inorganic nitrogen:phosphate ratios.

3.3.2 Inventories of Pacific and meteoric water freshwater equivalents

Fractional contributions of Pacific water (f_{PAC}) and meteoric water (f_{MW}), were converted into fractions of freshwater equivalent ($f_{FW\ eq}$) relative to Atlantic water with a reference salinity of 34.87 via the equations:

$$f_{MW,\ FW\ eq} = f_{MW}$$

$$f_{PAC,\ FW\ eq} = f_{PAC} \times (34.87 - 32.5) / 34.87$$

where the Pacific water endmember salinity is 32.5 (Table 3.1) and $f_{PAC,\ FW\ eq}$ refers to the fractional contribution of freshwater contained in Pacific water (relative to the reference salinity). Since meteoric water has a salinity of zero, its fraction is equal to its freshwater contribution. Depth profiles of Pacific and meteoric freshwater equivalents were then constructed by interpolating between the bottle values of these parameters. However, instead of interpolating onto a uniform depth grid, the CTD salinity data, averaged into 5 meter depth bins, was used as the independent variable in the interpolation to incorporate a more accurate shape of the vertical freshwater distribution. To determine inventories (in meters) of Pacific and meteoric freshwater equivalent at each station, the constructed profiles were integrated between the surface and 120 meters depth in the central Arctic and 195 meters depth in the southern Canada Basin assuming the top 10 meters were homogenous with respect to both salinity and water type contributions.

3.3.3 Sources of meteoric water

Potential alkalinity calculated from the bottle data was used to distinguish meteoric water contributions in the central Arctic and southern Canada Basin (Yamamoto-Kawai et al., 2005; 2009). Note that while dissolved barium proved useful for this purpose in the past (Guay and Falkner, 1997; Taylor et al., 2003), it displays non-conservative behavior in the absence of a sea-ice cover (Falkner et al., 1994; Abrahamsen et al., 2009). Potential alkalinity was calculated by correcting measured alkalinity for the effects of nitrate or ammonium utilization or production

via the photosynthesis and respiration of organic matter (Yamamoto-Kawai et al., 2009). Both potential alkalinity and salinity were then corrected for the influence of sea-ice melt/formation by subtracting the product of the sea-ice melt fractions and assigned sea ice melt salinity and total alkalinity from the observed values (Yamamoto-Kawai et al., 2005).

Linear regressions of corrected potential alkalinity and salinity were conducted for pooled data from the central Arctic (2007 and 2008) and from the southern Canada Basin (2008). The zero salinity intercepts were 740 ± 35 and 840 ± 36 μeq kg^{-1}, respectively.

In the central Arctic, Pacific water and North American river runoff are largely absent and sources of meteoric water are limited to Eurasian river runoff and direct net precipitation (Yamamoto-Kawai et al., 2005). Direct precipitation (alkalinity ~ 0) contributions must be very small (≤ 6%) as the potential alkalinity representing average meteoric water supplied to the central Arctic (740 μeq kg^{-1}), is very close to the average dissolved inorganic carbon measured in Eurasian rivers (~770 μmol kg^{-1}; Olsson and Anderson, 1997), which should closely approximate the total alkalinity as bicarbonate is the dominant carbonate species in these rivers (Yamamoto-Kawai et al., 2005).

The meteoric water balance in the Canada Basin is more complex as Pacific water and North American river runoff cannot be disregarded. Yamamoto-Kawai et al. (2005) estimated the maximum contribution of North American river runoff to the Canada Basin to be < 23%. Here, we utilize the same approach but with updated estimates for the Mackenzie River total alkalinity (1540 μeq kg^{-1}, Cooper et al., 2008) and the contribution of direct precipitation to the Arctic Ocean freshwater budget (24%, Serreze et al., 2006).

To derive an upper limit, direct precipitation is assumed to dilute the Mackenzie River contribution by 24% to 1170 μeq kg^{-1}. The total alkalinity of meteoric water entering the Arctic through Bering Strait relative to a salinity of 34.87 has been estimated to be 930 μeq kg^{-1} (Yamamoto-Kawai et al., 2005). Our estimate

from the central Arctic extrapolation (740 μeq kg^{-1}) is taken to represent Eurasian runoff in the following equations pertinent to the southern Canada Basin during spring 2008:

$$840 = 1170f_{Mackenzie+precip} + 930f_{Bering\ Strait} + 740f_{Eurasian}$$

$$f_{Mackenzie+precip} + f_{Bering\ Strait} + f_{Eurasian} = 1$$

$$f_{Eurasian} = 1 - f_{Mackenzie} - f_{Pacific}$$

A maximal $f_{Mackenzie+precip}$ of 23% is obtained when the Bering Strait inflow ($f_{Bering\ Strait}$) is negligible. Correcting this for dilution by direct precipitation (24%), the maximum North American runoff contribution is 18%. Thus, in accord with previous findings (Yamamoto-Kawai et al., 2005; 2008), Eurasian river runoff and the inflow of freshwaters via Bering Strait appear to be the dominant contributors to the meteoric water pool in this region.

3.4 Observations and Discussion

3.4.1 Distributions of Pacific water and river runoff

Inventories of Pacific water and meteoric water (expressed as meters of freshwater equivalent) at stations occupied during the 2007 and 2008 studies are shown in Figure 3.2. Of course, the Pacific equivalent freshwater inventories are much less than the total Pacific seawater contribution to the water column. For example, a 50-meter column of water with uniform salinity (S~32.5) consisting entirely of Pacific water yields an equivalent freshwater of only 50 x (34.87-32.5)/34.87 = 3.4 meters.

Figure 3.2 Inventories of freshwater equivalents of (a) Pacific water and (b) meteoric water from bottle chemistry data collected at depths of ~20, 60, 80, 100, and 120 meters in the central Arctic and ~20, 60, and 85, and 195 meters in the southern Canada Basin during 2007 (squares) and 2008 (circles).

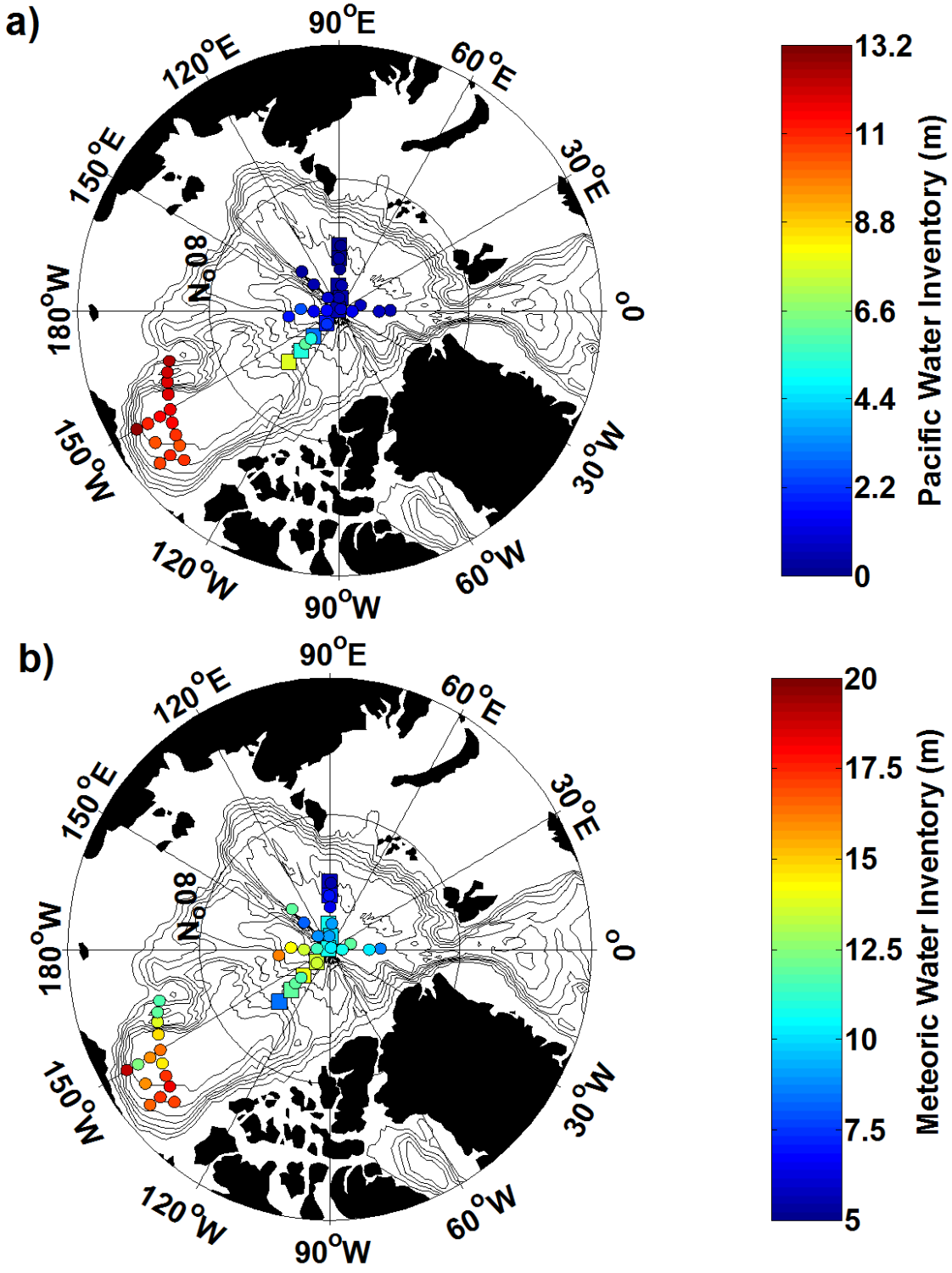
a)
90°E
120°E
60°E
150°E
30°E
180°W
0°
80°N
150°W
30°W
120°W
60°W
90°W
13.2
11
8.8
6.6
4.4
2.2
0
Pacific Water Inventory (m)
b)
90°E
120°E
60°E
150°E
30°E
180°W
0°
80°N
150°W
30°W
120°W
60°W
90°W
20
17.5
15
12.5
10
7.5
5
Meteoric Water Inventory (m)

Fig. 3.2

In the Makarov and Amundsen Basins, Pacific equivalent freshwater inventories were low (< 3 meters) at most stations during 2007 and 2008 (Fig. 3.2a). Pacific water influence increased southward from the North Pole along ~135ºW and was highest at station M1 over the Alpha Ridge. These results indicate cessation of the northward spread of Pacific water from the Canada Basin to the upper layers of the Makarov Basin observed during 2003-2005 (Morison et al., 2006; Alkire et al., 2007; Jones et al., 2008). This reversion potentially began as early as spring 2006 (Alkire et al., 2007; Morison et al., manuscript in preparation).

Pacific freshwater inventories were large (> 10 meters) throughout the southern Canada Basin; however, inventories were highest at stations W1-W4 over the Chukchi Borderland closest to Bering Strait. In contrast, the highest contributions from meteoric water (and somewhat lower Pacific inventories) occurred at stations east of 150ºW in the Canada Basin (Fig. 3.2b). As noted above, Eurasian river runoff is likely to be a major contributor to the meteoric water pool in this region. The predominance of Eurasian river water in the south-central Beaufort Gyre might appear to be an odd result. However, International Arctic Buoy Program based back-trajectories of sea-ice (Rigor et al., 2002; http://chemoc.coas.oregonstate.edu:16080/~kkfalkner/research/NPEO/NPEOintro.html) for some of our stations occupied in the southern Canada Basin during spring 2008 are traceable back to a Siberian shelf source over a 3+ year period. Interestingly, all the stations show recirculation in the Beaufort Gyre over several years and the back-trajectories are suggestive of entrainment of the Transpolar Drift Stream into the gyre. Strictly speaking the back-trajectories pertain to sea ice and not necessarily the circulation of waters over the depths of which meteoric waters were integrated, but river contributions tend to be highest near the surface at these stations.

In the central Arctic, meteoric water/Eurasian river runoff inventories (Fig. 3.2b) were higher at stations located in the Makarov Basin (though lower than in the Canada Basin) and lowest over the Arctic Mid-Ocean Ridge and central Amundsen

Basin during both 2007 and 2008. Assuming the stations occupied are representative of the mean state in the Amundsen and Makarov Basins during spring 2007 and 2008, the available data suggested preferential advection of Eurasian river runoff to the Makarov Basin as opposed to the Amundsen Basin in recent years. Such a distribution in river runoff can come about when Laptev Sea shelf waters circulate eastward alongshore past the Lomonosov Ridge. Numerous studies have suggested that the preferred pathway (northward versus eastward flow) of Laptev Sea waters is a function of summer wind forcing on the Siberian shelf (Steele and Boyd, 1998; Guay et al., 2001; Dmitrenko et al., 2005; 2008). In further support of this inference, Abrahamsen et al. (2009) recently showed that anomalous wind patterns over the Siberian seas during summer 2007 tended to confine Lena River runoff along the Laptev shelf and favored northward advection of shelf waters from the East Siberian Sea.

3.4.2 Continuous profiles of O_2, NO_3, and NO

3.4.2.1 Central Arctic 2007-2008

As noted earlier, freshwater sources (Pacific water and Eurasian river runoff) were present in significant amounts in the Makarov Basin stations (M1-M7) during both 2007 and 2008. In contrast, little freshwater occurred at Amundsen Basin stations (A5-A9) in 2007 and 2008. Accordingly, Makarov Basin stations had thicker and, in some cases, warmer halocline layers relative to those of the Amundsen Basin. The warmest halocline waters were present at Makarov Basin stations M1 and M2 (2007), which exhibited a relative θ maximum in the salinity range 32-33.5 (Fig. 3.3a) that is indicative of a summer Pacific origin. Larger Pacific contributions at stations M1 and M2 support this claim. Over this same salinity range, O_2 minima (Fig. 3.3b) and NO_3^- maxima (Fig. 3.3c) were present at stations M1 and M2 in 2007. Similarly depleted oxygen concentrations for central Arctic NPEO stations occupied in 2003 were attributed to summer Bering Sea waters that were shown to be influenced by respiratory activity in the sediments on their northward trajectories

(Falkner et al., 2005). Our continuous nitrate data (Fig. 3.3c & d) show this water type to be elevated in nutrients, consistent with the imprint of biological respiration.

Figure 3.3 Plots of (a, e) θ, (b, f) O_2, (c, g) NO_3^-, and (d, h) NO (= 9x[NO_3^-] + [O_2]) versus salinity for stations occupied in the Makarov (left, a-d) and Amundsen (right, e-h) Basins during 2007 (solid lines) and 2008 (dashed lines). Stations within the Makarov Basin are denoted M1-M7 whereas Amundsen Basin stations are denoted A5-A9. Colors correspond to station locations given in the inset maps (also see Figure 1) with southernmost stations in each transect being red progressing northward to cooler colors (green > cyan > blue) with black at the North Pole. Note axes have been expanded to focus on the halocline.

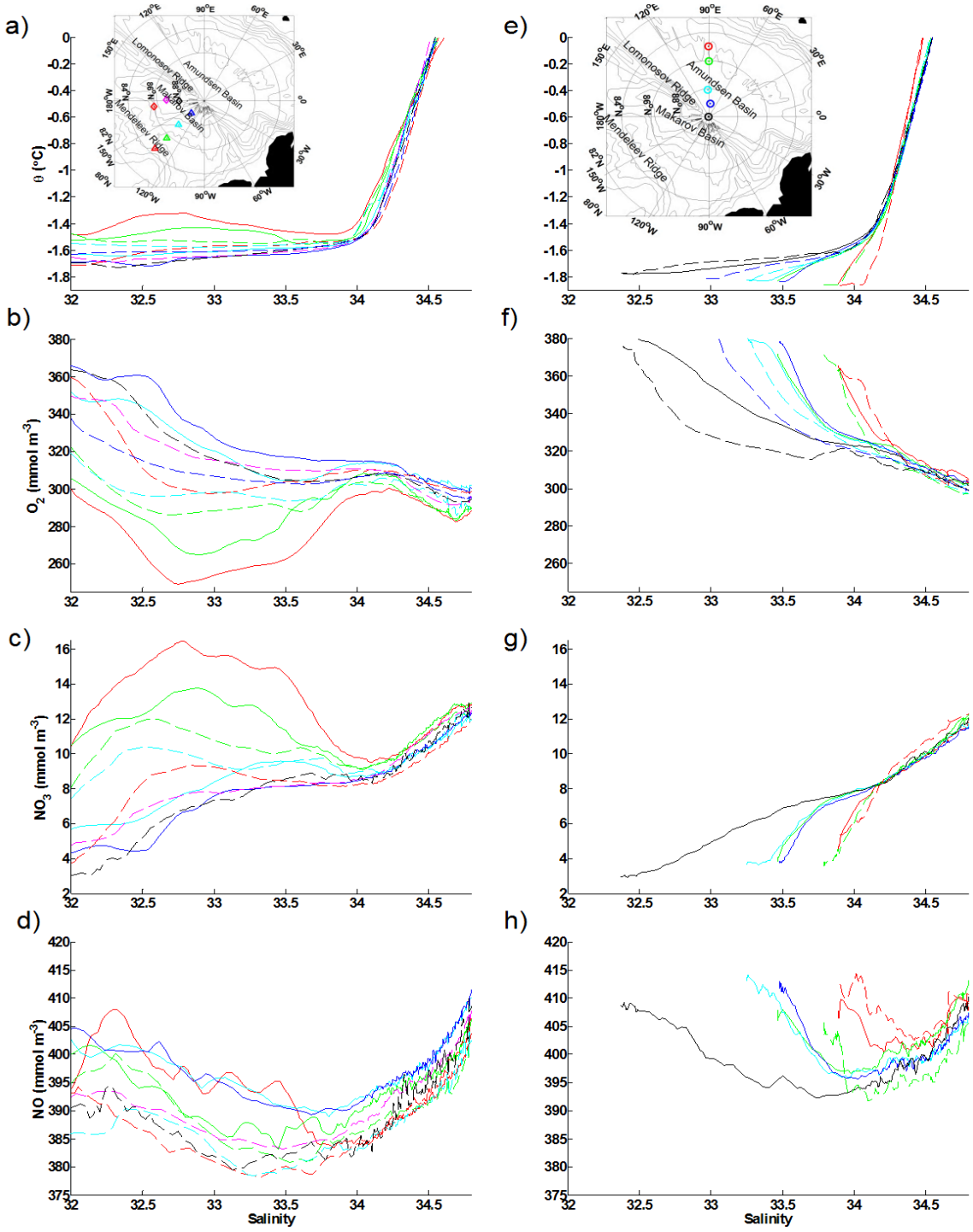
a)
e)
b)
f)
c)
g)
d)
h)
θ (°C)
O2 (mmol m-3)
NO3 (mmol m-3)
NO (mmol m-3)
Salinity
Lomonosov Ridge
Amundsen Basin
Mendeleev Ridge
Makarov Basin

Fig 3.3

In 2007, halocline layers were observed to be successively colder, better-ventilated, and more nutrient-deplete proceeding northward through the Makarov Basin (stations M3 and M4), past the North Pole (station A5), and into the Amundsen Basin (stations A6-A8) (Fig. 3.3). These observations are a consequence of the increasing influence of Atlantic origin halocline waters, which are relatively nutrient-poor and oxygen-rich, compared to Pacific-derived halocline waters moving from the Makarov to the Amundsen Basin (McLaughlin et al., 1996). In 2008, the halocline of Makarov Basin stations appeared colder, better ventilated, and depleted in nutrients relative to observations in 2007. In contrast, relatively little change was observed at Amundsen Basin stations between 2007 and 2008.

An O_2 maximum was observed in the salinity range of the lower halocline layer ($34.0 \leq S \leq 34.5$) at stations M1-M7 during both years within the Makarov Basin, but it was particularly pronounced in 2007 (Fig. 3.3b). This feature occurs between two minima, without which O_2 would have otherwise transitioned smoothly with increasing salinity (Falkner et al., 2005) as it did at Amundsen Basin stations (A5-A9, Fig. 3.3f). Nitrate concentrations grossly mirrored these trends (Fig. 3.3c, g) as expected from biological respiration. However, as is well known, denitrification over Arctic shelves (Wilson and Wallace, 1990) also contributes to variations in preformed nitrate concentrations and as a result, deviations from strictly Redfield type relationships between the nutrients and oxygen.

Observed variability in the structure of NO profiles, both vertically and between stations, significantly exceeds our conservative estimate of uncertainty (± 5 mmol m^{-3}). Profiles of NO (Fig. 3.3d, h) generally decreased from a surface maximum through the halocline toward a minimum in the salinity range 33.5-34.2 before increasing again toward a maximum associated with the Atlantic layer (S~34.8). Undulations occurring from 70 to 120 meters depth in the Makarov Basin during 2007 (Fig. 3.3d) were predominantly a function of similar structure in the nitrate data (Fig. 3.3c). While unusual, such structure does not appear to be a

sampling or data processing artifact since these features were coincident in both the up and down casts. We do not have an explanation for these features at this time.

Minima in NO were typically encountered at salinities < 34.0 in the Makarov Basin during both 2007 and 2008 (Table 3.2). Makarov Basin stations exhibited NO minima at salinities ranging between 33.2 and 34.0 in 2007 and at a salinity of 33.5 in 2008 (Fig. 3d). Station A5 (North Pole) exhibited similarly low NO values in the salinity range 33.2-33.9 in 2007 (Fig. 3.3g). Contrary to prior studies (Jones and Anderson, 1986; Anderson and Jones, 1992; Anderson et al., 1994; Salmon and McRoy, 1994; Rudels et al., 1996; McLaughlin et al., 1996; Guay and Falkner, 1997), these observations demonstrate that minimal NO values in a vertical profile are not always strictly associated with LHW (defined by the characteristic bend in θ-S space between salinities 34.1 and 34.3; Aagaard et al., 1981 and Jones and Anderson, 1986) in the central Arctic Ocean. This is not necessarily surprising as NO is known to vary greatly over the Siberian shelves (300-450 mmol m^{-3}) with median values similar to the minima associated with LHW (Wilson and Wallace, 1990).

Table 3.2 Values of NO (NO_{min}) and salinity (S_{min}) at the absolute NO minima (for salinities > 33.0 and depths > 50 meters) at each station occupied during the 2007 and 2008 field seasons. Also shown are the NO minima (NO_{LHW}) for the salinity range ($34.1 \leq S \leq 34.3$) associated with lower halocline water.

Year	Station	NO_{min}	S_{min}	NO_{LHW}
2007	A9	401	34.21	401
2007	A8	397	33.98	397
2007	A7	396	33.97	396
2007	A6	396	34.02	396
2007	A5	392	33.75	394
2007	M4	389	33.68	392
2007	M3	389	33.80	394
2007	M2	383	33.45	391
2007	M1	383	33.84	385
2008	A9	403	34.42	406
2008	A8	392	34.10	392
2008	M3	378	33.28	386
2008	M2	381	33.53	388
2008	M5	378	33.33	385
2008	M6	383	33.48	389
2008	M7	379	33.13	383
2008	W1	384	34.56	389
2008	W2	383	34.51	385
2008	W3	384	34.49	388
2008	W4	384	34.45	386
2008	L1	387	34.29	387
2008	L2	388	34.33	390
2008	L3	391	34.71	435
2008	L4	393	34.65	405
2008	C1	387	34.26	387
2008	C2	385	34.32	386
2008	C3	387	34.22	387
2008	B1	385	34.25	385
2008	B2	384	34.14	384
2008	C4	387	34.00	387
2008	B3	387	34.26	387

At Amundsen Basin stations (A6-A9), the NO minima occurred at somewhat higher salinities (~34.0) generally associated with LHW. The lower salinities at which NO minima occurred at Makarov Basin stations compared with Amundsen Basin stations (Table 3.2) requires that different sources of low salinity water ventilate their respective cold halocline layers. Modification and/or mixing of new sources in the density range of LHW upon crossing the Lomonosov Ridge have been suggested to explain observations of lower NO, warmer temperatures, and higher barium and silica concentrations in the LHW of the Canadian Basin (Salmon and McRoy, 1994; McLaughlin et al., 1996; Guay and Falkner, 1997).

For example, Salmon and McRoy (1994) suggested interleaving of Chukchi shelf waters with lower halocline waters to explain the higher silica concentrations and lower NO values associated with lower halocline waters in the Canada Basin. Guay and Falkner (1997) invoked additional inputs from Chukchi, Beaufort, and/or East Siberian shelf waters, influenced by brine rejection, interaction with sediments, and denitrification to explain relatively high barium concentrations measured in the lower halocline of Canada Basin.

Salmon and McRoy (1994) pointed out, however, that summer salinities on Siberian shelves tend to be insufficient to ventilate lower halocline water. Yet, these shelf waters are salty enough to contribute to the overlying cold halocline layer. Observations of NO minima in the cold halocline layer of Makarov Basin lend support to hypotheses arguing for a more direct role of shelf waters in the maintenance of NO minima associated with lower halocline water in the Canadian sector.

3.4.2.2 Southern Canada Basin/Beaufort Sea 2008

A generally linear increase in θ and decrease in O_2 with respect to salinity was observed at the westernmost stations (W1-W4) of the southern Canada Basin between 33.1 and 34.0 (Fig. 3.4a, b). These observations resemble those reported for summer

2002 by Woodgate et al. (2005) to be a consequence of diapyncal mixing between Pacific winter waters and lower halocline waters (Atlantic-origin) upwelled onto the Chukchi shelf/slope. At these stations, the NO decreased with salinity from relative maxima centered at salinities 32.9-33.1 to minima centered at a salinity of ~34.5 (Fig. 3.4d). The salinities at which the NO minima occurred were the highest observed among all of the stations occupied in the southern Canada Basin and central Arctic.

Figure 3.4 Plots of θ (a, e), O_2 (b, f), and NO_3^- (c, g), and (d, h) NO (= 9x[NO_3^-] + [O_2]) versus salinity for the western (left, a-d) and eastern (right, e-h) regions of the southern Canada Basin. Western region stations comprise W1-W4 and L1-L4 whereas eastern region stations comprise C1-C4 and B1-B3. Colors correspond to station locations given in the inset maps (also see Figure 1) using warmer (western) and cooler (eastern) color scales for western and eastern regions, respectively. Within each region, colors progress from cooler to warmer moving northward. Note axes have been expanded to focus on the halocline.

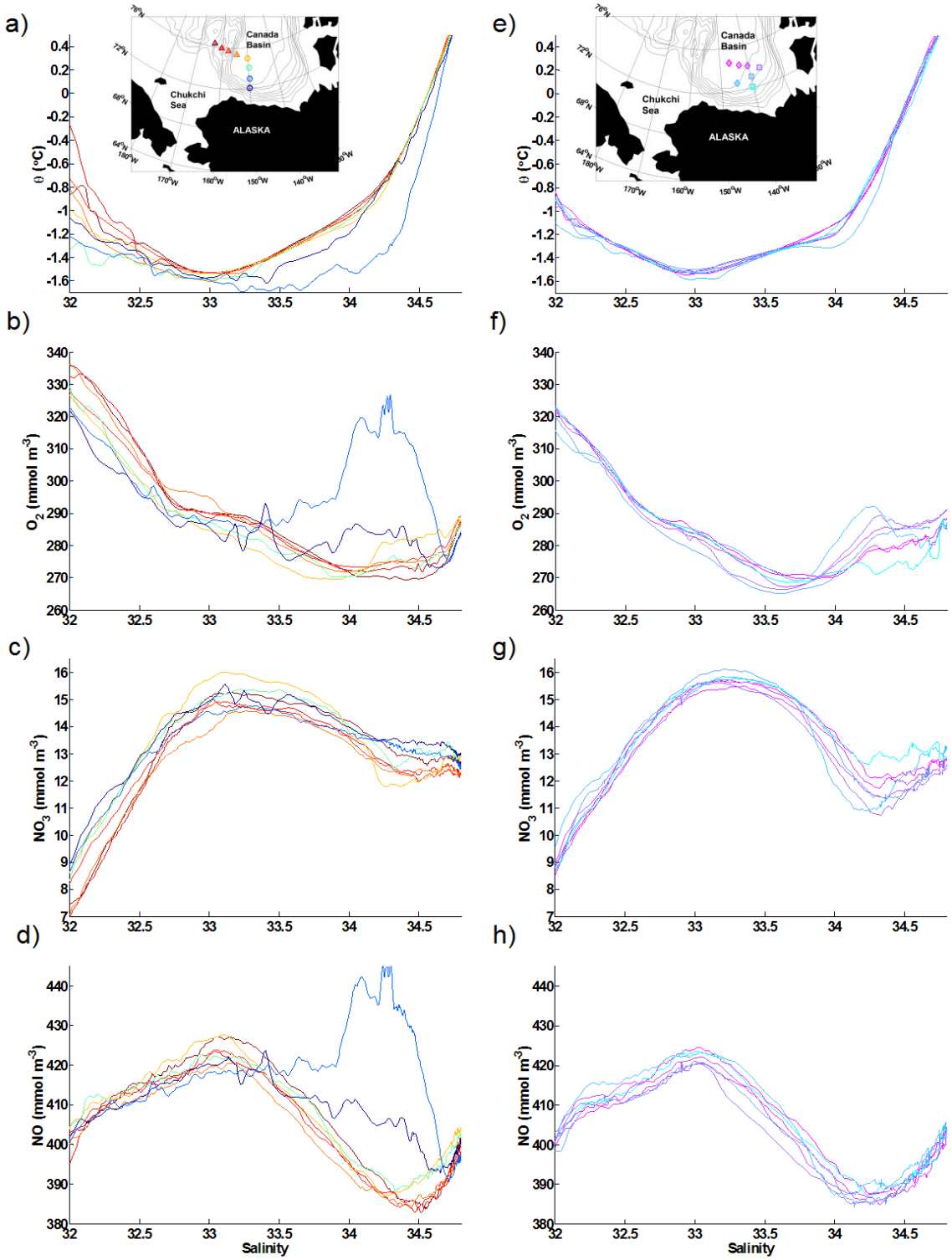
a)
e)
b)
f)
c)
g)
d)
h)
Canada Basin
Chukchi Sea
ALASKA
θ (°C)
O2 (mmol m-3)
NO3 (mmol m-3)
NO (mmol m-3)
Salinity

Fig. 3.4

Rudels et al. (2004) argued two branches of lower halocline water, the Fram Strait Branch (FSB) and Barents Sea Branch (BSB), circulated along different pathways and thus ventilated different basins of the Arctic interior. The warmer and more saline variety, BSB LHW, was suggested to circulate cyclonically along the continental slope forcing FSB LHW offshore to supply the halocline of the Amundsen and Makarov Basins and part of northern Canada Basin. In contrast, BSB LHW was expected to supply the lower halocline of the southern Canada Basin, particularly east of the Chukchi Cap. We suggest the NO minima observed at stations W1-W4 to be synonymous with BSB LHW. The low O_2 and high NO_3^- concentrations associated with these waters, relative to the FSB LHW ventilating the remaining Canada Basin stations, could be explained by the longer route taken by BSB LHW to enter the study area.

Stations L1 and L2, on the northern end of the 150ºW line, did not exhibit characteristics of diapycnal mixing, but featured O_2 minima (~270 mmol m^{-3}) between salinities 33.6 and 34.0 followed by an increase in O_2 through the lower halocline. Shimada et al. (2005) observed similar features in 2002-2003 and referred to them as a western Chukchi Pacific winter water/O_2-rich LHW assembly. Our observations (Fig. 3.4d) also indicated NO minima occurred at somewhat lower salinities (S~34.3) compared to stations W1-W4 (S~34.5). Stations located in the eastern region of Canada Basin (C1-C4 and B1-B3) also had hydrographic characteristics (Fig. 4e-f) resembling a western Chukchi PWW/O_2-rich LHW assembly (Shimada et al., 2005) with NO minima occurring between salinities 34.1 and 34.3 (Fig. 3.4h). These observations suggest ventilation by the FSB LHW (Rudels et al., 2004). Shimada et al. (2005) also inferred the O_2-rich LHW had origins in the Eurasian Basin where convection could produce high O_2 concentrations at the salinity and temperature of lower halocline water. This hypothesis was somewhat supported by Itoh et al. (2007) using oxygen saturation, θ, and potential vorticity to trace the cold and O_2-rich LHW to the Nansen Basin.

The different salinities at which NO minima occurred in the western versus eastern stations supports previous observations of two separate varieties of lower halocline water ventilating Canada Basin. The similarity in the respective NO minima, despite differences in O_2 concentrations, suggest these features share a similar formation mechanism. This most likely occurs, therefore, prior to the proposed split of the two branches upon crossing the Mendeleev Ridge (Rudels et al., 2004). The slightly lower NO of the BSB LHW (stations W1-W4) implies further modification, perhaps as a consequence of its close proximity to the shelf/slope.

Station L3 exhibited relatively high oxygen saturations (ranging from 85-87%) and cold potential temperatures (0.2-0.8ºC above freezing) in the salinity range 34.0-34.4 (Fig. 3.4a & c). Station L4 also had cold and well-ventilated waters in this salinity range, though not to the degree observed at L3. These high O_2 concentrations resulted in unusually high NO maxima in the salinity range ($34.1 \leq S \leq 34.5$) typically associated with the lower halocline NO minimum (Fig. 3.4d). All other stations occupied in the southern Canada Basin had warmer (0.7-1.5ºC above freezing) and less well-ventilated (O_2 saturation < 78%) waters in this same salinity range. These include stations exhibiting the relatively cold and O_2 rich FSB LHW. The high oxygen concentrations and cold potential temperatures of the lower halocline waters observed at these stations point to recent exchange with the atmosphere and contact with ice. Polynyas provide the appropriate conditions as elevated ice and therefore brine production tends to occur in association with the open waters (Aagaard et al., 1981; Cavalieri and Martin, 1994).

Unfortunately, no bottle data were collected within the O_2 maxima at these stations to help to chemically confirm recent surface water characteristics. Nitrate concentrations (Fig. 4c) alone cannot differentiate between Pacific winter waters and Atlantic-derived waters. However, images from the Moderate Resolution Imaging Spectroradiometer (MODIS) on satellites Terra and Aqua (http://rapidfire.sci.gsfc.nasa.gov/realtime/?calendar) confirm expanses of open water between Cape Lisburne and Point Barrow, Alaska beginning in late January and

extending through the end of April 2008. A recurrent coastal polynya was described for this region during 1990-2001 (Martin et al., 2004) and 2003 (Martin et al., 2005), supporting the possibility of recurrent ventilation of halocline waters. Both Woodgate et al. (2005b) and Weingartner et al. (1998) reported cold and saline ($S > 34$) water produced in polynyas opened during winter 1991-1992 by strong northeast winds. This dense water was carried alongshore with the coastal current and was carried into the Arctic Ocean via Barrow Canyon. Shimada et al. (2005) also reported near-freezing, high-salinity waters from time-series mooring data in Barrow Canyon between 1997 and 2003 and suggested upper halocline ventilation via polynya-produced dense waters.

Woodgate et al. (2005) discounted Shimada et al. (2005)'s suggestion that polynya influence aided the ventilation of upper halocline waters ($33 \leq S \leq 34$) in the southern Canada Basin as O_2 concentrations were not anomalously high and potential temperatures were above freezing. The 0.3-0.8ºC departure from the freezing point does argue against direct ventilation via ice formation at stations L3 and L4. However, the high O_2 concentrations suggest these waters were either in direct contact with the atmosphere or mixed with recently ventilated waters prior to injection into the lower halocline.

Another possible explanation for our observations could be upwelling of relatively warm Atlantic-derived waters onto the shelf/slope during winter months. Such upwelling events have been observed in Barrow Canyon during 1986-1987 (Aagaard and Roach, 1990) and 1990-1991 (Woodgate et al., 2005b). This is effectively the diapycnal mixing scenario discussed by Woodgate et al. (2005). However, θ, O_2, and salinity distributions at stations L3 and L4 do not illustrate the linear behavior that illustrates evidence of diapycnal mixing like that seen at stations W1-W4. Thus, if mixing did take place, significant cooling and ventilation must have occurred subsequently to produce the θ and O_2 concentrations observed prior to injection into the halocline. This scenario still requires an area of open water to allow interaction with the atmosphere.

Finally, we note Mathis et al. (2007) documented eddy propagation as a possible transport mechanism of well-ventilated, dense halocline waters off shore and into the basin interior. Our sampling scheme does not allow us to address the mechanism of transport.

3.5 Summary and Conclusions

High-resolution records of the NO parameter revealed that the NO minimum typically associated with lower halocline water ($34.1 \leq S \leq 34.5$) frequently occurred at lower salinities (33.2-34.2) in the Makarov Basin. In the Amundsen Basin, the NO minimum remained associated with LHW. These observations suggest the cold halocline layers in these basins were ventilated by different sources of low salinity waters (most likely from Siberian shelves) and support previous inferences suggesting direct shelf influence to the lower halocline of the Canadian Basin. Although physically-reasonable mechanisms for the injection of such signals from relatively fresh Arctic shelves into the saline lower halocline remain somewhat elusive, continuous profiles of NO offer a tool to constrain variability in the formation and modification of these waters.

Available bottle chemistry data indicate the differences observed in the halocline were coincident with a larger influence of Eurasian river runoff in the Makarov Basin relative to the Amundsen Basin during 2007-2008. These observations might be linked as a consequence of wind forcing over the Siberian shelves during summer 2007 favoring offshore advection northward of the East Siberian Sea (Abrahamsen et al., 2007). Assuming interaction with sediments or mixing with resident shelf waters prior to advection offshore, denitrification known to occur in East Siberian Sea sediments (Codispoti et al., 1991; Nitishinsky et al., 2007) could explain the low NO values observed in the cold halocline layer of the Makarov Basin. These inferences imply linkages between the fate of shelf waters and the formation of NO minima. Previous studies have also linked the offshore distribution of shelf waters to LHW formation (Steele and Boyd, 1998; Boyd et al., 2002; Kikuchi et al., 2004). The NO parameter might be used as an additional tool in understanding

variability in the formation and distribution of LHW types as well as other shelf influences on the overlying halocline.

At most stations in the southern Canada Basin, very low NO minima were coincident with lower halocline waters. At stations located over the Chukchi Borderland, NO generally decreased with increasing salinity throughout the halocline. This is indicative of diapycnal mixing between Pacific winter waters and Atlantic-derived lower halocline waters (Woodgate et al., 2005). Two different varieties of lower halocline water were characterized by the salinity at which the NO minimum occurred. In agreement with previous studies differentiating between different sources of lower halocline water, we observed O_2-poor LHW predominately ventilating the southwestern Canada Basin whereas O_2-rich LHW was found in the central and eastern portion of the basin. Despite these differences, both LHW varieties had similarly low NO minima.

In addition, very high NO values in the lower halocline were observed at the southernmost stations on the 150ºW line, suggesting ventilation of the halocline by waters in recent contact with the atmosphere. Recurrent and nearby coastal polynyas offer a source of open water where such waters may have been either formed or modified. Clearly, there are multiple mechanisms involved in the formation and ventilation of the halocline and under a changing wind and ice regime, their relative influences can be expected to vary in the future. Our study indicates that continuous sensor-based NO data will prove very useful for capturing such variability.

3.6 References

Aagaard, K., L.K. Coachman, E. Carmack (1981), On the halocline of the Arctic Ocean, *Deep-Sea Research 28A*: 529-545.

Aagaard, K., A.T. Roach (1990), Arctic Ocean-Shelf Exchange: Measurements in Barrow Canyon, *Journal of Geophysical Research 95*: 18163-18175.

Abrahamsen, E.P., Meredith, M.P., Falkner, K.K., Torres-Valdes, S., Leng, M.J., Alkire, M.B., Bacon, S., Polyakov, I., Ivanov, V., Kirillov, S. (2009), Tracer-derived freshwater budget of the Siberian Continental Shelf following the extreme Arctic summer of 2007, *Geophysical Research Letters 36*: doi:10.1029/2009GL037341.

Alkire, M.B., K.K. Falkner, I. Rigor , M. Steele, J. Morison (2007), The return of Pacific waters to the upper layers of the central Arctic Ocean, *Deep-Sea Research I 54*: 1509-1529.

Anderson, L.G. and E.P. Jones (1992), Tracing upper waters of the Nansen Basin in the Arctic Ocean, *Deep-Sea Research 39*: 425-433.

Boyd, T.J., M. Steele, R.D. Muench, J.T. Gunn (2002), Partial recovery of the Arctic Ocean halocline, *Geophysical Research Letters 29*: doi:10.1029/2001GL014047.

Broecker, W.S. (1974), "NO", A conservative water mass tracer, *Earth and Planetary Science Letters 23*: 100-107.

Carmack, E., F. McLaughlin, M. Yamamoto-Kawai, M. Itoh, K. Shimada, R. Krishfield, A. Proshutinsky (2008), Freshwater Storage in the Northern Ocean and the Special Role of the Beaufort Gyre in *Arctic-Subarctic Ocean Fluxes: Defining the Role of the Northern Seas in Climate*, eds. R.R. Dickson, J. Meincke, and P. Rhines, Springer, pp. 145-170.

Cavalieri, D.J., S. Martin (1994), The contribution of Alaskan, Siberian, and Canadian coastal polynyas to the cold halocline layer of the Arctic Ocean, *Journal of Geophysical Research 99*: 18343-18362.

Codispoti, L.A., Friederich, G.E., Sakamoto C.M., Gordon, L.I. (1991), Nutrient cycling and primary production in the marine systems of the Arctic and Antarctic, *Journal of Marine Systems 2*: 359-384.

Cooper, L.W., J.W. McClelland, R.M. Holmes, P.A. Raymond, J.J. Gibson, C.K. Guay, B.J. Peterson (2008), Flow-weighted values of runoff tracers (d18O, DOC, Ba, alkalinity) from the six largest Arctic rivers, *Geophysical Research Letters 35*: doi:10.1029/2008GL035007.

Dmitrenko, I., S. Kirillov, H. Eicken, N. Markova (2005), Wind-driven summer surface hydrography of the eastern Siberian shelf, *Geophysical Research Letters 32*: doi:10.1029/2005GL023022.

Dmitrenko, I.A., S.A. Kirillov, L.B. Tremblay (2008), The long-term and interannual variability of summer fresh water storage over the eastern Siberian shelf: Implications for climatic change, *Journal of Geophysical Research 113:* doi:10.1029/2007JC004304.

Ekwurzel, B., P. Schlosser, R.A. Mortlock, R.G. Fairbanks (2001), River runoff, sea ice meltwater, and Pacific water distribution and mean residence times in the Arctic Ocean, *Journal of Geophysical Research. 106*: 9075-9092.

Falkner, K.K., R.W. Macdonald, E.C. Carmack, T. Weingartner (1994), The potential of barium as a tracer of Arctic water masses, in *The Polar Oceans and Their Role in Shaping the Global Environment: The Nansen Centennial Volume, AGU Geophys. Monograph Series*, edited by O.M. Johannessen, R.D. Muench, and J.E. Overland, pp. 63-76, AGU Books, Washington DC.

Falkner, K.K., M. Steele, R.A. Woodgate, J.H. Swift, K. Aagaard, J. Morison (2005), Dissolved oxygen extrema in the Arctic Ocean halocline from the North Pole to the Lincoln Sea, *Deep-Sea Research I 52*: 1138-1154.

Guay, C.K. and K.K Falkner (1997), Barium as a tracer of Arctic halocline and river waters, *Deep-Sea Research II 44*: 1543-1569.

Guay, C.K., K.K Falkner, R.D. Muench, M. Mensch, M. Frank, R. Bayer (2001), Wind-driven transport pathways for Eurasian Arctic river discharge, *Journal of Geophysical Research 106*: 11469-11480.

Guay, C.K.H., F.A. McLaughlin, M. Yamamoto-Kawai (2009), Differentiating fluvial components of upper Canada Basin waters on the basis of measurements of dissolved barium combined with other physical and chemical tracers, *Journal of Geophysical Research 114*: doi:10.1029/2008JC005099.

Itoh, M., E. Carmack, K. Shimada, F. McLaughlin, S. Nishino, S. Zimmermann (2007), Formation and spreading of Eurasian source oxygen-rich halocline water into the Canadian Basin in the Arctic Ocean, *Geophysical Research Letters 34*: doi:10.1029/2007GL029482.

Johnson, K.S., L.J. Coletti (2002), In situ ultraviolet spectrophotometry for high resolution and long-term monitoring of nitrate, bromide and bisulfide in the ocean, *Deep-Sea Research I 49*: 1291-1305.

Johnson, K.S., J.A. Needoba (2008), Mapping the spatial variability of plankton metabolism using nitrate and oxygen sensors on an autonomous underwater vehicle, *Limnology and Oceanography 53*: 2237-2250.

Jones, E.P. and L.G. Anderson (1986), On the origin of the chemical properties of the Arctic Ocean halocline, *Journal of Geophysical Research. 91*: 10759-10767.

Jones, E.P., L.G. Anderson, S. Jutterstrom, L. Mintrop, J.H. Swift (2008), Pacific freshwater, river water and sea ice meltwater across the Arctic Ocean basins: Results

from the 2005 Beringia Expedition, *Journal of Geophysical Research 113*: doi:10.1029/2007JC004124.

Kikuchi, T., K. Hatakeyama, J. Morison (2004), Distribution of convective Lower Halocline Water in the eastern Arctic Ocean, *Journal of Geophysical Research 109*: doi:10.1029/2003JC002223.

Martin, S., R. Drucker, R. Kwok, B. Holt (2004), Estimation of the thin ice thickness and heat flux for the Chukchi Sea Alaskan coast polynya from Special Sensor Microwave/Imager data, 1990-2001, *Journal of Geophysical Research 109*: doi:10.1029/2004JC002428.

Martin, S., R. Drucker, R. Kwok, B. Holt. (2005), Improvements in the estimates of ice thickness and production in the Chukchi Sea polynyas derived from AMSR-E, *Geophysical Research Letters 32*: doi:10.1029/2004GL022013.

Mathis, J.T., R.S Pickart, D.A. Hansell, D. Kadko, N.R. Bates (2007), Eddy transport of organic carbon and nutrients from the Chukchi Shelf: Impact on the upper halocline of the western Arctic Ocean, *Journal of Geophysical Research 112*: doi:10.1029/2006JC003899.

McLaughlin, F.A., E. Carmack, R. Macdonald (1996), Physical and geochemical properties across the Atlantic/Pacific water mass front in the southern Canadian Basin, *Journal of Geophysical Research 101*: 1183-1197.

McLaughlin, F.A., E.C. Carmack, R.W. Macdonald, H. Melling, J.H. Swift, P.A. Wheeler, B.F. Sherr, E.B. Sherr (2004), The joint roles of Pacific and Atlantic-origin waters in the Canada Basin, 1997-1998, *Deep-Sea Research I 51*: 107-128.

Morison, J., R. Andersen, N. Larson, E. D'Asaro, T. Boyd (1994), The Correction for Thermal-Lag Effects in Sea-Bird CTD Data, *Journal of Atmosphere & Ocean Techology 11*: 1151-1164.

Morison, J., M. Steele, R. Andersen (1998), Hydrography of the upper Arctic Ocean measured from the nuclear submarine *U.S.S. Pargo*, *Deep-Sea Research I 45*: 15-38.

Morison, J., M. Steele, T. Kikuchi, K. Falkner, W. Smethie (2006), The relaxation of central Arctic Ocean hydrography to pre-1990s climatology, *Geophysical Research Letters 33*: doi:10.1029/2006GL026826.

Nitishinsky, M., L.G. Anderson, J.A. Holemann (2007), Inorganic carbon and nutrient fluxes on the Arctic Shelf, *Continental Shelf Research 27*: 1584-1599.

Olsson, K., L. Anderson (1997), Input and biogeochemical transformation of dissolved carbon in the Siberian shelf seas, *Continental Shelf Research 17*: 819-833.

Pfirman, S., W. Haxby,, M. Jeffries, D. Bauch (2004), Drifting Arctic sea ice archives changes in ocean surface conditions, *Geophysical Research Letters 31*: doi:10.1029/2004GL020666.

Rigor, I.G., J.M. Wallace, R.L. Colony (2002), Response of Sea Ice to the Arctic Oscillation, *Journal of Climate 15*: 2648-2663.

Rudels, B., L.G. Anderson, E.P. Jones (1996), Formation and evolution of the surface mixed layer and halocline of the Arctic Ocean, *Journal of Geophysical Research 101*: 8807-8821.

Rudels, B., E.P. Jones, U. Schauer, P. Eriksson (2004), Atlantic sources of the Arctic Ocean surface and halocline waters, *Polar Research 23*: 181-208.

Sakamoto, C.M., K.S Johnson, L.J. Coletti (2009), Improved algorithm for the computation of nitrate concentrations in seawater using an in situ ultraviolet spectrophotometer, *Limnology and Oceanography Methods 7*: 132-143.

Salmon, D.K. and C.P. McRoy (1994), Nutrient-based tracers in the Western Arctic: a new lower halocline water defined, in *The Polar Oceans and Their Role in Shaping the Global Environment: The Nansen Centennial Volume, Geophys., Monogr. Ser.*, vol 85, edited by O.M Johannessen, R.D. Muench, and J.E. Overland, pp. 47-61, AGU, Washington, D.C.

Seabird (2009), Application Note No. 64: SBE43 Dissolved Oxygen Sensor – Background Information, Deployment Recommendations, and Cleaning and Storage, http://www.seabird.com/application_notes/AN64.htm, last modified 06 Jul 2009.

Serreze, M.C., A.P. Barrett, A.G. Slater, R.A. Woodgate, K. Aagaard, R.B. Lammers, M. Steele, R. Moritz, M. Meredith, C.M. Lee (2006), The large-scale freshwater cycle of the Arctic, *Journal of Geophysical Research. 111*: doi:10.1029/2005JC003424.

Shimada, K., M. Itoh, S. Nishino, F. McLaughlin, E. Carmack, A. Proshutinsky (2005), Halocline structure in the Canada Basin of the Arctic Ocean, *Geophysical Research Letters 32*: doi:10.1029/2004GL021358.

Steele, M., J.H. Morison, T.B. Curtin (1995), Halocline water formation in the Barents Sea, *Journal of Geophysical Research 100*: 881-894.

Steele, M. and T. Boyd (1998), Retreat of the cold halocline layer in the Arctic Ocean, *Journal of Geophysical Research 103*: 10,419-10,435.

Steele, M., J. Morison, W. Ermold, I. Rigor, M. Ortmeyer, K. Shimada (2004), Circulation of summer Pacific halocline water in the Arctic Ocean, *Journal of Geophysical Research 109*: doi:10.1029/2003JC002009.

Taylor, J.R., K.K Falkner, U. Schauer, M. Meredith (2003), Quantitative considerations of dissolved barium as a tracer in the Arctic Ocean, *Journal of Geophysical Research 108*: doi:10.1029/2002JC001635.

Weingartner, T.J., D.J. Cavalieri, K. Aagaard, Y. Sasaki (1998), Circulation, dense water formation, and outflow on the northeast Chukchi shelf, *JGR 103*, 7647-7661.
Wilson, C. and D.W.R. Wallace (1990), Using the nutrient ratio NO/PO as a tracer of continental shelf waters in the central Arctic Ocean, *J. Geophys. Res. 95*: 22193-22208.

Woodgate, R.A., K. Aagaard, J.H. Swift, K.K. Falkner, W.M. Smethie, Jr. (2005), Pacific ventilation of the Arctic Ocean's lower halocline by upwelling and diapycnal mixing over the continental margin, *Geophysical Research Letters 32*: doi:10.1029/2005GL023999.

Woodgate, R.A., K. Aagaard, T.J. Weingartner (2005b), A year in the physical oceanography of the Chukchi Sea: Moored measurements from autumn 1990-1991, *Deep-Sea Research II 52:* 3116-3149.

Yamamoto-Kawai, M., N. Tanaka, S. Pivovarov (2005). Freshwater and brine behaviors in the Arctic Ocean deduced from historical data of $\delta^{18}O$ and alkalinity (1929-2002 A.D.), *J. Geophys. Res. 110*, doi:10.1029/2004JC002793.

Yamamoto-Kawai, M., F.A. McLaughlin, E.C. Carmack, S. Nishino, K. Shimada (2008), Freshwater budgets of the Canada Basin, Arctic Ocean, from salinity, $\delta^{18}O$, and nutrients, *J. Geophys. Res. 113*, doi:10.1029/2006JC003858.

Yamamoto-Kawai, M., F.A. McLaughlin, E.C. Carmack, S. Nishino, K. Shimada, N. Kurita (2009), Surface freshening of the Canada Basin, 2003-2007: River runoff versus sea ice meltwater, *J. Geophys. Res. 114*, doi:10.1029/2008JC005000.

4. SEA-ICE MELT AND METEORIC WATER DISTRIBUTIONS IN BAFFIN BAY AND THE CANADIAN ARCTIC ARCHIPELAGO

Matthew B. Alkire[1], Kelly K. Falkner[1], Tim Boyd[2]

[1]College of Oceanic & Atmospheric Sciences, Oregon State University, Corvallis, OR , USA
[2]Scottish Association for Marine Science, Dunstaffnage Marine Laboratory, Oban, Argyll, Scotland, UK

This chapter will undergo some revision, including additional figures and text, before submission to the *Journal of Marine Systems* for publication planned for April, 2010

4.1 Abstract

Salinity, $\delta^{18}O$, and nutrient data were used to estimate contributions of sea-ice melt and meteoric water to the upper waters of the Canadian Arctic Archipelago (CAA) and Baffin Bay during late summer 1997 and 2003. Comparison of salinity-$\delta^{18}O$ relationships in profiles within the study area to those throughout the Arctic Ocean shows the CAA inherits a net sea-ice formation signal from the Arctic Ocean at least in summer. Two main, linear salinity-$\delta^{18}O$ trends emerge in the study region that result from seawater combining with brine enriched shelf water and above that, this shelf water mixing with meteoric water and sea-ice melt. Using these inherited characteristics as a starting point, local, seasonal sea-ice meltwater contributions were calculated.

Positive, local sea-ice melt fractions were generally limited to the upper 20-50 meters but were ubiquitous over the study region. Largest contributions up to 6% were present in areas of northeast Baffin Bay, southeastern Kennedy Channel, northern Jones Sound, and Davis Strait. Local sea-ice melt did penetrate to > 150 meters depth in eastern Davis Strait. Though distributions of local sea-ice meltwater were generally similar to previous reports, the fractions themselves were somewhat lower, resulting in the greater contributions of Pacific water and meteoric water over sea-ice melt to the total freshwater in the top 20-50 meters. Meteoric water contributions were comparable (6-9%) but Pacific water content was lower in 2003 (40-70%) than in 1997 (70-85%) in Smith Sound, demonstrating that these water types do not necessarily co-circulate.

4.2 Introduction

The Canadian Arctic Archipelago (CAA) is a major conduit by which the Pacific and Atlantic Oceans are connected through the Arctic Ocean and it accounts for approximately half of the freshwater exported from the Arctic to the North Atlantic (Serreze, et al., 2006). This freshwater, in the form of relatively fresh seawater and to a lesser extent as ice, is delivered to the Labrador Sea where North Atlantic Intermediate Water is formed. By

strengthening stratification at sites of convective overturning, freshwater exported from the CAA could potentially impede this key northern limb of global ocean overturning circulation. Hence it is important to gain an understanding of what controls freshwater distributions and fluxes in the region. In this paper, we quantify the sea-ice melt and meteoric (riverine plus precipitation) components of the freshwater distributions in Baffin Bay and the CAA using $\delta^{18}O$ and salinity information to account for both the inherited and local freshwater signals.

4.3 Background

4.3.1 Hydrographic setting

Exchange of water is limited in the CAA by the relatively shallow sills in various straits and sounds bridging adjacent Arctic basins from the Beaufort to Lincoln Seas with Baffin Bay. To reach Baffin Bay, Arctic-origin waters must transit either Nares Strait (sill depth ~220m), Cardigan Strait/Hell Gate (~180/125m), or Barrow Strait (~125m) to Smith, Jones, and Lancaster Sounds, respectively, to reach Baffin Bay (Melling et al., 2008). A small fraction of waters exiting the Arctic through the CAA is also diverted to Hudson Bay via Fury and Hecla Straits. Toward the south of our study region, Davis Strait (sill depth ~650m) and Hudson Strait (200m) connect Baffin Bay and Foxe Basin/Hudson Bay respectively to the Labrador Sea.

We restrict our review of hydrographic properties of Baffin Bay for the purpose of this paper to the upper 500 m. Above this depth waters are comprised of two main types: warm and saline ($33.7 \leq S \leq 34.55$) West Greenland Intermediate Waters (WGIW) entering via the eastern channel of Davis Strait and cold and relatively fresh ($S < 33.7$) waters originating largely from the Arctic Ocean. The seawater component of Arctic Ocean waters entering the CAA channels of Baffin Bay have a predominately Pacific origin but Atlantic-derived waters are also present in proportions that tend to increase with depth and to the north (Munchow et al., 2007; Falkner et al., 2010). The surface 100-200 meters are additionally imprinted by sea-ice melt and formation processes, river runoff, direct precipitation, and glacial

melt. These influences can both be inherited from upstream as well as come about locally.

The large scale circulation in Baffin Bay is generally cyclonic (Fig. 4.1; Tang et al., 2004). As the West Greenland Current enters eastern Davis Strait, a large portion re-circulates back through western Davis Strait while the remainder continues north along the Greenland shelf and slope. As it turns westward, it is joined by throughflows from the CAA passages and becomes the southward flowing Baffin Island Current.

Although net flow is from the Arctic Ocean through the CAA, flow in the passages in not unidirectional (Coote and Jones, 1982). A variable fraction of the West Greenland Current continues northward through eastern Smith Sound (Munchow et al., 2007) but it is likely that the majority of this re-circulates in Kane Basin and returns southward. Likewise, Baffin Bay waters tend to flow into the northern sides of Jones and Lancaster Sounds and what exits on the southern sides is through flow mixed with Baffin Bay water (Fissel et al., 1988).

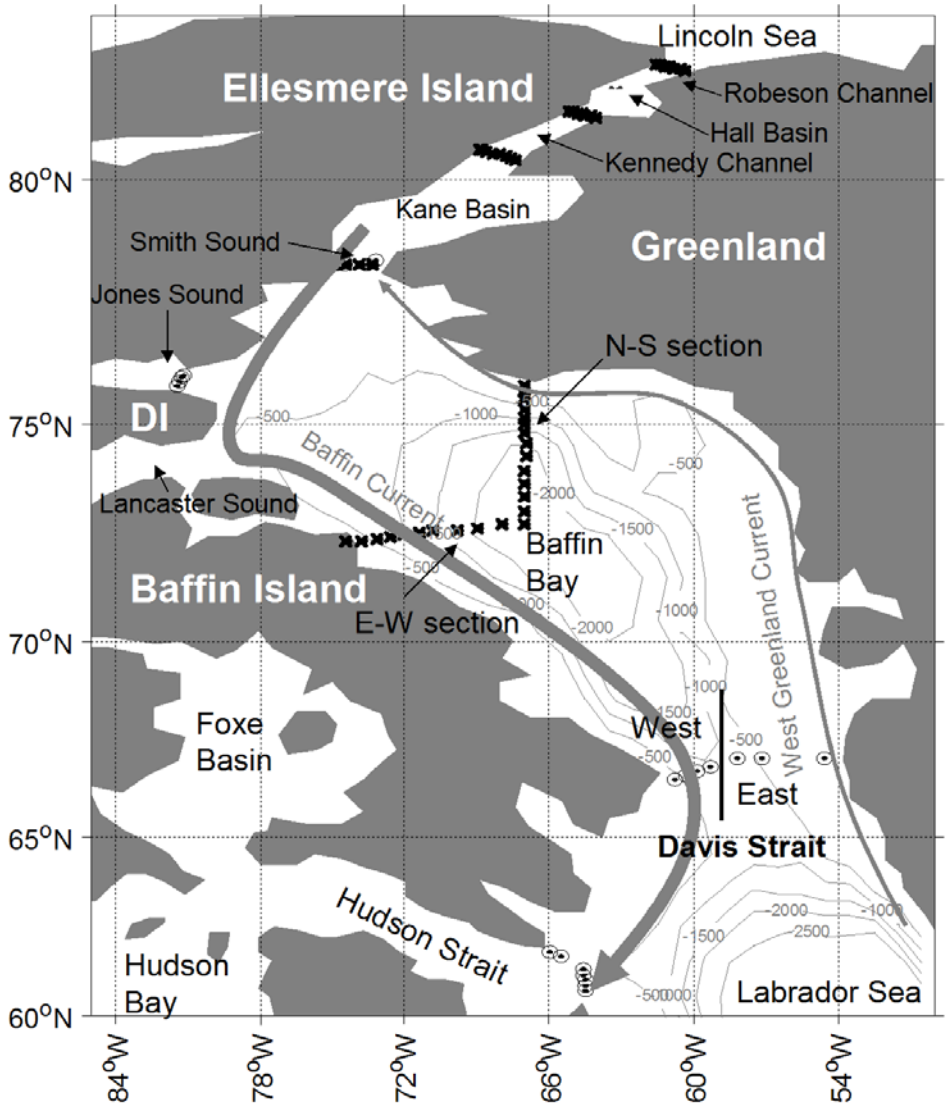

Figure 4.1. Map of study area. Stations occupied during 1997 and 2003 are plotted as circless and x's, respectively. Note the acronym DI stands for Devon Island. Nares Strait consists (from north to south) the Robeson Channel (separating Lincoln Sea and Hall Basin), Kennedy Channel (separating Hall Basin and Kane Basin), and Smith Sound (separating Kane Basin and Baffin Bay). Isobaths range from 500 to 2500 meters (500 meter intervals).

4.3.2 Review of approaches for quantifying water types in high latitude waters

In this paper, we emphasize oxygen isotopes of water, the measurement of which is expressed in delta notation relative to a standard (Vienna Mean Standard Ocean Water):

$$\delta^{18}O = \{(R_{sample} - R_{VSMOW}) / R_{VSMOW}\} \times 1000$$

where $R = {}^{18}O/{}^{16}O$. Both equilibrium thermodynamic and kinetic effects favor the accumulation of lighter isotopes of water in the vapor phase and heavier isotopes in the liquid phase (Craig and Gordon, 1961). Repeated evaporation and precipitation cycles result in northern latitude meteoric waters being depleted in ^{18}O (-15 to -22‰; Cooper et al., 2008) relative to seawater (-1 to +0.5‰; Yamamoto-Kawaii et al., 2008). Simple mixing of a meteoric water source with seawater should produce an approximately linear relationship between salinity and $\delta^{18}O$ (Paren and Potter, 1984). Several investigators (e.g., Redfield and Friedman, 1969; Tan and Strain, 1980; Ostlund and Hut, 1984; Kipphut, 1990; Tan and Strain, 1996; Cooper et al., 1997) have extrapolated linear fits of their $\delta^{18}O$ versus salinity observations to zero salinity intercepts in order to infer high latitude freshwater sources (e.g., glacial meltwater, sea-ice melt, and/or meteoric water contributions).

The situation becomes more complicated when more than one freshwater source and/or sea-ice formation contributes to the salinity-$\delta^{18}O$ relationship. When sea-ice forms, heavier isotopes are preferentially incorporated into the solid phase to a small extent (fractionation factor of +1.9-2.3‰; Macdonald et al., 1995). At the same time, salt is excluded from the ice. The bulk of the salt is excluded during the initial formation of sea ice and the residual trapped brine tends to migrate into channels that drain as the ice ages (Weeks and Ackley, 1986). The initial salinity of newly-formed sea ice can be as large as 10 or 20; however, after one year, the salinity typically decreases to 4-6 and multi-year ice can have even lower salinities (Weeks and Ackley, 1986).

To account for meteoric water and ice formation or melting influences, numerous investigators have applied conservation equations for salinity, $\delta^{18}O$, and mass (or volume) assuming known endmember characteristics (e.g., meteoric water or MW, sea-ice melt or SIM, and seawater or SW):

$$S_{SIM} \times f_{SIM} + S_{MW} \times f_{MW} + S_{SW} \times f_{SW} = S_{observed}$$

$$\delta^{18}O_{SIM} \times f_{SIM} + \delta^{18}O_{MW} \times f_{MW} + \delta^{18}O_{SW} \times f_{SW} = \delta^{18}O_{observed}$$

$$f_{SIM} + f_{MW} + f_{SW} = 1$$

where f is the mass (or volume) fraction contributed by a given component. Note that sea-ice formation will generate a negative melt signal.

In a conceptually idealized case, sea ice formed during winter circulates with the water containing its rejected brine. When it eventually melts, wind over the open water brings about mixing with the brine and the system becomes reset to a zero ice formation tracer signal. While this has been a reasonable approximation for describing the interior Arctic Ocean, differential transport of water and ice, particularly at the perimeter of the domain, can lead to substantial net segregation and so the tracer signal may not be reset. We shall return to this point again later.

Independent tracers have been used to quantify additional components. Atlantic and Pacific contributions to seawater have been addressed using silicic acid (Bauch et al., 1995), phosphate (Ekwurzel et al., 2001), and dissolved inorganic nitrogen to phosphate relationships (Jones et al., 1998; Jones et al., 2003; Taylor et al., 2003; Alkire et al., 2007; Yamamoto-Kawai et al., 2008). River water has also been further apportioned into North American versus Eurasian sources using barium (Guay and Falkner, 1997; Taylor et al., 2003; Guay et al., 2009) and total alkalinity (Anderson et al., 2004; Yamamoto-Kawai et al., 2005).

4.3.3 Previous Baffin Bay Water Component Studies

Tan and Strain (1980) published the first attempt to interpret $\delta^{18}O$ in our study region. They presumed that waters just below the surface were primarily affected by mixing of salty seawater with a meteoric source and so regressed $\delta^{18}O$-salinity data that visually appeared to be linear over varying sub-surface depths, ranging from 5-

150 meters, which they referred to as a “deepwater regression line”. Differences between measured isotope values and those estimated from the regression line were interpreted to indicate the seasonal sea ice melt contributions local to Baffin Bay. They found high concentrations of sea-ice meltwater, with maxima up to ~18%, within the top ~50 meters of Baffin Bay and western Davis Strait. Comparisons with the contributions of meteoric water (estimated as the difference between the total freshwater and that contributed by sea-ice meltwater, relative to the maximum salinity measured at each station) were interpreted to suggest that more than 25% of samples with detectable sea-ice meltwater contained more meltwater than meteoric water.

Strain and Tan (1993) later revised their approach in order to address a few unsatisfactory issues. They acknowledged that selection of data to regress for a reference line was highly subjective. The slopes of their reference (“deepwater”) lines varied considerably from profile to profile and extrapolations to zero salinity yielded apparent $\delta^{18}O$ endmembers that were either more enriched or depleted than the dominant meteoric input to the region. To better understand the nature of these issues, they carried out a box modeling study in which they demonstrated that partitioning of meltwater and brine could alter $\delta^{18}O$ and salinity profile shapes throughout the melt and freeze seasons and so significantly alter the slope and intercepts of apparent mixing lines. They concluded that their previous treatment could under-estimate meltwater fractions, though they expected errors to be relatively small (Strain and Tan, 1993).

Tan and Strain (1996) next applied their box model to salinity and $\delta^{18}O$ data collected in Foxe Basin and Hudson Bay to try to more faithfully represent the reference mixing line prior to the start of the melt season. However, certain data selection aspects remain subjective and only seasonal sea-ice meltwater and not the inherited contribution was quantified.

In this paper, we first apply conservation equations to our data to determine net contributions of meteoric water and sea ice melt/formation. We reduce uncertainties by estimating Pacific and Atlantic contributions to the sea water end-

member. We then modify the approach of Tan and Strain (1996) to estimate sea ice melt local to Baffin Bay as detailed in the sections 3.5 and 3.6 below.

4.4 Sampling and Analyses

4.4.1 Field Programs

Samples were collected as part of two field missions to the region. The first was comprised of Legs 1-3 of the US-Canadian Joint Ice Ocean Studies (JOIS) conducted on the *CCGS Louis S. St. Laurent* between August 1 and September 2, 1997. The second was the Canadian Archipelago Throughflow Study (CATS) conducted on the USGCS Healy between July 26 and August 11, 2003. Hydrographic station transects were acquired at Hudson and Davis Straits and Smith and Jones Sounds in 1997, and Robeson and Kennedy Channels, Smith Sound and Baffin Bay in 2003 (Fig. 1). The full 1997 and 2003 data are sets are available online via the Institute of Ocean Sciences, Department of Fisheries and Oceans, Canada (http://www.dfo-mpo.gc.ca/libraries-bibliotheques/data-stat-hydro-eng.htm) and the National Snow and Ice Data Center (http://nsidc.org/data/index.html).

4.4.2 Sample collection

Water sample collection and chemical analyses have been described in detail elsewhere (Falkner et al., 2010). Briefly, conductivity-temperature-depth (CTD) casts and seawater samples were collected via deployment of a rosette system from the A-frames of the two ships during their respective cruises. In 1997, an Integrated CTD of Falmouth Scientific Inc. was combined with 23 ten-liter PVC bottles developed by Brooke Ocean Technology. In 2003, a Seabird SBE9*plus* CTD outfitted with an SBE43 dissolved oxygen sensor was deployed in the rosette along with 24 twelve-liter Ocean Test Equipment PVC bottles.

4.4.3 Chemical methods

Bottle salinities were determined at sea after a 12-hour equilibration to a controlled room temperature using a model 8400A Guideline Autosal salinometer. Precision is estimated to be ±0.003 in 1997 and ±0.001 in 2003. In 1997, nutrients were determined at sea via a Technicon Autoanalyser II following published

procedures with modifications (Armstrong et al., 1967; Bernhardt and Wilhelms, 1967). Precision is estimated to be ±1%. In 2003, nutrients were determined with similar precision at sea using a hybrid Alpkem RFA 300 and Technicon AA-II (AutoAnalyzer II) – based system and the JGOFS/WOCE suggested protocols (Gordon et al., 1994). The Si, NO_3^-+NO_2^-, and NO_2^- channels were RFA-based, the phosphate and NH_4^+ channels, AA-II.

Oxygen isotopes were analyzed by the CO_2 equilibration method on the COAS Finnegan Mat 251 mass spectrometer at Oregon State University. Results are reported in del units relative to VSMOW. Precision (1σ) is estimated to be ± 0.03‰.

4.4.4 Assignment of endmember characteristics

Salinity and isotope endmember characteristics (Table 1) were assigned as follows. Sea-ice meltwater characteristics were chosen to represent first-year ice now typically observed over much of the Arctic as well as in the Canadian Archipelago and Baffin Bay (Strain and Tan, 1993; Rigor et al., 2004). Meteoric water $\delta^{18}O$ represents the flow-weighted average of Arctic river runoff (Cooper et al., 2008) as it is expected that the majority of meteoric water enters the study area from the Arctic and that local meteoric waters (precipitation and runoff) have comparable isotopic signatures (Tan and Strain, 1980; Ostlund and Hut, 1984; Tan and Strain, 1996).

Table 4.3 Endmember definitions for water type analyses.

Water Type	**Salinity**	**$\delta^{18}O$**	**Unc.***
Sea-ice melt	6 ± 2	0.05 ± 2	0.03
Pacific seawater	32.5 ± 1	-0.8 ± 0.3	0.14
Atlantic seawater	34.87 ± 0.03	0.24 ± 0.05	0.14
Meteoric Water	0	-18.8 ± 2	0.03

*Maximum uncertainty in water type fractions derived from varying salinity and $d^{18}O$ definitions within limits of variability specified. Note larger uncertainty in Pacific and Atlantic fractions is due to inherent uncertainty in the dissolved inorganic:phosphate ratios defined (Taylor et al., 2003).

Natural variability in the salinity and $\delta^{18}O$ characteristics of meteoric waters and sea-ice meltwater should be taken into account for estimating uncertainties in the calculated fractional contributions of these water types. Maximum absolute ranges of $\leq 3\%$ in the contributions result from propagating the extremes of the range of observed variability. For example, using the values for sea-ice meltwater representative of aged ice (S=4, $\delta^{18}O$ = -2‰) generally yields meteoric water fractions ~1% higher (on average) relative to calculations using our mid-range endmember assignments. Thus, the water type analysis is robust to typical sea-ice melt and meteoric water variability within the limits of uncertainty reported in Table 4.1.

Pacific and Atlantic water assignments, characterized to represent the inflow entering the Arctic Ocean via Bering and Fram Straits, respectively, were adopted from Yamamoto-Kawai et al. (2008). This choice is clearly suitable for Pacific water, which can be traced back to the Bering Strait; however, Atlantic water enters the study region both through the CAA passages and via Davis Strait. We examined salinity and $\delta^{18}O$ data for salinities > 33 and between depths of 150 and 500 meters where the influence from both Pacific water and Baffin Bay Deep and Bottom Waters is negligible. The data show a linear trend and a regression yields a $\delta^{18}O$ value of 0.24 ± 1.86‰ (95% confidence interval) for an Atlantic water salinity (34.87). Thus, we treat Atlantic water as a single endmember within these uncertainties for our purposes (Table 4.1).

4.4.5 Water component analysis

Relationships between dissolved fixed inorganic nitrogen to phosphate (DIN-P) are utilized to distinguish Pacific and Atlantic seawater contributions (Jones et al., 1998; Taylor et al., 2003; Alkire et al., 2007; Yamamoto-Kawai et al., 2008). Respiratory processes occurring on the relatively shallow continental shelves deplete DIN relative to phosphorus in Pacific source waters that enter at Bering Strait (Devol et al., 1997). As they enter the interior Arctic Ocean they are subject to more usual Redfield type photosynthesis and respiration. Atlantic waters are not depleted in

DIN, but are also subject to Redfield type processes. Thus, on a plot of DIN versus phosphorus the Atlantic line lies to the left of the Pacific line. The distance of observed values that fall between the lines can be used to calculate the proportions of Pacific and Atlantic water in a seawater sample. Pacific and Atlantic water endmember DIN-P relationships were adopted from Yamamoto-Kawai et al. (2008). Since river runoff tends to look like Atlantic water in DIN-P space, that component is effectively included in the Atlantic estimate (Jones et al., 1998; Taylor et al., 2003).

Pacific and Atlantic seawater contributions were calculated as described by Alkire et al. (2007). Pacific waters appeared to be limited to the top ~150 meters throughout the study region (Falkner et al., 2010). It is cautioned that significant denitrification occurs at depth in Baffin Bay (Falkner et al., 2010) and probably in the shallow sediments of Foxe Basin and Hudson Bay. The assumptions behind the DIN-P analysis are not applicable to such waters. We therefore limited our analysis to waters above 500 meters depth in Baffin Bay.

Estimated Pacific and Atlantic proportions were used to calculate characteristics of a general seawater endmember for each sample in accordance with Table 4.1. Combining this seawater with meteoric water and sea-ice meltwater endmembers (Table 4.1), equations conserving salinity, oxygen isotopes, and volume (see section 4.3.2) were simultaneously solved to determine fractional contributions of these components to each water sample. Pacific and Atlantic contributions were then refined by multiplying the resultant seawater endmember fraction associated with the seawater endmember by the initial proportions of Pacific and Atlantic waters.

4.4.6 Estimating the local, seasonal sea ice melt component

Through simple linear extrapolations, Tan and Strain (1980) reported "apparent" freshwater (S=0) endmember $\delta^{18}O$ values ranging from -33.1 to -45.1‰ in Baffin Bay. These are very different from what would be expected for a simple linear mixing scheme between average Arctic meteoric water and Atlantic water ($\delta^{18}O$ = 0.546*S – 18.8). Our profile data in the CAA and Baffin Bay during 1997 and 2003

would yield similar extrapolations (Figs. 4.2-4.3). Barring dominance by glacial meltwater, an average meteoric water source with such a highly-depleted isotopic signature is not physically realistic. Estimates of glacial meltwater input from all of Greenland in 2000-2004 range from 160-230 km^3yr^{-1} (Luthcke et al., 2006; Rignot et al., 2008). Such a flux tends to be small compared to the estimated total freshwater flux entering Baffin Bay through CAA passages (3200 km^3yr^{-1}; Serreze et al., 2006). It is noted that the melt from Greenland appears to be on an increasing trend so this assumption doesn't necessarily hold for the future nor in close proximity to the ice sheet. Thus we view it more likely that the highly-negative intercepts are an artifact of mixing seawater with sub-surface water enriched by brine during sea ice formation, which is in agreement with the conclusions of Strain and Tan (1993). Where do such waters acquire their brine signatures?

Although we cannot completely discount contributions by ice formation local to Baffin Bay, examination of regional data suggests that brine enriched waters are delivered from the Arctic Ocean. Bauch et al. (2009) reported brine-enriched bottom water on the southern Laptev shelf, presumably produced via net ice formation in the persistent polynya that occurs there. Entrainment of this shelf bottom water into the Arctic Ocean halocline was observed at the Laptev shelf break where it mixes with Atlantic water. Mixing also occurred at shallower depths with lower-salinity shelf waters, influenced by Lena River input, generating a separate trend in salinity-$\delta^{18}O$ space.

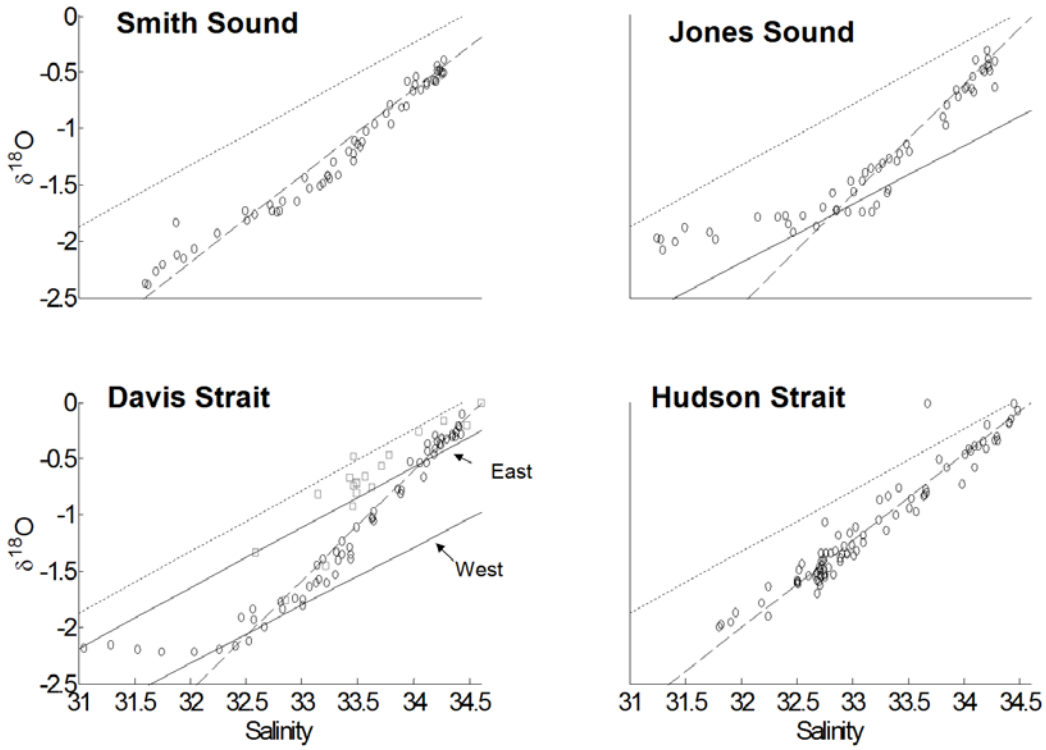

Figure 4.2. Salinity vs. $\delta^{18}O$ plots for sections occupied during summer 1997. Included in each plot are data from the upper 500 meters (circles), the 150-500 meter pooled regression line (dashed line), the typical meteoric water-Atlantic water mixing line specified for the Arctic interior (dotted line), and an additional mixing line (solid line) connecting meteoric water and a brine-enriched halocline water endmember (see secion 3.6 for details). Note no brine-enriched halocline water was estimated in Smith Sound and Hudson Strait sections. The Davis Strait section was further separated into west (black circles) and east (gray squares) regions in accordance with their very different hydrographic regimes.

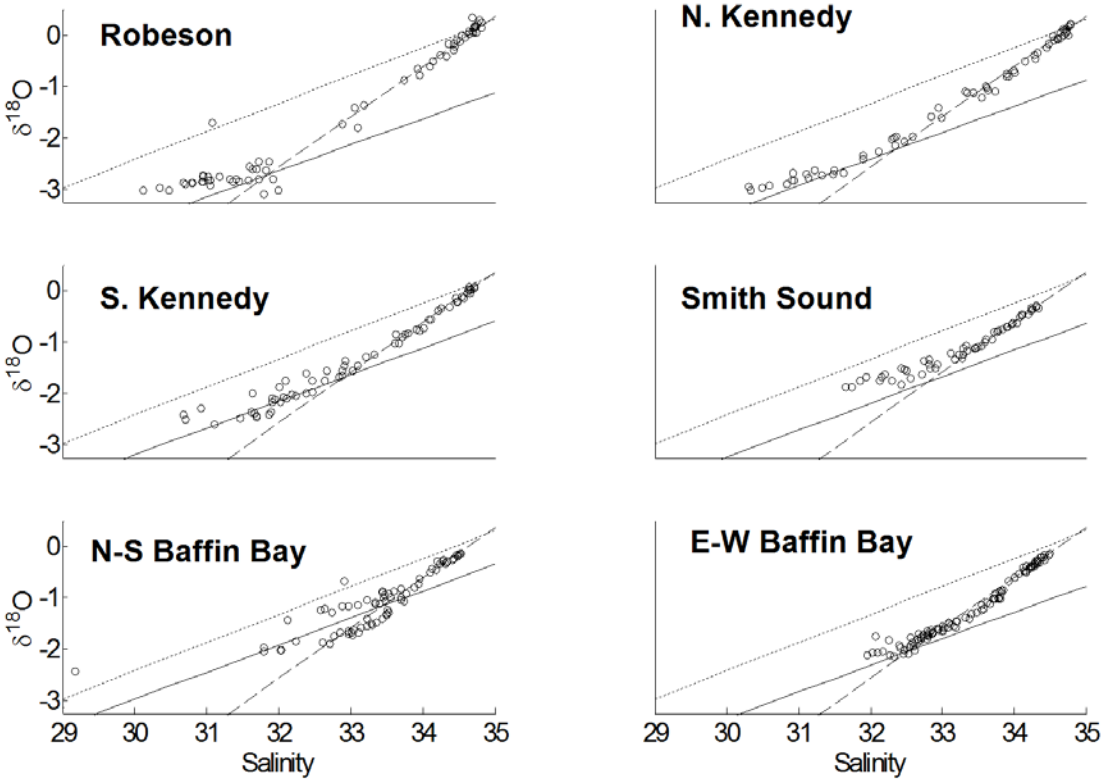

Figure 4.3. Same as for Figure 4.2 but for sections occupied during summer 2003.

Examination of archived data for the Arctic Ocean from 1958-2001 (Seawater Oxygen-18 Database, Schmidt et al., 1999) reveals that very rarely do salinity-$\delta^{18}O$ slopes and intercepts adhere to a strictly meteoric-Atlantic water mixing trend. This holds true not only on the Arctic shelves, but in portions of the deep basins as well. In Figure 4.5, salinity-$\delta^{18}O$ relationships are shown for the marginal seas and deep basins of the Arctic Ocean. Data from the Barents Sea mostly plot above the meteoric-Atlantic water mixing line as result of freshening by sea-ice melt (Fig. 4.5a). Meteoric water influence is more pronounced in the Kara (Fig. 4.5b), Laptev (Fig. 4.5c), East Siberian (Fig. 4.5d), and Chukchi (Fig. 4.5g) Seas where much of the data conform to a meteoric-Atlantic water mixing trend. However, even here where river water would be expected to be prominent, clear departures from the trend signal a significant brine influence between salinities 31-33.5. The Beaufort Sea (Fig. 4.5h)

and Eurasian (Fig. 4.5e) and Canadian (Fig. 4.5f) Basins all show significant brine influence throughout the salinity range 30-34.2, that does not appear to be rectified by seasonal mixing processes and closely resemble observations in the CAA and Baffin Bay (Figs. 4.2-4.3, 4.5i).

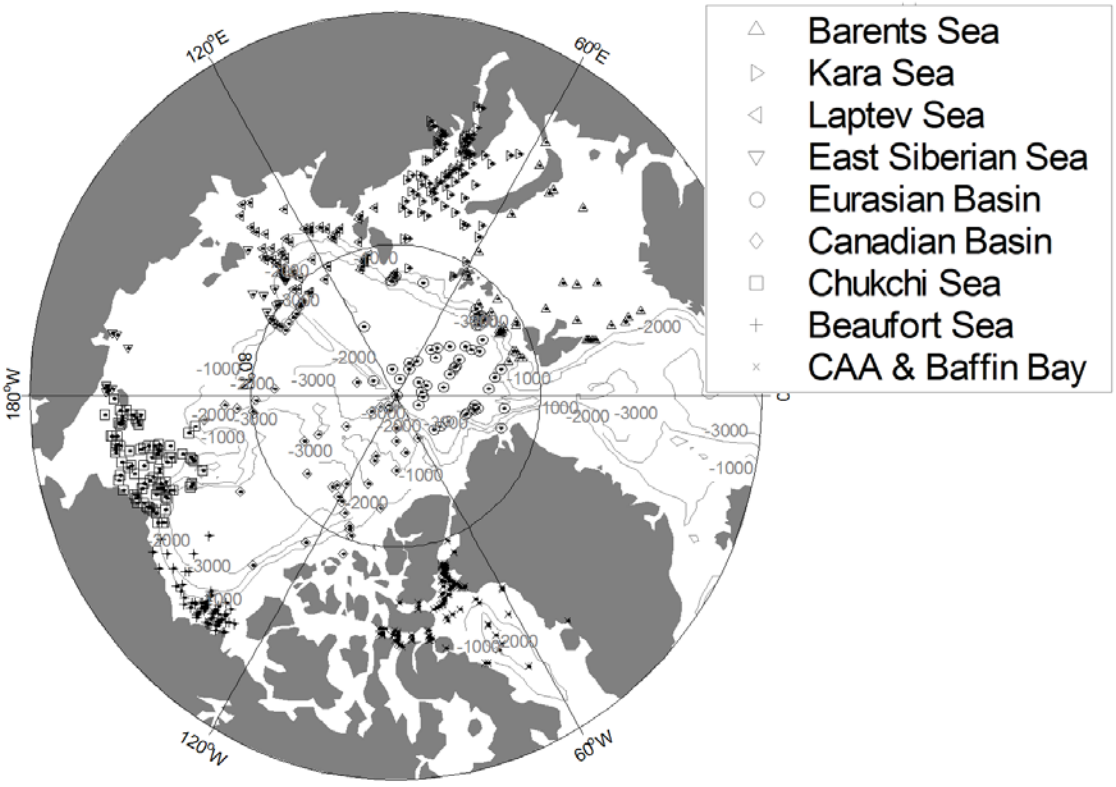

Figure 4.4. Map of Oxygen-18 Database stations occupied between 1957 and 2001 (Schmidt et al., 1999). Stations were grouped into geographic regions (Barents Sea, Kara Sea, Laptev Sea, East Siberian Sea, Chukchi Sea, Beaufort Sea, Canadian Basin, Eurasian Basin, and the Canadian Arctic Archipelago and Baffin Bay) for separate regression analyses. Also included in each diagram is the typical meteoric-Atlantic water mixing line, departures from which are typically used to identify the presence of sea-ice meltwater or brine. Isobaths range from 1000 to 300 meters (1000 meter intervals).

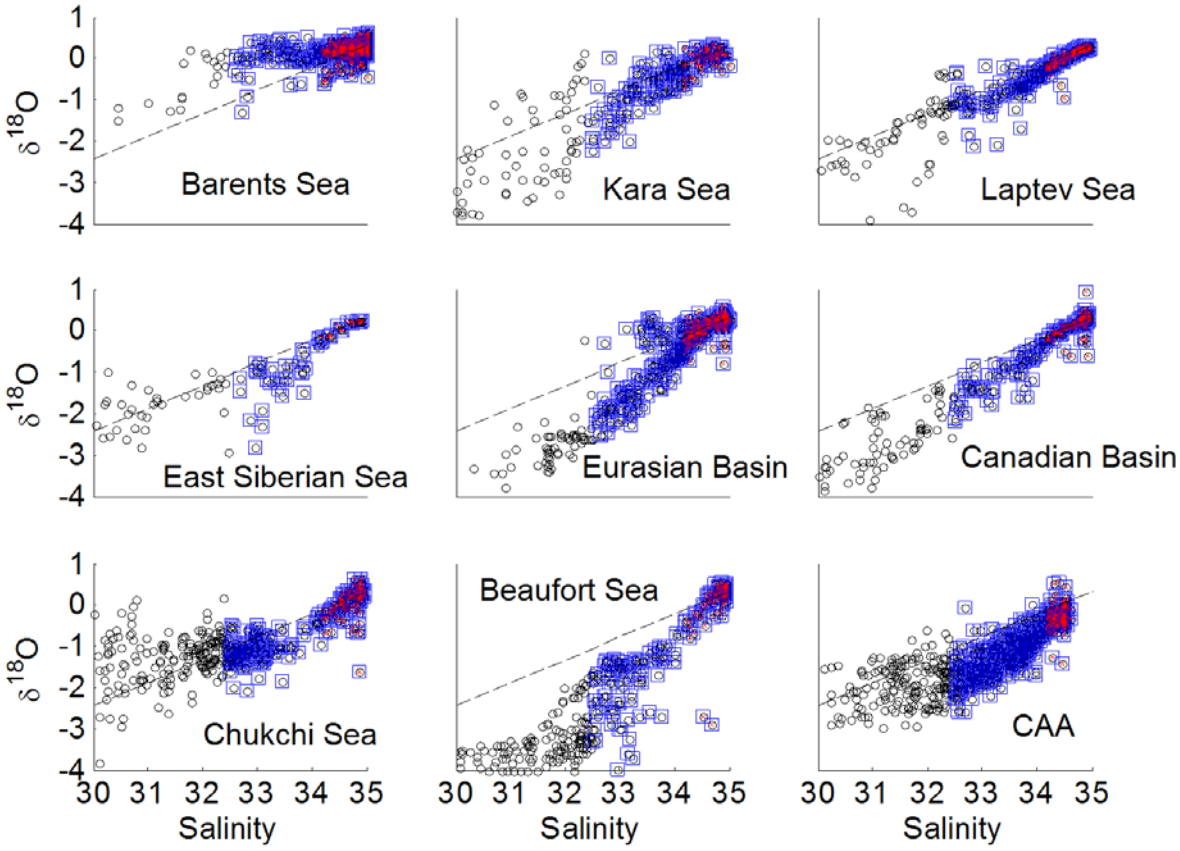

Figure 4.5. Plots of salinity versus $\delta^{18}O$ for separate regions from the Oxygen-18 Database (Schmidt et al., 1999). Data are color-coded according to salinity range: black circles (salinity > 30), blue squares (salinity > 32.5), and red diamonds (salinity > 34.2). The dotted lines plotted in each frame represent the average Arctic meteoric water mixing line.

This net ice formation signal observed is apparently advected from the Arctic Ocean through the CAA and Nares Strait. We suspect that Canadian Basin waters supply Lancaster and Jones Sounds while both the Canadian and Eurasian Basins supply Nares Strait and Smith Sound. It has been previously suggested the upper ~100 meters of Robeson Channel resemble waters from either the Eurasian (Muench, 1971) or Canadian (Melling et al., 1984) Basins while waters below 200 meters have characteristics similar to the Canadian Basin (Muench, 1971). Our unpublished

August 2003 hydrographic tracer data set shows a blend of Canadian and Eurasian Basin waters flowing through Robeson Channel. Thus, the brine that accompanies flow through Nares Strait may originate widely along Arctic shelves via sea-ice formation processes that are not rectified by seasonal melting and mixing.

Figure 4.6 illustrates and identifies trends in salinity-$\delta^{18}O$ following the work of Bauch et al. (2009). One mixing line directly connects Atlantic water to an average Arctic meteoric water source and another connects brine-enriched halocline water directly to Atlantic water. The halocline water endmembers for the Smith Sound and Robeson Channel sections (2003) have salinities of 32.81 and 31.85, respectively. The salinity and $\delta^{18}O$ values of the halocline water are expected to range somewhat depending on the intensity of ice formation and depth of the shelf of origin as pointed out by Bauch et al. (2009). The observations tend to fall in a broad envelope over the lower salinity (< 33) range that reflect variable mixing of brine enriched halocline water with typical meteoric water or with surface waters affected by additional sea-ice melt/formation or both.

To quantify sea-ice formation/melt influence local to Baffin Bay, we treat Baffin Bay as a two-layer system, with an upper layer having the possible influences just described and an underlying layer that is a mix between Atlantic-origin and shelf, brine-enriched waters. We take linear regressions of data between 150 and 500 meters for each section (Table 4.2) as our Atlantic-halocline water mixing reference. Little, if any, influence from local sea-ice meltwater is expected to penetrate to these depths (Muench, 1971; Tan and Strain, 1980; Wallace, 1985). As a check on our conceptual model, we find that extrapolation of such regression lines for our stations to Atlantic water salinity (34.87) yields isotope values consistent with our assigned endmember value (Table 4.1).

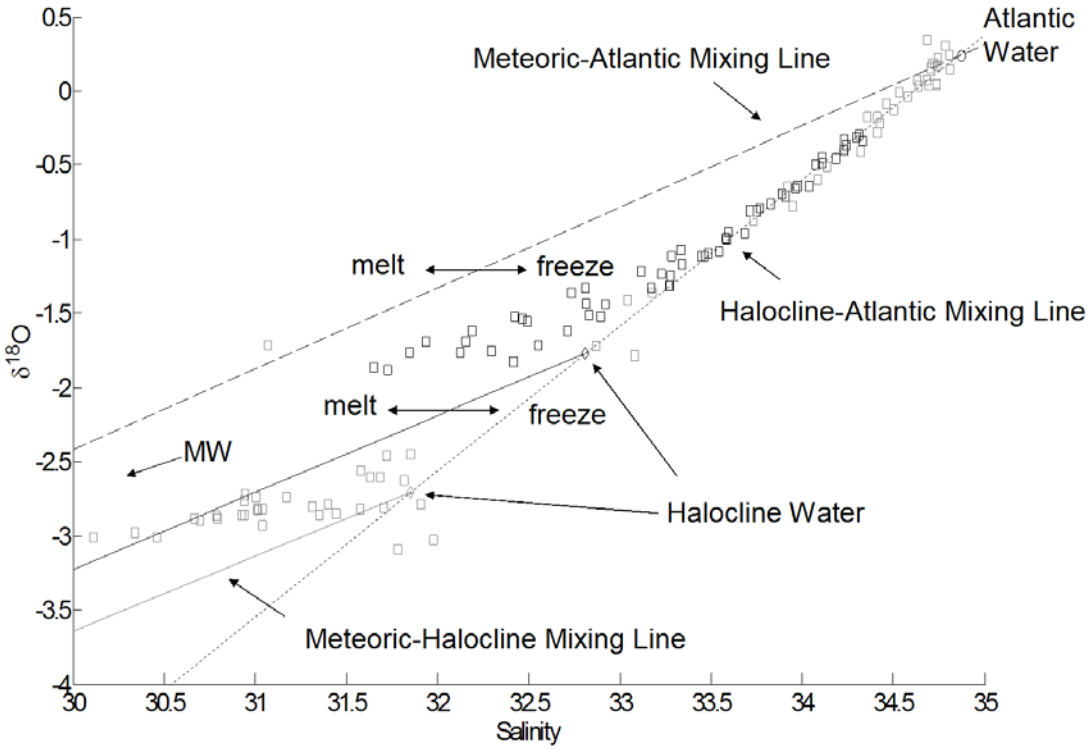

Figure 4.6. Schematic of mixing in a two-layer system with brine-enriched halocline waters advected from the Arctic interior represented as a separate water type. Mixing between meteoric waters and this Arctic halocline water is represented by the solid line. Samples containing local sea-ice melt or brine in the Canadian Archipelago and Baffin Bay will plot above or below this line, respectively. Deeper waters having no local sea-ice melt influence can be described relative to Arctic inflow, as mixing between a seawater (i.e., Atlantic water) endmember and either meteoric water (dashed line) or halocline water (dotted line). Included in the diagram are data from Smith Sound (black squares) and Robeson Channel (gray squares), occupied in 2003. Note, the higher salinities plot along a common Atlantic-halocline water mixing line, but diverge along separate meteoric-halocline water mixing lines at different salinities.

Regression parameters calculated for each section were generally very similar to one another (within the range 0.9-1.0), with the exception of stations in E-W Baffin Bay (2003), northern Kennedy Channel (2003), Smith Sound (1997), and Hudson Strait (1997). Further restricting the data to $S \geq 34$ for the E-W Baffin Bay and northern Kennedy Channel regressions however, returned parameters coherent with

most other sections. This was not the case for Smith Sound (1997) or Hudson Bay (1997), so we treated them separately. We otherwise pooled together data from all other sections to obtain a common $\delta^{18}O$-S relationship for 150-500 meters over the entire study area ($\delta^{18}O = 0.98 \pm 0.03 * S - 34.0 \pm 1.0$). The similarity among regression parameters derived from most sections suggests deeper waters inherited from the Arctic are little altered along their southward flow pathway and thus can be combined. In further support of this assumption, the pooled regression parameters resemble those calculated from the Canadian ($\delta^{18}O = 0.83 \pm 0.03 * S - 28.7 \pm 1.0$) and Eurasian ($\delta^{18}O = 0.89 \pm 0.03 * S - 30.9 \pm 1.1$) Basins in the Arctic Ocean over a salinity range (32.5-35) expected to include the largest influence from brine. We note, however, results for local sea-ice meltwater fractions are comparable (±1%) when utilizing parameters derived separately for each section.

Having estimated the mixing line between Atlantic water and the brine-enriched halocline water, we now must determine the mixing lines between the halocline water and average meteoric water for each section. This requires the assignment of endmember characteristics for the halocline water, which lies somewhere along the halocline-Atlantic water mixing line (Fig. 4.6). According to our model, positive deviations away from the halocline-Atlantic water mixing line indicates a transition into shallower waters where direct mixing with either sea-ice melt or average meteoric water occurs.

Table 4.2. Coefficients from simple linear regression of salinity and Δ data for sections occupied in 1997 and 2003. Data included in the regression were collected between 150 and 500 meters depth to ensure minimal influence from local sea-ice meltwater.

Section	Slope	Lower Slope (95% CI)	Upper Slope (95% CI)	Int.	Lower Int. (95% CI)	Upper Int. (95% CI)	R	n	$\delta^{18}O_{AW}$
2003									
Robeson Channel	0.97	0.63	1.31	-33.5	-45.3	-21.8	0.8181	20	0.28
N. Kennedy Channel	1.07	0.92	1.21	-36.9	-41.7	-32.0	0.9704	18	0.26
N. Kennedy Channel (S ≥ 34)	1.01	0.75	1.27	-35.0	-43.9	-26.1	0.9075	17	0.24
S. Kennedy Channel	0.95	0.85	1.05	-33.0	-36.5	-29.5	0.9832	16	0.22
Smith Sound	0.93	0.84	1.01	-32.0	-35.0	-29.1	0.9837	19	0.22
N-S Baffin Bay	0.99	0.87	1.10	-34.1	-38.0	-30.3	0.9717	22	0.24
E-W Baffin Bay	1.14	1.09	1.19	-39.2	-40.9	-37.6	0.9900	45	0.34
E-W Baffin Bay (S ≥ 34)	0.90	0.79	1.00	-31.0	-34.8	-27.3	0.9537	30	0.20
1997									
Smith Sound	0.77	0.66	0.88	-26.8	-30.6	-23.0	0.9446	26	0.02
Jones Sound	0.94	0.82	1.06	-32.6	-36.7	-28.6	0.9595	25	0.18
Hudson Strait	0.77	0.70	0.84	-26.6	-29.0	-24.3	0.9627	42	0.21
Davis Strait	1.00	0.93	1.07	-34.4	-36.8	-32.1	0.9809	35	0.27
Pooled*	0.98	0.95	1.00	-34.0	-34.9	-33.0	0.9830	179	0.25

*Pooled data excludes sections from Smith Sound 1997 and Hudson Strait

Table 4.3. Salinity and $\delta^{18}O$ values representing the halocline water endmember estimated at each section (see section 3.6 for details). Note no brine-enriched halocline water was estimated in Smith Sound and Hudson Strait sections. Data from Davis Strait was split into east and west sections in accordance with their very different hydrographic regimes (warm and saline Atlantic water versus relatively cold and fresh Arctic outflow) above ~150 meters.

Section	Salinity	$\delta^{18}O$
1997		
Smith Sound	-	-
Jones Sound	32.83	-1.76
Hudson Strait	-	-
Davis Strait (east)	34.05	-0.55
Davis Strait (west)	32.56	-2.03
2003		
Robeson Channel	31.85	-2.71
N. Kennedy Channel	32.35	-2.23
S. Kennedy Channel	32.92	-1.67
Smith Sound	32.81	-1.77
N-S Baffin Bay	33.44	-1.16
E-W Baffin Bay	32.55	-2.03

In order to estimate the point at which this transition occurs (i.e., the halocline water endmember; Table 4.3), we take the highest salinity sample for which deviations away from the halocline-Atlantic water mixing line are "significantly" positive. Deviations were calculated for each section by subtracting observed $\delta^{18}O$ values from those that would plot along the halocline-Atlantic mixing line at the associated salinity. Deviations were considered to be significant if they exceeded a threshold value = 0.3‰. The threshold value was chosen such that it could be applied to each section and result in at least one sample at each station showing influence from sea-ice melt. Decreasing the threshold value from 0.3 to 0.2‰ did not alter the estimated halocline water endmembers in most sections; however, in northern Kennedy Channel and Smith Sound 2003, salinity and $\delta^{18}O$ assignments

decreased by ~ 1 unit. This resulted in a maximum decrease in local sea-ice meltwater fractions of ≤ 3%.

In order to determine local sea-ice melt contributions to water above the brine-enriched layer, a reference line for each section was derived by connecting the assigned halocline water properties to those of the meteoric water endmember (-18.8‰). We note no brine-enriched halocline water was estimated in Smith Sound and Hudson Strait 1997 sections. In contrast to all other sections, salinity-$\delta^{18}O$ data generally fell along the linear mixing line between Atlantic water and halocline water. These sections apparently had very little local sea-ice meltwater influence, fractions of which were calculated using the Atlantic-halocline mixing line as the reference line.

Local, seasonal sea-ice melt fractions for each section were calculated relative to the defined reference line using the formulation of Tan and Strain (1980):

$$f_{SIM,\ seasonal} = \{\delta_{obs} - (AS_{obs} + B)\} / \{\delta_{SIM} - (AS_{SIM} + B)\}$$

where $f_{SIM,\ seasonal}$ = local, seasonal sea-ice melt fraction; δ_{obs} and S_{obs} are the observed $\delta^{18}O$ and salinity; A and B are the slope and intercept of the reference line; and S_{SIM} and δ_{SIM} are the assigned sea-ice melt endmember values (Table 4.1). With the exception of Smith Sound and Hudson Strait 1997 sections, local, seasonal sea-ice melt fractions are calculated only for samples with salinities ≤ the estimated halocline water salinity at each section. Samples with larger salinities plot on or close to the halocline-Atlantic water line and are therefore presumed part of the deeper, inherited regime unaffected by surface processes.

4.5 Water Type Distributions

We now describe and compare sea-ice melt and meteoric water distributions derived from the water component analysis of the outflow from the Arctic Ocean and sea-ice meltwater local to the study region for each section occupied during 1997 and 2003 cruises. For simplicity we will refer to the sea-ice melt fractions as having either an Arctic or local origin. Distributions of Pacific water have been described in detail elsewhere (Munchow et al., 2007; Falkner et. al., 2010) and therefore will only

be briefly described here. We note the re-occupation of Smith Sound in 2003 allows comparison with conditions in 1997. Otherwise, data were obtained in different geographical locales in the two time frames.

4.5.1 Smith Sound 1997

Pacific fractions were both high (> 70%) and widespread across the entire section over the top ~100 meters depth (Fig. 4.7). Meteoric water fractions ranged between 4 and 10% in the upper 150-200 meters with highest contributions in the topmost ~50 meters of the eastern stations. Sea-ice melt fractions derived from the water component analysis exhibited highly-negative fractions (≤ -6%; hereafter referred to as Arctic sea-ice melt) extending over the entire section in the top ~100 meters. However, local sea-ice melt contributions were small and positive (1-3%), but limited to depths ≤ 20 meters. In fact, the westernmost station had no significant local sea-ice melt contribution. Recall that, below the depth of local sea-ice melt influence, fractions of sea-ice melt are taken directly from the water component analysis and differences between the Arctic and local distributions are limited to salinities ≤ estimated for the halocline water endmember.

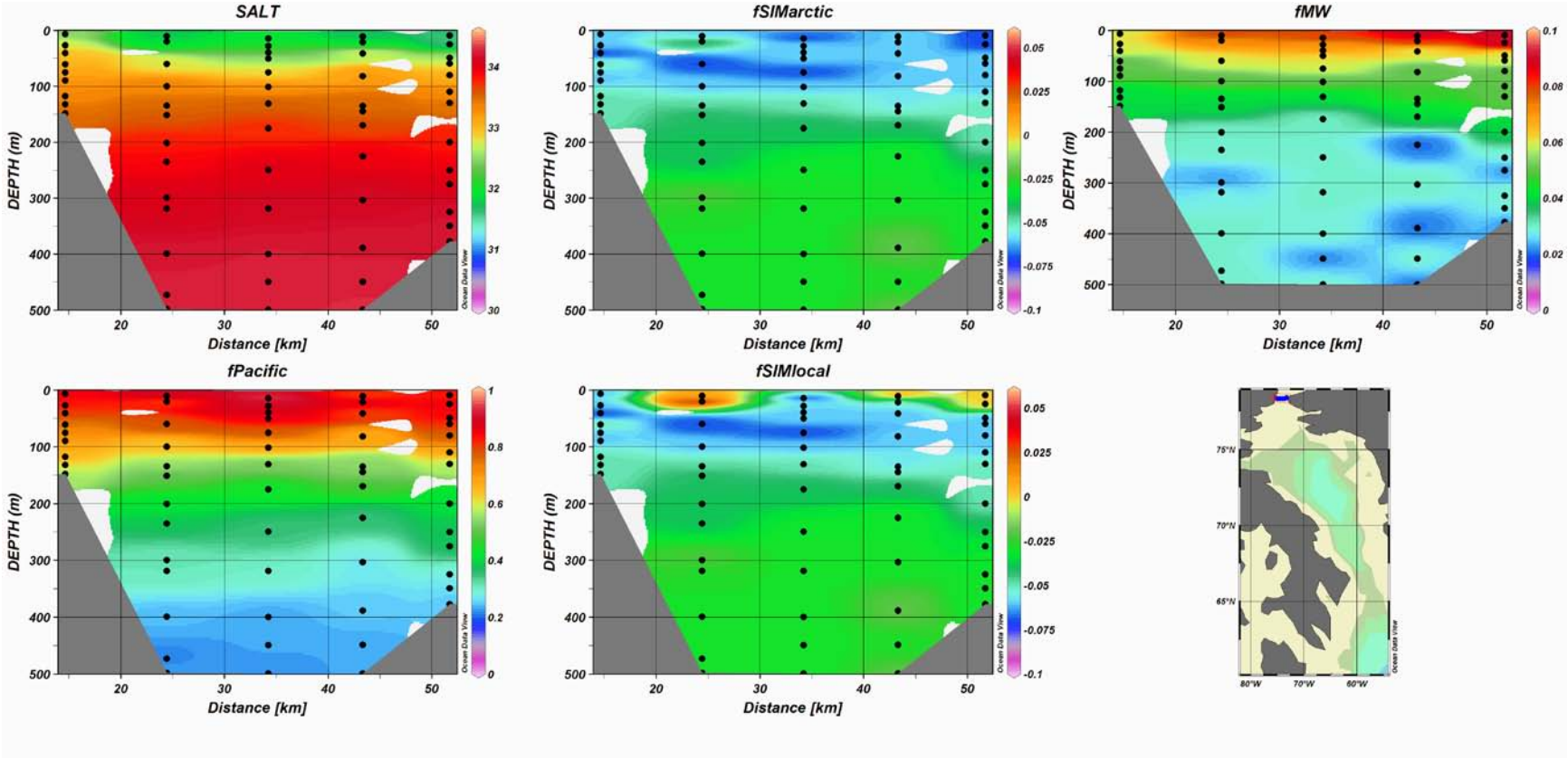

Figure 4.7. Smith Sound 1997. Color contours for upper 500 meters of salinity (top left) and water type fractions: sea-ice meltwater (top middle), meteoric water (top right), and Pacific water (bottom left) calculated using the component water type analysis relative to the Arctic inflow through the Canadian Archipelago and Baffin Bay and local sea-ice meltwater (bottom middle). In each plot, sections extend from west/left to east/right (Smith Sound and Davis Strait) or north/left to south/right (Jones Sound and Hudson Strait). Contours were drawn using the VG gridding algorithm in *Ocean Data View* with x and y scale lengths set to 100 and 35 per mille, respectively (Schlitzer, 2001).

4.5.2 Jones Sound 1997

Relatively high Pacific water fractions (> 70%) were observed at or near the surface on both sides of the section (Fig. 4.8). On the northern end where waters typically flow into the sound, highest fractions occurred in the sub-surface at 50-75 meters. We note coincidence of this core of relatively high Pacific water fractions with highly-negative sea-ice melt fractions indicating significant brine influence. These characteristics likely derive from Arctic-origin that transit Nares Strait and enter northern Jones Sound via a branch of the Baffin Current. The highest fractions of Pacific water occurred in the upper 50 meters at the southern end of the sound where waters typically flow into Baffin Bay. Meteoric water fractions were highest in the top 20-50 meters on the northern/inflow end with slightly smaller fractions (> 6%) occurring over the remaining section. Local sea-ice melt was prevalent over most of the section except at the northernmost stations where fractions were negative (-3%) and meteoric water influence was highest. Positive sea-ice melt fractions were restricted to the upper 20-25 meters over the section except at the southernmost station where the penetration depth was > 40 meters.

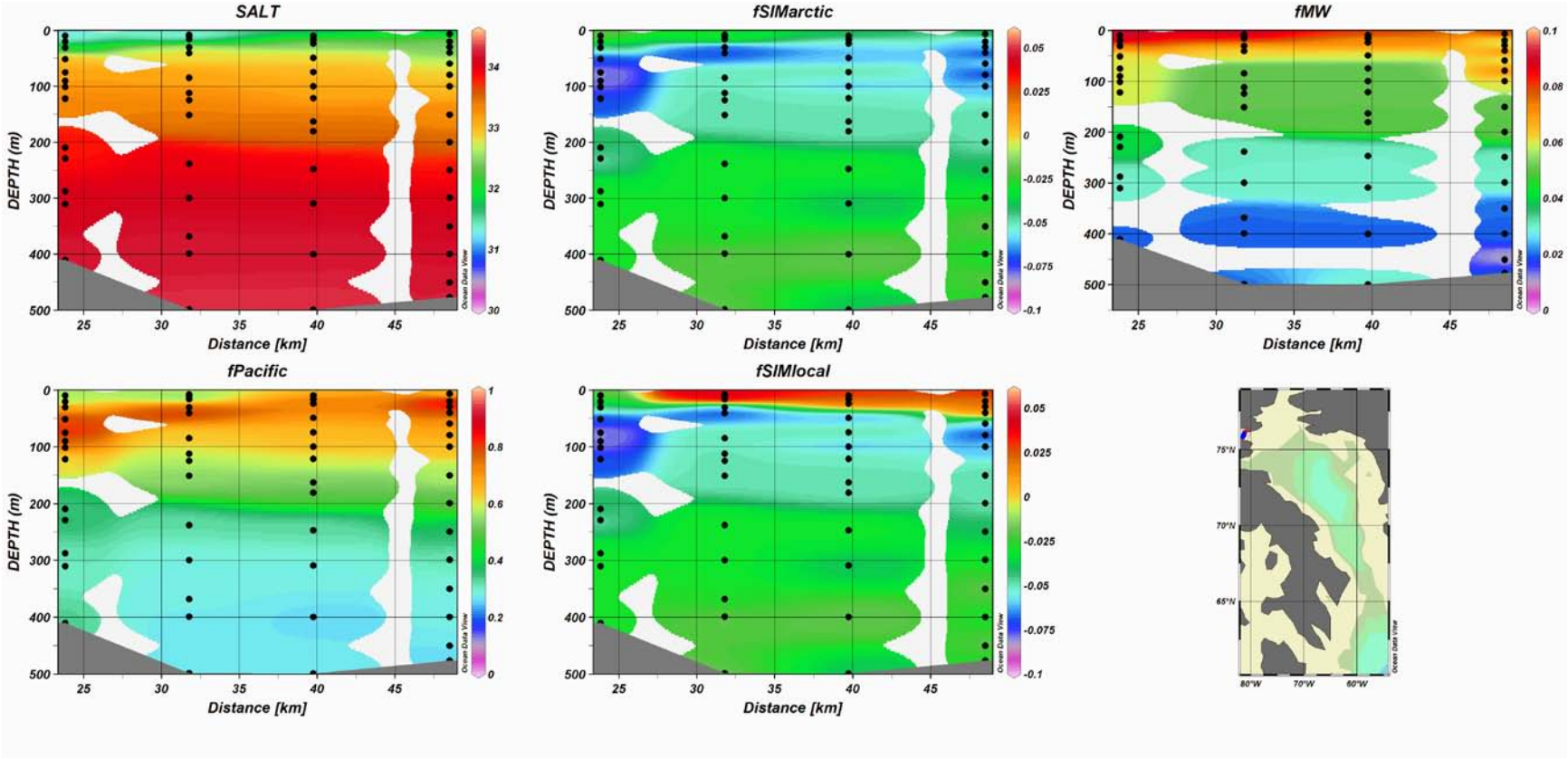

Figure 4.8. Same as for Figure 4.7 but for Jones Sound 1997.

4.5.3 Davis Strait 1997

Consistent with the understanding of circulation in Baffin Bay, Pacific water contribution in Davis Strait is concentrated on the western side in the top ~200 meters (Fig. 4.9). Warmer and more saline waters of Atlantic-origin comprise both deeper waters and shallow waters on the eastern side. These contrasting hydrographic regimes in the upper water column prompted a split of stations into western and eastern regions (see Fig. 4.1) for purposes of calculating local sea-ice melt fractions (see section 4.4.6). Failure to split the stations resulted in negative sea-ice melt fractions in the western half of the strait, amounting to under-estimations of up to 4%.

The highest meteoric water fractions accompany the most negative Arctic sea-ice melt fractions and largest Pacific water contributions in the western half of the strait. While significant ($\geq$ 4%) meteoric water influence occurred across the entire strait, highest fractions ($\geq$ 7%) were prevalent in the western half, coincident with the largest influence from Pacific water. Local sea-ice melt exerts a significant influence ($\geq$ 2%) in the top 20-25 meters in the western half of the strait and penetrates to depths > 150 meters in the eastern half.

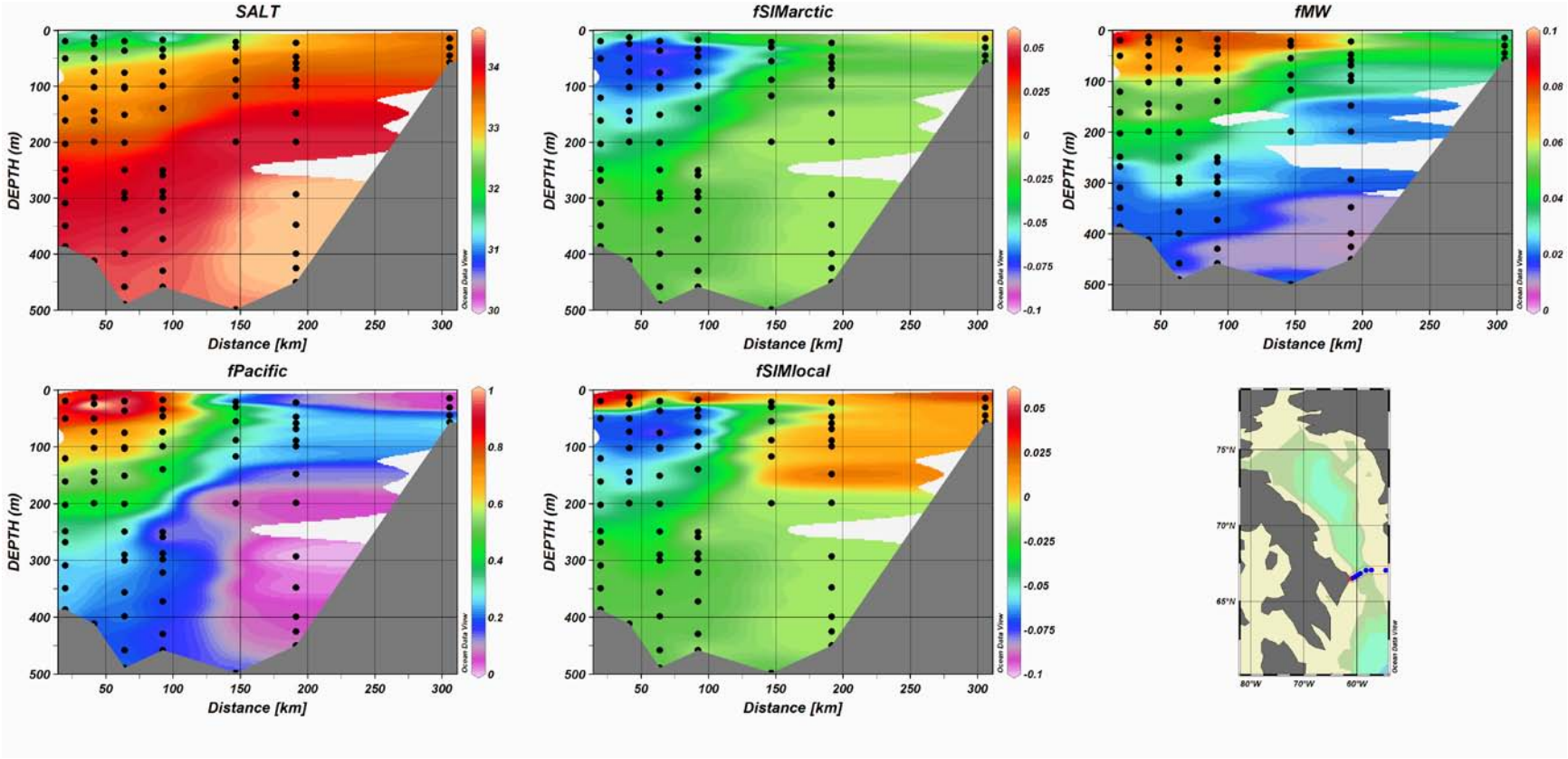

Figure 4.9. Same as for Figure 4.7 but for Davis Strait 1997.

4.5.4 Hudson Strait 1997

Potential denitrification occurring in the sediments of Hudson Bay renders interpretations of Pacific fractions flowing out of Hudson Strait questionable. The sub-surface Pacific water maximum present on the northern/inflow end of the strait is likely a real feature (Fig. 4.10). Relatively low (< 50%) Pacific fractions were present in the upper water column across the strait and very low fractions (< 25%) occurred below 150-200 meters in the center of the strait. The low Pacific values observed suggest that the water tidally-pumped through Hudson Strait are dominantly of Atlantic origin and are not significantly overprinted by respiratory processes.

A core of relatively high (≥ 8%) meteoric water was observed within the upper ~100 meters on the southern/outflow end of the strait. The sea-ice melt fractions exhibited no obvious pattern except that fractions tended to be somewhat lower on the northern versus the southern end of the strait. Local sea-ice melt fractions (-2%) were only slightly more positive than Arctic fractions (-4%) and were fairly uniform over the section except for some patches of where 0-1% fractions were present. The slightly negative (but near-zero) and fairly uniform sea-ice melt fractions observed throughout Hudson Strait indicate tidal mixing in the strait could result in a closer balance between ice melt and formation (Tan and Strain, 1996). Net sea-ice melt fractions close to zero are generally observed in the deeper, Atlantic-dominated waters of Baffin Bay and those entering via Davis Strait. This further suggests a dominant, tidally-pumped Atlantic water signature in Hudson Strait.

Our findings are somewhat coherent with previous $\delta^{18}O$ distributions in Foxe Basin and Hudson Strait that suggested a narrow band of river runoff exits Hudson Strait on the southern side (Tan and Strain, 1996). However, the dominance of sea-ice meltwater in the central and northern Hudson Strait during summer 1982 was not observed in this locale during 1997.

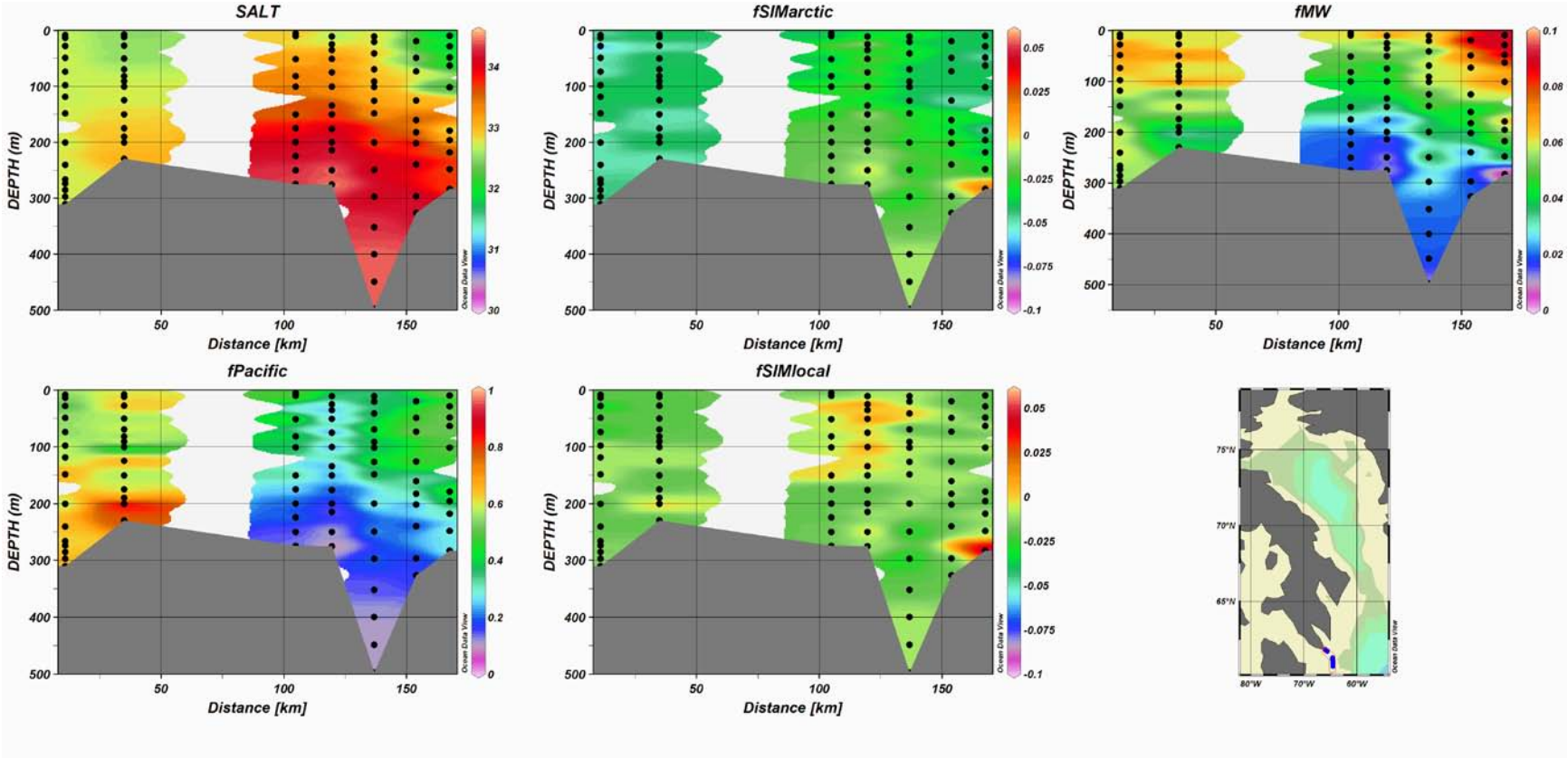

Figure 4.10. Same as for Figure 4.7 but for Hudson Strait 1997

4.5.5 Robeson Channel 2003

The highest fractions of Pacific water were present in the top 150-200 meters of Robeson Channel (Fig. 4.11) and coincided with high fractions of meteoric water (≥ 10%) and generally highly-negative (≤ -7%) Arctic sea-ice melt fractions. The highest meteoric water fractions (11-13%) were observed throughout Robeson Channel to depths > 75 meters. The coincidence of this large meteoric water signal was generally accompanied by high fractions of Pacific water and thus signaled a dominant Arctic origin.

Local sea-ice meltwater was present down to ~100 meters but highest fractions were concentrated in the top 10-20 meters. Below ~100 meters, sea-ice melt fractions ranged between -2% and 1%, and deeper waters were comprised predominately of Atlantic waters with little to no influence from sea-ice meltwater or brine.

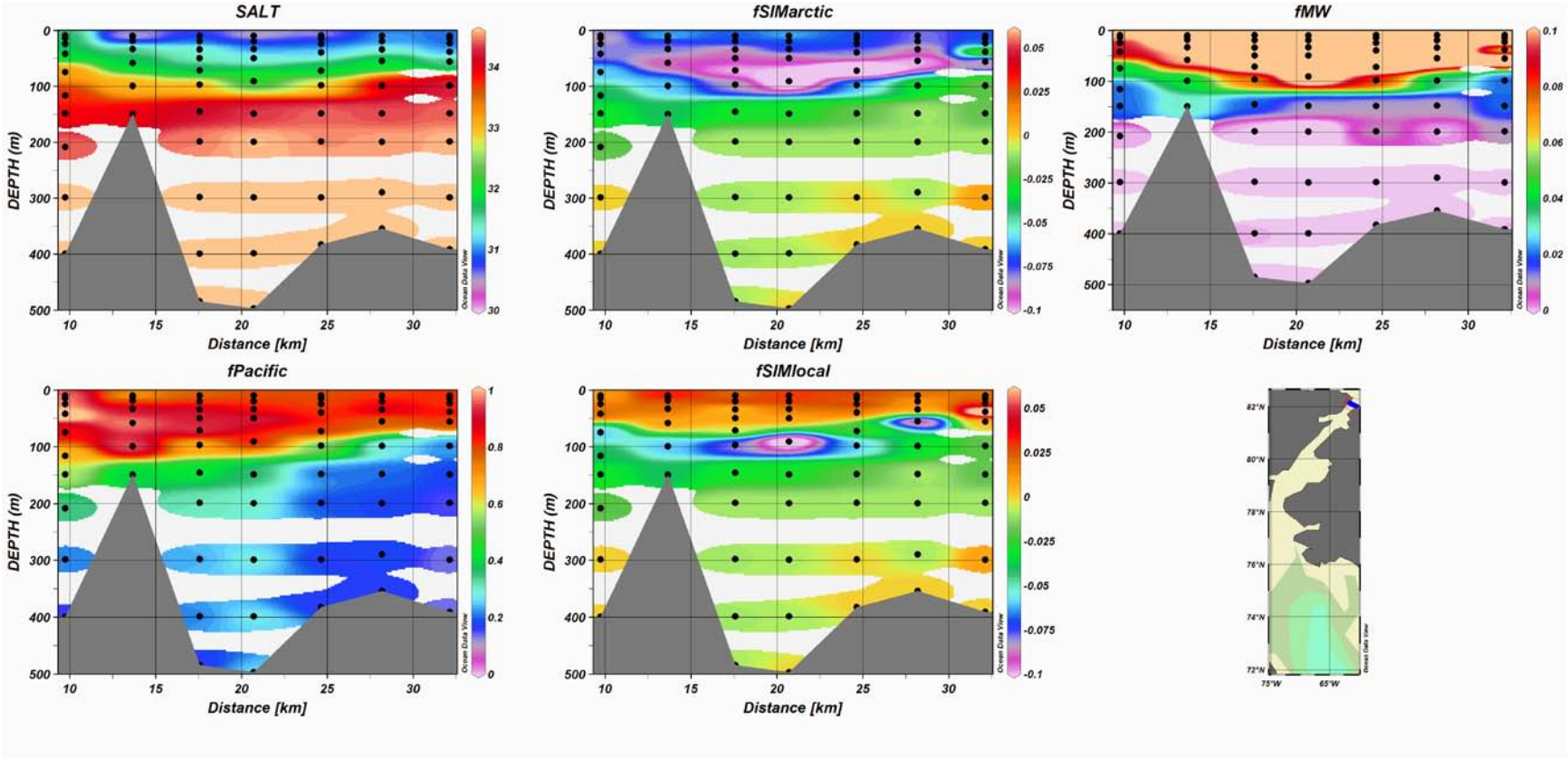

Figure 4.11. Robeson Channel 2003. Color contours for upper 500 meters of salinity (top left) and water type fractions: sea-ice meltwater (top middle), meteoric water (top right), and Pacific water (bottom left) calculated using the component water type analysis relative to the Arctic inflow through the Canadian Archipelago and Baffin Bay and local sea-ice meltwater (bottom middle). In each plot, sections extend from west/left to east/right. Contours were drawn using the VG gridding algorithm in *Ocean Data View* with x and y scale lengths set to 100 and 35 per mille, respectively (Schlitzer, 2001).

4.5.6 Northern Kennedy Channel 2003

Moving southward into Kennedy Channel (Fig. 4.12), Pacific water, meteoric water, and local sea-ice melt fractions were somewhat lower than those observed in Robeson Channel. Meteoric water fractions were ≥ 10% in the top 20-50 meters across the section and positive, local sea-ice melt fractions penetrated to ~50 meters depth near the middle of the section. Large fractions of meteoric water and sea-ice meltwater were limited to shallower depths at the eastern and western ends of the section.

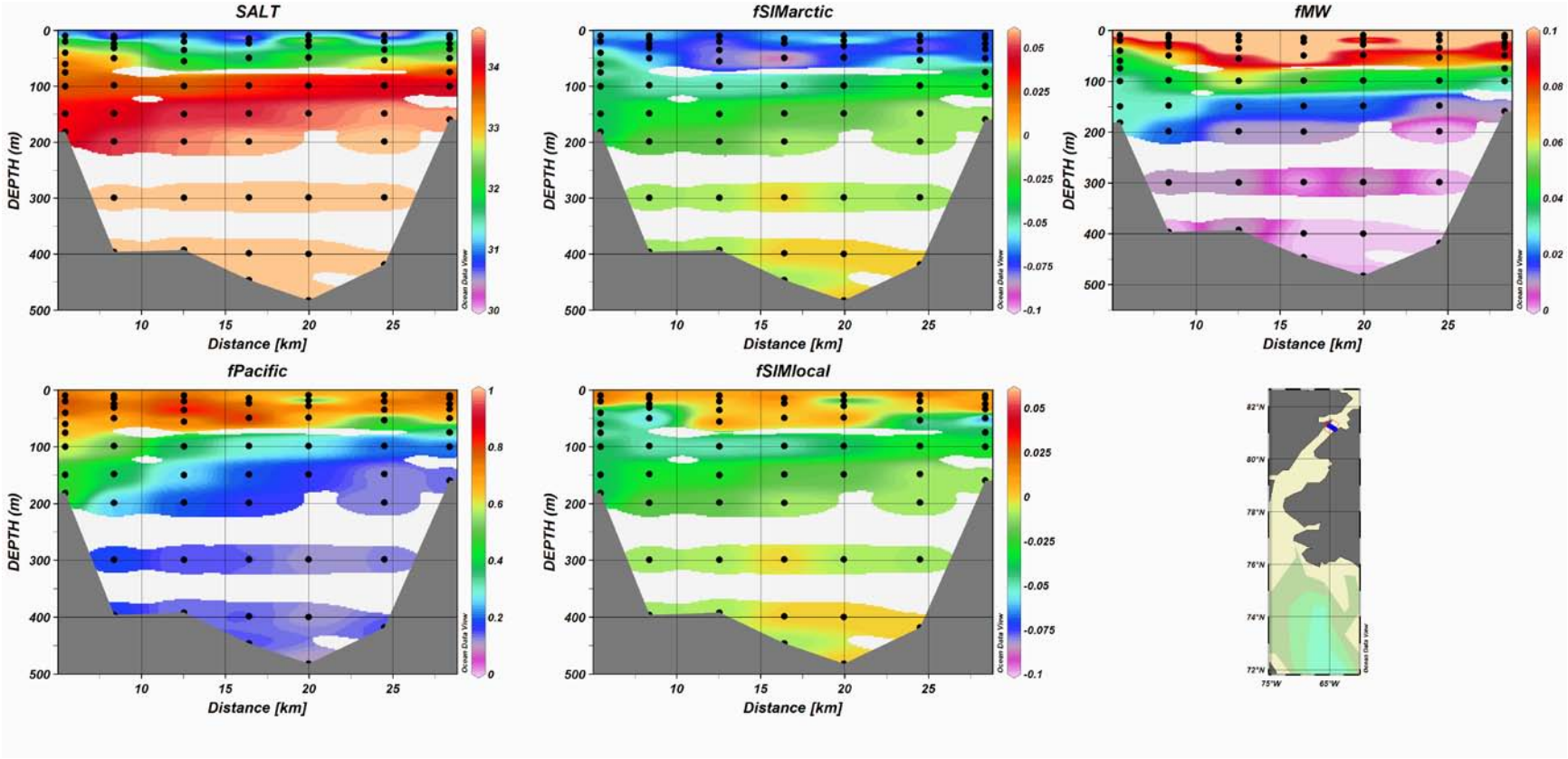

Figure 4.12. Same as for Figure 4.11 but for northern Kennedy Channel 2003.

4.5.7 Southern Kennedy Channel 2003

The southern Kennedy Channel section shows the first sign of shallow Atlantic water influence moving northward through Nares Strait (Fig. 4.13). Although Pacific water influence remains high across the length of the strait, fractions decreased in the eastern portion of the channel around what appears to be a front-like structure. A similar frontal structure is observed in the Arctic sea-ice melt distribution as brine-enriched (highly-negative) waters encounter slightly more positive fractions. Local sea-ice melt fractions were also somewhat higher east of the front. Meteoric water fractions were slightly lower (8-11%) than those observed in northern Kennedy Channel; however the distribution was similarly limited to the top 100-120 meters and was spread out evenly across the channel. The front-like structure observed in the Pacific and sea-ice melt distributions was not detected in the meteoric water distribution.

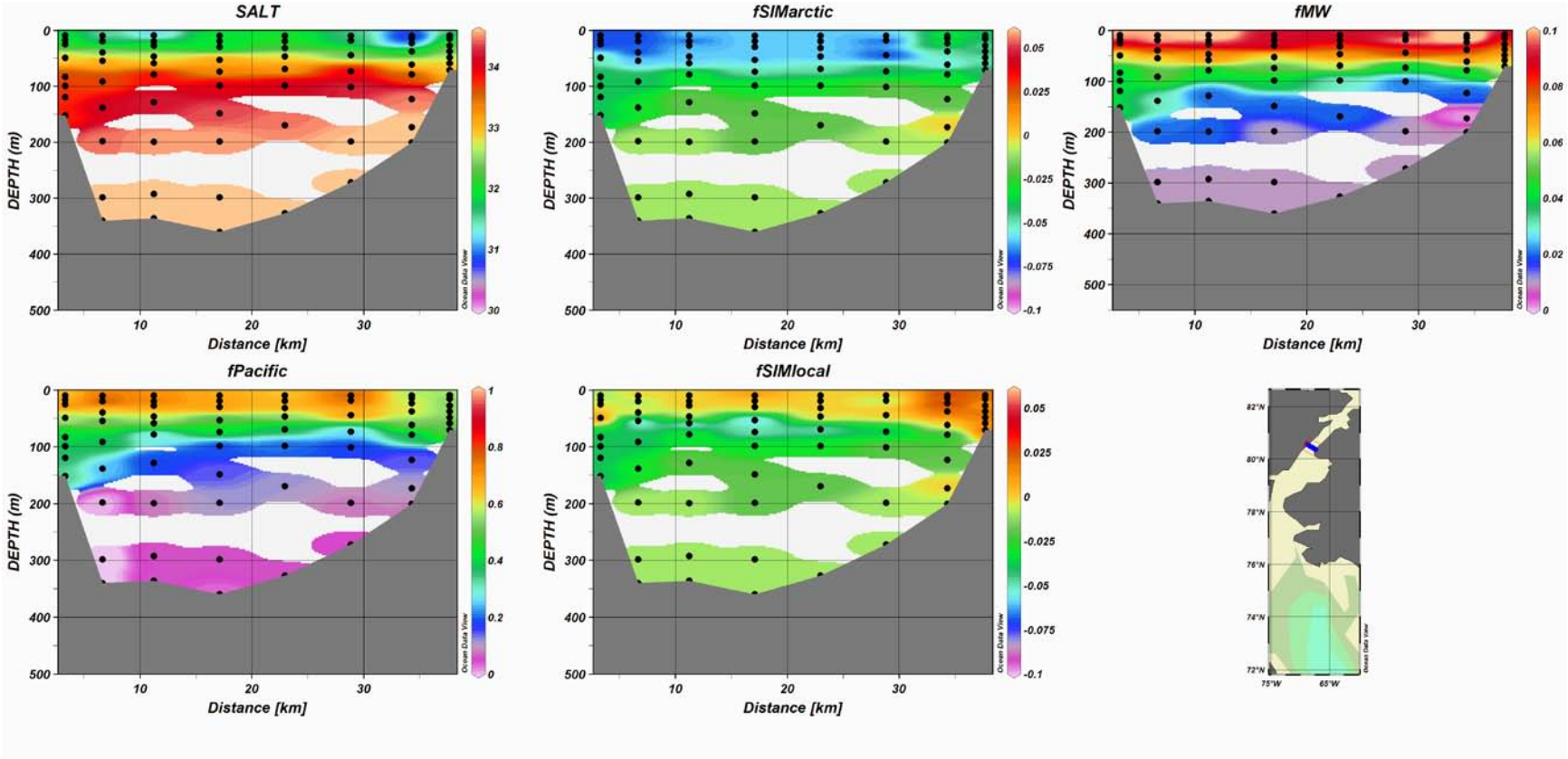

Figure 4.13. Same as for Figure 4.11 but for southern Kennedy Channel 2003.

4.5.8 Smith Sound 2003

The Pacific water distribution observed in Smith Sound during 2003 (Fig. 4.14) implies a somewhat lower influence relative to that observed in 1997 (Fig. 4.7). Falkner et al. (2010) have discussed this difference in detail and suggest the larger presumed flow of Pacific water through Nares Strait during 1997 could have been a consequence of the large positive anomaly in the Arctic Oscillation and resulting hydrographic shifts observed in the Arctic Ocean over the early to mid 1990s. Meteoric water distributions did not differ much between 1997 and 2003. In contrast, sea-ice meltwater fractions appeared to be somewhat higher in 2003. Arctic sea-ice meltwater fractions were highly negative across the upper ~150 meters of the section during 1997 (Fig. 4.7); however, during 2003 these fractions were more positive (-2%) and fairly uniform with depth (Fig. 4.14). Local sea-ice melt fractions were slightly higher and penetrated to greater depths (~50 meters), particularly in the eastern half of the sound, in 2003 versus 1997.

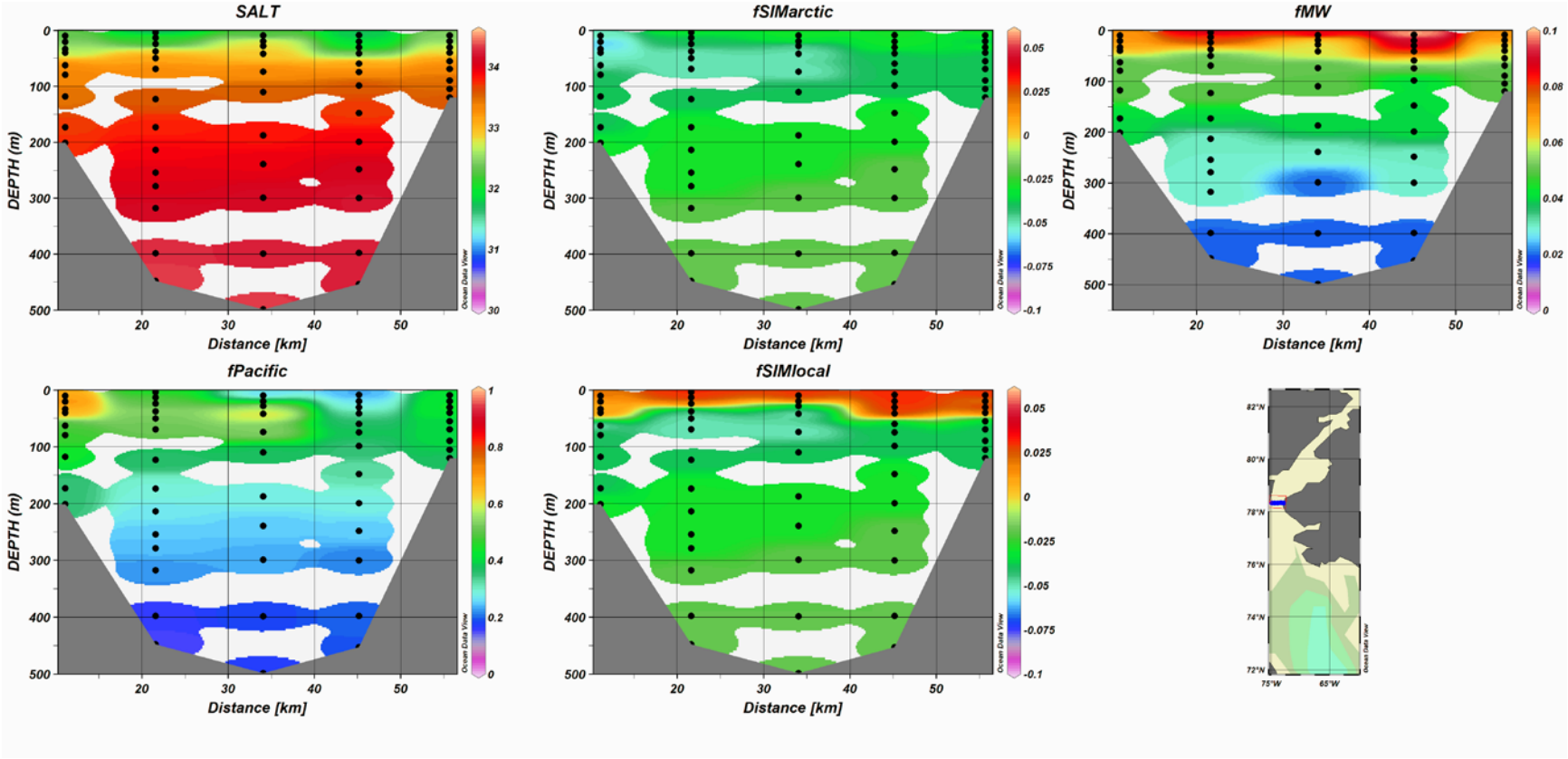

Figure 4.14. Same as for Figure 4.11 but for Smith Sound 2003.

4.5.9 Baffin Bay 2003

The Baffin Bay section (Fig. 4.15) consists of two halves extending first eastward from the Baffin Island continental shelf toward the center of the bay and then northward toward Hayes Peninsula, Greenland (see Fig. 4.1). Arctic-origin water, signified by relatively large fractions of Pacific water and highly-negative Arctic sea-ice melt fractions, was present in western and central Baffin Bay between 0 and 200 meters depth. The greatest concentration (>60%) and vertical extent (~150 meters) of Pacific water was observed closest to Baffin Island. Maximum fractions of Pacific water were ~80%, which was slightly higher than those measured in Smith Sound. This could suggest additional input from Lancaster and Jones Sounds via the western archipelago (Falkner et al., 2010).

Meteoric water fractions were highest (8-9%) above ~20 meters depth and extended across both sections of Baffin Bay. However, significant meteoric water fractions (≥ 6%) were present between 50 and 150 meters in the east-west section but generally absent in the north-south section, except for the southernmost few stations. This larger meteoric water influence concentration in the western half of Baffin Bay was accompanied by highly-negative sea-ice melt fractions and higher Pacific water influence. This indicated an Arctic-origin for, at least, the sub-surface meteoric water influence observed.

Fractions of Arctic sea-ice melt were also more negative in the east-west branch of the section compared to observations in Smith Sound. Local sea-ice meltwater fractions ranged between 0 and 3% in the top ~20 meters across the section with meltwater influence > 5% observed above 10 meters depth at the northernmost station. Below ~20 meters, sea-ice melt fractions decreased to minimum values of -6 to -7% at ~100 meters depth over the majority of the section (as far east as ~67ºW and north to ~73ºN) before increasing to values between -2 and -1%.

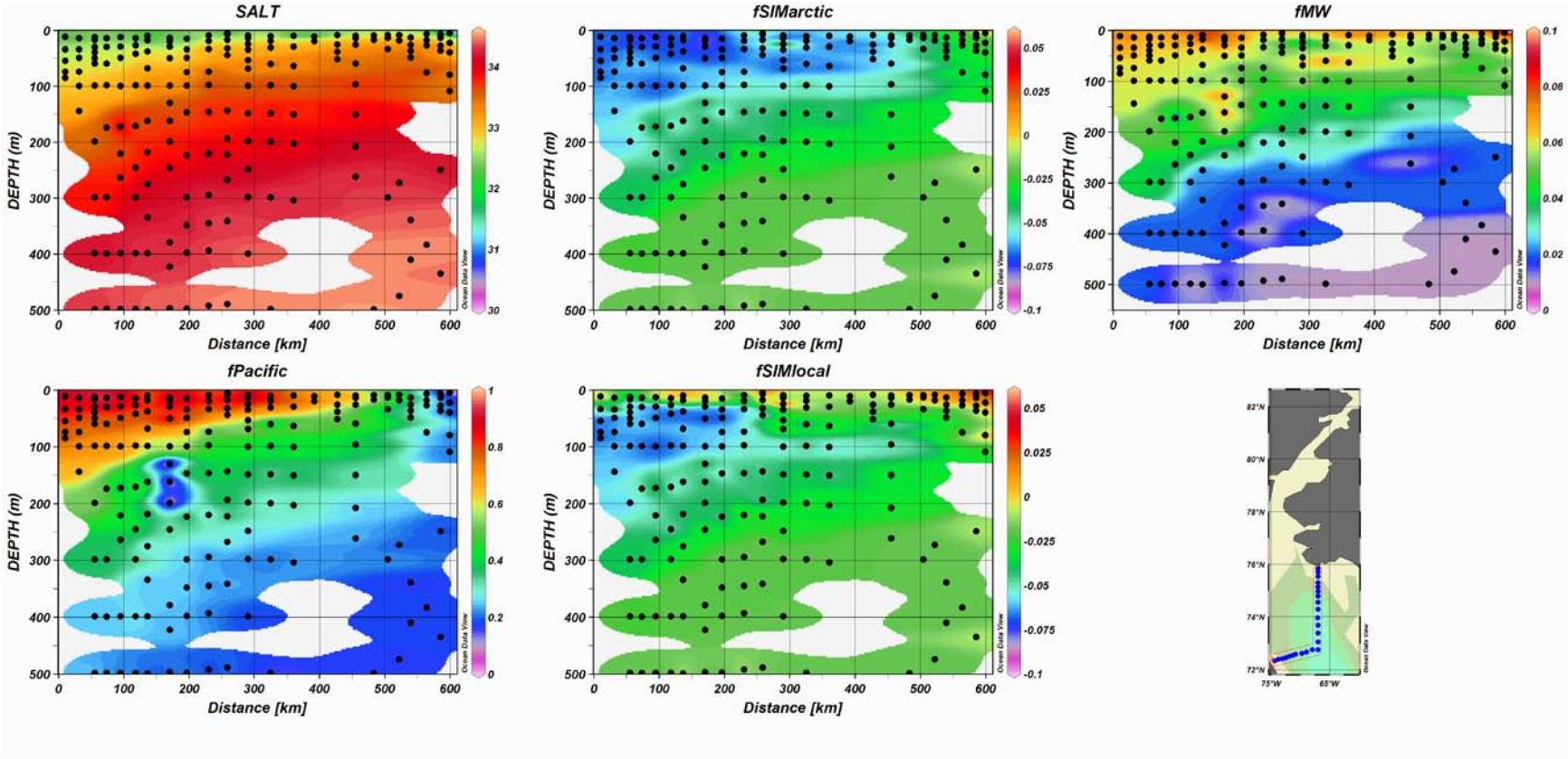

Figure 4.15. Same as for Figure 4.11 but for Baffin Bay 2003. Plot composited from east-west and south-north Baffin Bay sections (see Fig. 4.1).

4.6 Summary and Conclusions

As first discussed by Strain and Tan (1993), a conservation-equation approach to a water component analysis with endmembers appropriate to the Arctic can obscure local sea-ice melt in Baffin Bay. Via satellite imagery and ship observations, we know that there is seasonal ice drift and melt in Baffin Bay (Kwok et al. 2007). We have attempted to estimate local contributions through considerations of an appropriate reference framework.

It has long been appreciated that Arctic-origin waters flowing southward through multiple channels, including Jones, Lancaster, and Smith Sounds contribute significantly to Baffin Bay (Muench, 1971; Jones and Coote, 1980; Coote and Jones, 1982; Melling et al., 1984). However, the inheritance of a net ice formation signal in salinity-$\delta^{18}O$ relationships from the Arctic interior to Baffin Bay has not been exploited in calculations of local sea-ice melt influence. Our results suggest previous studies not taking this inherited Arctic brine signature into account (Tan and Strain 1980; 1996) have potentially over-estimated local sea-ice meltwater fractional contributions by 0-6%.

Here, we have presented a two layer mixing scheme adapted from the work of Bauch et al. (2009) to estimate local sea-ice melt. A common, salinity-$\delta^{18}O$ mixing line between Atlantic seawater and brine-enriched halocline water was estimated from data collected from depths where local sea-ice processes should have limited influence (Muench, 1971; Bourke et al., 1989; Tang et al., 2004). The endmember characteristics of the brine-enriched halocline water varied somewhat among sections, indicating potential variability in seawater sources (Pacific versus Atlantic), shelf inputs, meteoric water sources, winter mixed layer depth, etc. Local sea-ice meltwater fractions were calculated relative to a second mixing line between this brine-enriched halocline water and an average, high-latitude meteoric water source.

Positive, local sea-ice melt fractions were generally limited to the upper 20-50 meters and were typically ubiquitous over the length of the sections. The deepest

penetration of positive sea-ice melt fractions was observed in eastern Davis Strait (Fig. 9), down to > 150 meters depth. The largest contributions (≥ 5%) were present in northeast Baffin Bay (Fig. 15), southeastern Kennedy Channel (Fig. 4.13), northern Jones Sound (Fig. 4.8), and eastern Davis Strait (Fig. 4.9). Meteoric and Pacific water were found to be the dominant sources of freshwater to the Canadian Arctic Archipelago and Baffin Bay during summer 1997 and 2003.

Sections occupied across Smith Sound in 1997 and 2003 offered the only direct, temporal comparison between the two study years. An apparent decrease in the Pacific influence to Smith Sound was observed between 1997 and 2003. This is consistent with a relaxation of the Arctic Oscillation toward more neutral conditions following anomalous cyclonic forcing (positive AO index) during the early to mid 1990s and a subsequent reduction in Pacific water export through Nares Strait (Falkner et al., 2010). In contrast to the observed reduction in Pacific influence, meteoric water distributions were found to be quite similar between these two years. Assuming an Arctic-origin for the meteoric water in Smith Sound, the similar influence observed in 1997 and 2003 despite the large contrast in Pacific influence suggests these Arctic inflows might be de-coupled at least part of the time.

Low Pacific values observed in Hudson Strait during 1997 suggest a dominance of Atlantic over Pacific seawater and indicated sedimentary denitrification thought to occur in Hudson Bay did not affect the waters sampled during the study period. Whether or not this observation is anomalous requires further study. In agreement with the conclusions of Tan and Strain (1996), we find a narrow band of meteoric water exits Hudson Strait on the southern side. However, salinity-$\delta^{18}O$ relationships suggested little influence from local sea-ice meltwater across the strait. Instead, samples generally fell along a linear mixing line between Atlantic water and a mixture of brine-enriched halocline water and meteoric water. Similar observations were found in Smith Sound in 1997.

Halocline-Atlantic water mixing lines such as those observed during this study, particularly in Smith Sound and Hudson Strait 1997 sections where very little

local sea-ice meltwater is present, closely resemble a linear mixing line one would expect in the presence of glacial meltwater. Salinity and $\delta^{18}O$ data collected next to the outflow of the Petermann Glacier (Fig. 4.16), where we are confident the relationships observed are a result of glacial meltwater, are indistinguishable from data collected in Smith Sound and Hudson Strait during 1997. We have interpreted the latter data a consequence of input from brine-enriched halocline waters inherited from Arctic shelves. Therefore, future studies attempting to address contributions of glacial runoff from the Greenland Ice Sheet to the eastern and western Greenland shelves cannot do so using salinity and $\delta^{18}O$ data alone. Simple interpretations will be complicated by brine-enriched halocline waters exported from the Arctic interior through the Canadian Arctic Archipelago and Fram Strait. Additional tracers are needed to distinguish between net sea-ice formation signatures and influence from glacial runoff in these regions.

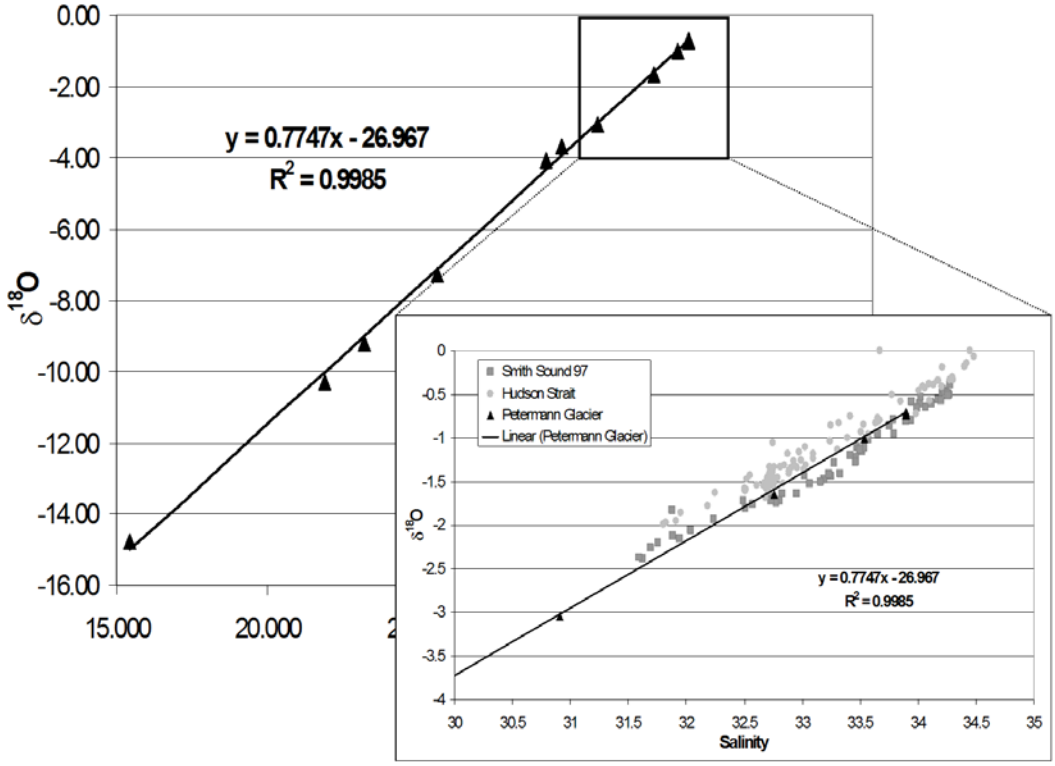

Figure 4.16. Salinity versus $\delta^{18}O$ for samples collected next to Peterman Glacier outflow (black triangles) and a comparison (inset) to data collected from Smith Sound (gray squares) and Hudson Strait (light gray circles) during summer 1997.

4.7 References

Alkire, M.B., K.K. Falkner, I. Rigor , M. Steele, J. Morison (2007), The return of Pacific waters to the upper layers of the central Arctic Ocean, *Deep-Sea Research I 54*: 1509-1529.

Anderson, L.G., S. Jutterstrom, S. Kaltin, E.P. Jones, G. Bjork (2004), Variability in river runoff distribution in the Eurasian Basin of the Arctic Ocean, *Journal of Geophysical Research 109*: doi:10.1029/2003JC001773.

Armstrong, F.A.J, et al. (1967), The measurement of upwelling and subsequent biological processes by means of Technicon Autoanalyser and associated equipment, *Deep-Sea Research 14*: 381-389.

Bauch, D., I.A. Dmitrenko, C. Wegner, J. Holemann, S.A. Kirillov, L.A. Timokhov, H. Kassens (2009), Exchange of Laptev Sea and Arctic Ocean halocline waters in

response to atmospheric forcing, *Journal of Geophysical Research 114*: doi:10.1029/2008JC005062.

Bernhardt, H. and A. Wilhelms (1967), The continuous determination of low level iron, soluble phosphate and total phosphate with the autoanalyser, paper presented at Technicon Symposium.

Bourke, R.H., V.G. Addison, R.G. Paquette (1989), Oceanography of Nares Strait and Northern Baffin Bay in 1986 with emphasis on deep and bottom water formation, *Journal of Geophysical Research 94*: 8289-8302.

Cooper, L.W., T.E. Whitledge, J.M. Grebmeier (1997), The nutrient, salinity, and stable oxygen isotope composition of Bering and Chukchi Seas waters in and near the Bering Strait, *Journal of Geophysical Research 102*: 12563-12573.

Cooper, L.W., J.W. McClelland, R.M. Holmes, P.A. Raymond, J.J. Gibson, C.K. Guay, B.J. Peterson (2008), Flow-weighted values of runoff tracers (d18O, DOC, Ba, alkalinity) from the six largest Arctic rivers, *Geophysical Research Letters 35*: doi:10.1029/2008GL035007.

Coote, A.R., E.P. Jones (1982), Nutrient distributions and their relationships to water masses in Baffin Bay, *Canadian Journal of Fisheries and Aquatic Sciences 39*: 1210-1214.

Craig, H. and L.I. Gordon (1965), Deuterium and oxygen 18 variations in the ocean and the marine atmosphere, in *Stable Isotopes in Oceanographic Studies and Paleotemperatures*, edited by E. Tongiorgi, pp. 9-130, Consiglio Nazionale delle Ricerche, Pisa, Italy.

Devol, A.H., Codispoti, L.A., J.P. Christensen (1997), Summer and winter denitrification rates in western Arctic shelf sediments, *Continental Shelf Research 17*: 1029-1050.

Falkner, K.K., R.W. Macdonald, E.C. Carmack, T. Weingartner, T. (1994), The potential of barium as a tracer of Arctic water masses, in *The Polar Oceans and Their Role in Shaping the Global Environment: The Nansen Centennial Volume, AGU Geophys. Monograph Series*, edited by O.M. Johannessen, R.D. Muench, and J.E. Overland, pp. 63-76, AGU Books, Washington DC.

Falkner, K.K., M.C. O'Brien, H. Melling, E.C. Carmack, F.A. McLaughlin, A. Munchow, E.P. Jones (2010), Interannual variability of dissolved nutrients in the Canadian Archipelago and Baffin Bay with implications for freshwater flux, *manuscript in preparation*.

Fissel, D.B. et al. (1988), *Non-tidal flows in the Northwest Passage*, 143 pp., Institute of Ocean Sciences, Sidney, BC.

Gordon, L.I., J.J.C. Jr., A.A. Ross, J.M. Krest (1994), A suggested protocol for continuous flow automated analysis of seawater nutrients (phosphate, nitrate, nitrite and silicic acid) in the WOCE Hydrographic Program and the Joint Global Ocean Fluxes Study, WOCE Operations Manual, Vol. 3: The Observational Program, Section 3.1: WOCE Hydrographic Program, Part 3.1.3: WHP Operations and Methods., pp. 52 loose-leaf, Woods Hole, MA.

Guay, C.K. and K.K Falkner (1997), Barium as a tracer of Arctic halocline and river waters, *Deep-Sea Research II 44*: 1543-1569.

Guay, C.K.H., F.A. McLaughlin, M. Yamamoto-Kawai (2009), Differentiating fluvial components of upper Canada Basin waters on the basis of measurements of dissolved barium combined with other physical and chemical tracers, *Journal of Geophysical Research 114*: doi:10.1029/2008JC005099.

Jones, E.P., A.R. Coote (1980), Nutrient distributions in the Canadian Archipelago: indicators of summer water mass and flow characteristics, *Canadian Journal of Fisheries and Aquatic Sciences 37:* 589-599.

Jones, E.P., L.G. Anderson, J.H. Swift (1998). Distribution of Atlantic and Pacific waters in the upper Arctic Ocean: Implications for circulation, *Geophysical Research Letters 25*: 765-768.

Jones, E.P., J.H. Swift, L.G. Anderson, M. Lipizer, G. Civitarese, K.K. Falkner, G. Kattner, F. McLaughlin (2003), Tracing Pacific water in the North Atlantic Ocean, *Journal of Geophysical Research 108*: doi:10.1029/2001JC001141.

Kipphut, G. W. (1990), Glacial meltwater input to the Alaska Coastal Current: Evidence from oxygen isotope measurements, *Journal of Geophysical Research 95:* 5177-5181.

Kwok, R (2007), Baffin Bay ice drift and export : 2002–2007, *Geophysical Research Letters 34*: doi:10.1029/2007GL031204.

Luthcke, S.B., H.J. Zwally, W. Abdalati, D.D. Rowlands, R.D. Ray, R.S. Nerem, F.G. Lemoine, J.J. McCarthy, D.S. Chinn (2006), Recent Greenland ice mass loss by drainage system from satellite gravity observations, *Science 314*: 1286-1289.

Macdonald, R.W., D.W. Paton, E.C. Carmack (1995), The freshwater budget and under-ice spreading of Mackenzie River water in the Canadian Beaufort Sea based on

salinity and $^{18}O/^{16}O$ measurements in water and ice, *Journal of Geophysical Research 100*: 895-919.

Melling, H., T.A. Agnew, K.K. Falkner, D.A. Greenberg, C.M. Lee, A. Munchow, B. Petrie, S.J. Prinsenberg, R.M. Samelson, R.A. Woodgate (2008) in *Arctic-Subarctic Ocean Fluxes: Defining the Role of the Northern Seas in Climate*, eds. R.R. Dickson, J. Meincke, and P. Rhines, Springer, pp. 193-247.

Muench, R.D. (1971), The physical oceanography of the northern Baffin Bay region, Ph.D. thesis: University of Washington, Seattle.

Munchow, A., K.K. Falkner, H. Melling (2007), Spatial continuity of measured seawater and tracer fluxes through Nares Strait, a dynamically wide channel bordering the Canadian Archipelago, *Journal of Marine Research 65*: 759-788.

Nguyen, A.T., D. Menemenlis, R. Kwok (2009), Improved modeling of the Arctic halocline with a subgrid-scale brine rejection parameterization, Journal of Geophysical Research 114: doi:10.1029/2008JC005121.

Ostlund, H.G. and G. Hut (1984), Arctic Ocean water mass balance from isotope data, *Journal of Geophysical Research 89*: 6373-6381.

Paren, J. G. and J. R. Potter (1984), Isotopic tracers in polar seas and glacier ice, *Journal of Geophysical Research 89*: 749-750.

Redfield, A.C. and I. Friedman (1969), The effect of meteoric water, melt water and brine on the composition of Polar Sea water and of the deep waters of the ocean, *Deep-Sea Research*: 197-224.

Rignot, E., J.E. Box, E. Burgess, E. Hanna (2008), Mass balance of the Greenland ice sheet from 1958-2007, *Geophysical Research Letters 35*: doi:10.1029/2008GL035417.

Rigor, I.G., J.M. Wallace (2004), Variations in the age of Arctic sea-ice and summer sea-ice extent, *Geophysical Research Letters 31*: doi:10.1029/2004GL019492.

Schlitzer, R. (2001) Ocean Data View, http://www.awi-bremerhaven.de/GEO/ODV.

Schmidt, G.A., G.R. Bigg, E.J. Rohling (1999), "Global Seawater Oxygen-18 Database," http:data.giss.nasa.gov/o18data/

Serreze, M. C., A. P. Barrett, et al. (2006), The large-scale freshwater cycle of the Arctic, *Journal of Geophysical Research 111*: doi:10.1029/2005JC003424.

Strain, P.M. and F.C. Tan (1993), Seasonal evolution of oxygen isotope-salinity relationships in high-latitude surface waters, *Journal of Geophysical Research 98*: 14589-14598.

Tan, F.C. and P.M. Strain (1980), The distribution of sea ice meltwater in the Eastern Canadian Arctic, *Journal of Geophysical Research 85*: 1925-1932.

Tan, F.C. and P.M. Strain (1996), Sea ice and oxygen isotopes in Foxe Basin, Hudson Bay, and Hudson Strait, Canada, *Journal of Geophysical Research 101*: 20869-20876.

Tang, C.C.L., C.K. Ross, T. Yao, B. Petrie, B.M. DeTracey, E. Dunlap (2004), The circulation, water masses and sea-ice of Baffin Bay, *Progress in Oceanography 63*: 183-228.

Taylor, J.R., K.K Falkner, U. Schauer, M. Meredith (2003), Quantitative considerations of dissolved barium as a tracer in the Arctic Ocean, *Journal of Geophysical Research 108*: doi:10.1029/2002JC001635.

Weeks, W. F. and S. F. Ackley (1986), The growth, structure and properties of sea ice, *The Geophysics of Sea Ice*. N. Untersteiner. New York, Plenum Press. 146**:** 9-164.

Yamamoto-Kawai, M., N. Tanaka, S. Pivovarov (2005). Freshwater and brine behaviors in the Arctic Ocean deduced from historical data of $\delta^{18}O$ and alkalinity (1929-2002 A.D.), *Journal of Geophysical Research 110*: doi:10.1029/2004JC002793.

Yamamoto-Kawai, M., F.A. McLaughlin, E.C. Carmack, S. Nishino, K. Shimada (2008), Freshwater budgets of the Canada Basin, Arctic Ocean, from salinity, $\delta^{18}O$, and nutrients, *Journal of Geophysical Research. 113*: doi:10.1029/2006JC003858.

5. CONCLUSIONS

This research program has quantified the distribution of the various water types comprising the upper 150-300 meters of the central Arctic Ocean and passages of the Canadian Archipelago and Baffin Bay to derive insights regarding ocean circulation and processes. This has been accomplished via the application of multiple geochemical tracers to distinguish freshwater components comprising the Arctic and subarctic seas: Pacific water, meteoric water (direct precipitation plus river runoff from both North American and Eurasian continents), and sea-ice melt/formation. Application of in-situ sensor technology has revealed unsurpassed detail of surface and halocline water variability and shown the system can be under-sampled using traditional bottle casts. Methods used to calculate local sea-ice meltwater contributions in the Canadian Arctic Archipelago and Baffin Bay are altered so that they take into account brine signatures inherited from the Arctic interior.

Water type distributions derived from chemical data collected annually during spring months between 2000 and 2008 reveal rapid variation in the position of the front roughly separating waters of Pacific and Atlantic origins in the upper ~150 meters of the central Arctic. Pacific water partially returned to the Makarov Basin between 2003 and 2005 via expansion of the Beaufort Gyre and a shift in the alignment of the Transpolar Drift from an alignment roughly over the Mendeleev-Alpha Ridge system toward the Lomonosov Ridge. Back-trajectories of sea-ice motion derived from data collected via the International Arctic Buoy Program indicate Pacific waters entering the Arctic via Bering Strait were advected westward along the Siberian continental slope between 2003 and 2005 and moved offshore into the Transpolar Drift offshore of the New Siberian Islands. This shift in the Pacific water distribution was short-lived, however, as Pacific waters again retreated from the Makarov Basin between 2006 and 2008.

Eurasian river runoff was observed to dominate the meteoric water contributions observed both in the central Arctic between 2000 and 2008 and the

southern Canada Basin during spring 2008. A change in the distributions of Eurasian river runoff in the central Arctic was observed between 2006 and 2008. During this period, contributions of Eurasian river runoff to the top ~120 meters were found to be larger in the Makarov Basin relative to the Amundsen Basin. This is in contrast to the expected distribution as low-salinity shelf waters of the Laptev Sea are expected to move offshore along the Amundsen Basin flank of the Lomonosov Ridge. These observations might be linked as a consequence of wind forcing over the Siberian shelves during summers 2006-2008 favoring offshore advection northward of the East Siberian Sea.

The first, high-resolution vertical profiles of nitrate were collected in the central Arctic Ocean during spring 2007 and 2008. Combined with similarly-collected high-resolution profiles of dissolved oxygen, profiles of the NO parameter were also collected in this region for the first time. These high-resolution records revealed that the NO minimum typically associated with lower halocline water ($34.1 \leq S \leq 34.5$) frequently occurred at lower salinities (33.2-34.2) in the Makarov Basin during spring 2007 and 2008. In the Amundsen Basin, the NO minimum remained associated with LHW. These observations suggest the cold halocline layers in these basins were ventilated by different sources of low salinity waters (most likely from Siberian shelves) and support previous inferences suggesting direct shelf influence to the lower halocline of the Makarov and Canada Basins.

These observations are correlated with an increased contribution of Eurasian river runoff to the Makarov Basin during this period. We speculate the low NO values observed in the cold halocline layer of the Makarov Basin could be explained by direct interaction with East Siberian Sea sediments known to undergo respiratory processes such as denitrification and/or annamox or mixing with resident shelf waters prior to advection offshore. These inferences have implications both on linkages between the fate of shelf waters and the formation of NO minima and the use of the NO parameter to observe variability in halocline water formation and ventilation in the future.

Vertical profiles of the NO parameter collected in the southern Canada Basin support multiple sources of lower halocline waters to this region, including Fram Strait Branch and Barents Sea Branch lower halocline waters advected from the Eurasian Basin, diapycnal mixing of upwelled Atlantic-origin waters, and polynya influence.

Salinity, $\delta^{18}O$, and nutrient data collected from the Canadian Arctic Archipelago and Baffin Bay during two separate summer cruises in 1997 and 2003 were analyzed to determine the magnitude and distribution of various freshwater components (Pacific water, meteoric water, and sea-ice melt) including local sea-ice meltwater.

Waters moving southward from the Arctic interior through the Canadian Arctic Archipelago and Baffin Bay carry a signal of net sea-ice formation identified by salinity-$\delta^{18}O$ relationships. These inherited relationships are important for determining contributions of local sea-ice meltwater to subarctic regions. Previous studies of Baffin Bay freshwater components were restricted in that they considered only local sea-ice melt and did not take this inherited signature into account. Here, conservation equations are applied to calculate contributions of meteoric water and net sea-ice melt/formation. Uncertainties are reduced by estimating Pacific and Atlantic contributions to the seawater end-member. Local sea-ice melt fractions are then calculated relative to a reference line describing linear mixing between brine-enriched halocline water and meteoric water. We believe this is a more accurate description of water type mixing in the upper layers of Baffin Bay and thus return better estimates of the influence from local sea-ice melt.

Our results suggest previous studies which did not take the inherited net sea-ice formation signature into account may have over-estimated local sea-ice melt contributions by 0-6%. Temporal comparisons can be made for sections in Smith Sound that were occupied during both 1997 and 2003. Meteoric water contributions were comparable but Pacific water content was lower in 2003 than in 1997, demonstrating that these water types do not necessarily co-circulate. Sea-ice melt

fractions were also somewhat lower across Smith Sound in 1997 relative to 2003, implying an enhanced net sea-ice formation signal from the Arctic, a decrease in local sea-ice melt, or both.

Geochemical tracers allow quantitative separation of multiple freshwater sources to the upper layers of the Arctic Ocean which cannot be conducted using temperature and salinity alone. The tracer data collected via aerial hydrographical surveys as part of the North Pole Environmental Observatory provide data essential to begin filling gaps in our understanding of high-latitude oceanographic processes which exist due to the heavy bias toward late summer measurements. Such targeted hydrographic sampling can be used to compliment newer, Lagrangian data sets such as those collected from Ice Tethered Profilers (ITPs). However, the focus of these studies on regions of the central Arctic most susceptible to change is not sufficient to describe spatial and temporal variability in the upper layers of the Arctic Ocean.

More hydrographic sampling is required in the marginal seas surrounding the Arctic to address mechanisms of halocline water formation and biogeochemical cycles affecting the various tracers used to discriminate among water types. This is particularly true for winter months where a general lack of winter data in regions such as the Laptev and East Siberian Sea shelves prevents direct experiments testing hypotheses regarding halocline water formation and advection. Such studies will only become more necessary as the extent and volume of sea ice continues to decline as feedbacks between the ice extent and the maintenance of the halocline may help drive conditions to an ice free state during summer. The advancement of sensor technology and its integration into autonomous platforms (such as ITPs) will facilitate the collection of much needed, high-resolution data in regions and time periods otherwise difficult to sample. Such data are necessary in understanding both physical and biogeochemical shelf processes and their connections to water type formation.

Future studies should not only focus on the applications of geochemical tracers, but the response of these tracers to on-going change. For example, the non-conservative behavior of barium in the absence of sea-ice cover has rendered this

tracer unreliable to distinguish between North American and Eurasian river runoff. The effects of a declining sea-ice cover on the biogeochemistry of high-latitude waters are not yet well understood. Recent research has described, for example, an ecosystem shift in the Bering Sea from generally benthic to pelagic conditions resulting, in part, from a longer open water season. Increased primary productivity could have consequences not only on atmosphere-ocean CO_2 fluxes, but also on the rain of organic matter to the sediments of the broad and shallow Arctic continental shelves. An increase in the rain of organic carbon could potentially affect bottom water oxygen conditions and lead to more widespread denitrification. This could render the nutrient relationships used to identify Pacific versus Atlantic seawater ineffective.

In addition, increased flow of glacial runoff to both the West and East Greenland shelves can potentially contribute a significant source of freshwater to these regions as the climate continues to warm. Salinity-$\delta^{18}O$ relationships in these regions are complicated by the mixing of brine-enriched halocline waters originating on Arctic shelves and deeper, Atlantic waters. At present, export of brine-enriched, Arctic-origin waters are believed to dominate these relationships; however, this may not always be the case. Futures studies require additional tracers to separate these two components. Furthermore, the impact of a seasonally ice-free Arctic on the balance between sea-ice melt and formation and its implications on export of brine-enriched halocline waters also requires attention.

Obviously, there are still many questions to be answered regarding the response of biogeochemistry, freshwater distributions, circulation, and their interaction as the Arctic region continues to warm and the sea-ice cover deteriorates.

BIBLIOGRAPHY

Aagaard, K., L.K. Coachman, E. Carmack (1981), On the halocline of the Arctic Ocean, *Deep-Sea Research 28A*: 529-545.

Aagaard, K., A.T. Roach (1990), Arctic Ocean-Shelf Exchange: Measurements in Barrow Canyon, *Journal of Geophysical Research 95*: 18163-18175.

Abrahamsen, E.P., Meredith, M.P., Falkner, K.K., Torres-Valdes, S., Leng, M.J., Alkire, M.B., Bacon, S., Polyakov, I., Ivanov, V., Kirillov, S. (2009), Tracer-derived freshwater budget of the Siberian Continental Shelf following the extreme Arctic summer of 2007, *Geophysical Research Letters 36*: doi:10.1029/2009GL037341.

Alkire, M.B., K.K. Falkner, I. Rigor , M. Steele, J. Morison (2007), The return of Pacific waters to the upper layers of the central Arctic Ocean, *Deep-Sea Research I 54*: 1509-1529.

Anderson, L.G. and E.P. Jones (1992), Tracing upper waters of the Nansen Basin in the Arctic Ocean, *Deep-Sea Research 39*: 425-433.

Anderson, L.G., S. Jutterstrom, S. Kaltin, E.P. Jones, G. Bjork (2004), Variability in river runoff distribution in the Eurasian Basin of the Arctic Ocean, *Journal of Geophysical Research 109*: doi:10.1029/2003JC001773.

Armstrong, F.A.J, et al. (1967), The measurement of upwelling and subsequent biological processes by means of Technicon Autoanalyser and associated equipment, *Deep-Sea Research 14*: 381-389.

Bauch, D., I.A. Dmitrenko, C. Wegner, J. Holemann, S.A. Kirillov, L.A. Timokhov, H. Kassens (2009), Exchange of Laptev Sea and Arctic Ocean halocline waters in response to atmospheric forcing, *Journal of Geophysical Research 114*: doi:10.1029/2008JC005062.

Bernhardt, H. and A. Wilhelms (1967), The continuous determination of low level iron, soluble phosphate and total phosphate with the autoanalyser, paper presented at Technicon Symposium.

Bourke, R.H., V.G. Addison, R.G. Paquette (1989), Oceanography of Nares Strait and Northern Baffin Bay in 1986 with emphasis on deep and bottom water formation, *Journal of Geophysical Research 94*: 8289-8302.

Boyd, T.J., M. Steele, R.D. Muench, J.T. Gunn (2002), Partial recovery of the Arctic Ocean halocline, *Geophysical Research Letters 29*: doi:10.1029/2001GL014047.

Broecker, W.S. (1974), "NO", A conservative water mass tracer, *Earth and Planetary Science Letters 23*: 100-107.

Camill, P. (2005), Permafrost thaw accelerates in boreal peatlands during late-20th century climate warming, *Climate Change 68*: 135-152.

Carmack, E.C., K. Aagaard, J.H. Swift, R.W. Macdonald, F.A. McLaughlin, E.P. Jones, R.G. Perkin, J.N. Smith, K.M. Ellis, L.R. Kilius (1997), Changes in the temperature and tracer distributions within the Arctic Ocean Section, *Deep-Sea Research II 44*: 1487-1502.

Carmack, E., F. McLaughlin, M. Yamamoto-Kawai, M. Itoh, K. Shimada, R. Krishfield, A. Proshutinsky (2008), Freshwater Storage in the Northern Ocean and the Special Role of the Beaufort Gyre in *Arctic-Subarctic Ocean Fluxes: Defining the Role of the Northern Seas in Climate*, eds. R.R. Dickson, J. Meincke, and P. Rhines, Springer, pp. 145-170.

Cavalieri, D.J., S. Martin (1994), The contribution of Alaskan, Siberian, and Canadian coastal polynyas to the cold halocline layer of the Arctic Ocean, *Journal of Geophysical Research 99*: 18343-18362.

Codispoti, L.A., Friederich, G.E., Sakamoto C.M., Gordon, L.I. (1991), Nutrient cycling and primary production in the marine systems of the Arctic and Antarctic, *Journal of Marine Systems 2*: 359-384.

Comiso, J.C. (2002), A rapidly declining perennial sea ice cover in the Arctic, *Geophysical Research Letters 29*: doi:10.1029/2002GL015650.

Cooper, L.W., T.E. Whitledge, J.M. Grebmeier (1997), The nutrient, salinity, and stable oxygen isotope composition of Bering and Chukchi Seas waters in and near the Bering Strait, *Journal of Geophysical Research 102*: 12563-12573.

Cooper, L.W., J.W. McClelland, R.M. Holmes, P.A. Raymond, J.J. Gibson, C.K. Guay, B.J. Peterson (2008), Flow-weighted values of runoff tracers (d18O, DOC, Ba, alkalinity) from the six largest Arctic rivers, *Geophysical Research Letters 35*: doi:10.1029/2008GL035007.

Coote, A.R., E.P. Jones (1982), Nutrient distributions and their relationships to water masses in Baffin Bay, *Canadian Journal of Fisheries and Aquatic Sciences 39*: 1210-1214.

Craig, H. and L.I. Gordon (1965), Deuterium and oxygen 18 variations in the ocean and the marine atmosphere, in *Stable Isotopes in Oceanographic Studies and*

Paleotemperatures, edited by E. Tongiorgi, pp. 9-130, Consiglio Nazionale delle Ricerche, Pisa, Italy.

Devol, A.H., Codispoti, L.A., J.P. Christensen (1997), Summer and winter denitrification rates in western Arctic shelf sediments, *Continental Shelf Research 17*: 1029-1050.

Dmitrenko, I., S. Kirillov, H. Eicken, N. Markova (2005), Wind-driven summer surface hydrography of the eastern Siberian shelf, *Geophysical Research Letters 32*: doi:10.1029/2005GL023022.

Dmitrenko, I.A., S.A. Kirillov, L.B. Tremblay (2008), The long-term and interannual variability of summer fresh water storage over the eastern Siberian shelf: Implications for climatic change, *Journal of Geophysical Research 113:* doi:10.1029/2007JC004304.

Ekwurzel, B., P. Schlosser, R.A. Mortlock, R.G. Fairbanks (2001), River runoff, sea ice meltwater, and Pacific water distribution and mean residence times in the Arctic Ocean, *Journal of Geophysical Research. 106*: 9075-9092.

Falkner, K.K., R.W. Macdonald, E.C. Carmack, T. Weingartner (1994), The potential of barium as a tracer of Arctic water masses, in *The Polar Oceans and Their Role in Shaping the Global Environment: The Nansen Centennial Volume, AGU Geophys. Monograph Series*, edited by O.M. Johannessen, R.D. Muench, and J.E. Overland, pp. 63-76, AGU Books, Washington DC.

Falkner, K.K., M. Steele, R.A. Woodgate, J.H. Swift, K. Aagaard, J. Morison (2005), Dissolved oxygen extrema in the Arctic Ocean halocline from the North Pole to the Lincoln Sea, *Deep-Sea Research I 52*: 1138-1154.

Falkner, K.K., M.C. O'Brien, H. Melling, E.C. Carmack, F.A. McLaughlin, A. Munchow, E.P. Jones (2010), Interannual variability of dissolved nutrients in the Canadian Archipelago and Baffin Bay with implications for freshwater flux, *manuscript in preparation*.

Fissel, D.B. et al. (1988), *Non-tidal flows in the Northwest Passage*, 143 pp., Institute of Ocean Sciences, Sidney, BC.

Gordon, L.I., J.J.C. Jr., A.A. Ross, J.M. Krest (1994), A suggested protocol for continuous flow automated analysis of seawater nutrients (phosphate, nitrate, nitrite and silicic acid) in the WOCE Hydrographic Program and the Joint Global Ocean Fluxes Study, WOCE Operations Manual, Vol. 3: The Observational Program, Section 3.1: WOCE Hydrographic Program, Part 3.1.3: WHP Operations and Methods., pp. 52 loose-leaf, Woods Hole, MA.

Grebmeier, J.M., J.E. Overland, S.E. Moore, E.V. Farley, E.C. Carmack, L.W. Cooper, K.E. Frey, J.H. Helle, F.A. McLaughlin, S.L. McNutt (2006), A major ecosystem shift in the Northern Bering Sea, *Science 311*: doi:10.1126/science.1121365.

Guay, C.K. and K.K Falkner (1997), Barium as a tracer of Arctic halocline and river waters, *Deep-Sea Research II 44*: 1543-1569.

Guay, C.K., K.K. Falkner (1998), A survey of dissolved barium in the estuaries of major Arctic rivers and adjacent seas, *Continental Shelf Research 18*: 859-882.

Guay, C.K., K.K Falkner, R.D. Muench, M. Mensch, M. Frank, R. Bayer (2001), Wind-driven transport pathways for Eurasian Arctic river discharge, *Journal of Geophysical Research 106*: 11469-11480.

Guay, C.K.H., F.A. McLaughlin, M. Yamamoto-Kawai (2009), Differentiating fluvial components of upper Canada Basin waters on the basis of measurements of dissolved barium combined with other physical and chemical tracers, *Journal of Geophysical Research 114*: doi:10.1029/2008JC005099.

Itoh, M., E. Carmack, K. Shimada, F. McLaughlin, S. Nishino, S. Zimmermann (2007), Formation and spreading of Eurasian source oxygen-rich halocline water into the Canadian Basin in the Arctic Ocean, *Geophysical Research Letters 34*: doi:10.1029/2007GL029482.

Johnson, K.S., L.J. Coletti (2002), In situ ultraviolet spectrophotometry for high resolution and long-term monitoring of nitrate, bromide and bisulfide in the ocean, *Deep-Sea Research I 49*: 1291-1305.

Johnson, K.S., J.A. Needoba (2008), Mapping the spatial variability of plankton metabolism using nitrate and oxygen sensors on an autonomous underwater vehicle, *Limnology and Oceanography 53*: 2237-2250.

Jones, E.P., A.R. Coote (1980), Nutrient distributions in the Canadian Archipelago: indicators of summer water mass and flow characteristics, *Canadian Journal of Fisheries and Aquatic Sciences 37:* 589-599.

Jones, E.P. and L.G. Anderson (1986), On the origin of the chemical properties of the Arctic Ocean halocline, *Journal of Geophysical Research. 91*: 10759-10767.

Jones, E.P., L.G. Anderson, J.H. Swift (1998), Distribution of Atlantic and Pacific waters in the upper Arctic Ocean: Implications for circulation, *Geophysical Research Letters 25*: 765-768.

Jones, E.P., J.H. Swift, L.G. Anderson, M. Lipizer, G. Civitarese, K.K. Falkner, G. Kattner, F. McLaughlin (2003), Tracing Pacific water in the North Atlantic Ocean, *Journal of Geophysical Research 108*: doi:10.1029/2001JC001141.

Jones, E.P., L.G. Anderson, S. Jutterstrom, L. Mintrop, J.H. Swift (2008), Pacific freshwater, river water and sea ice meltwater across the Arctic Ocean basins: Results from the 2005 Beringia Expedition, *Journal of Geophysical Research 113*: doi:10.1029/2007JC004124.

Karcher, M.J., J.M. Oberhuber (2002), Pathways and modification of the upper and intermediate waters of the Arctic Ocean, *Journal of Geophysical Research 107*: doi:10.1029/2000JC000530.

Karcher, M.J., R. Gerdes, F. Kauker, C. Koberle (2003), Arctic warming: Evolution and spreading of the 1990s warm event in the Nordic seas and the Arctic Ocean, *Journal of Geophysical Research 108*: doi:10.1029/2001JC001265.

Kikuchi, T., K. Hatakeyama, J. Morison (2004), Distribution of convective Lower Halocline Water in the eastern Arctic Ocean, *Journal of Geophysical Research 109*: doi:10.1029/2003JC002223.

Kipphut, G. W. (1990), Glacial meltwater input to the Alaska Coastal Current: Evidence from oxygen isotope measurements, *Journal of Geophysical Research 95:* 5177-5181.

Kwok, R (2007), Baffin Bay ice drift and export : 2002–2007, *Geophysical Research Letters 34*: doi:10.1029/2007GL031204.

Luthcke, S.B., H.J. Zwally, W. Abdalati, D.D. Rowlands, R.D. Ray, R.S. Nerem, F.G. Lemoine, J.J. McCarthy, D.S. Chinn (2006), Recent Greenland ice mass loss by drainage system from satellite gravity observations, *Science 314*: 1286-1289.

Macdonald, R.W., D.W. Paton, E.C. Carmack (1995), The freshwater budget and under-
ice spreading of Mackenzie River water in the Canadian Beaufort Sea based on salinity and $^{18}O/^{16}O$ measurements in water and ice, *Journal of Geophysical. Research 100*: 895-919.

Macdonald, R.W., T. Harner, J. Fyfe (2005), Recent climate change in the Arctic and its impact on contaminant pathways and interpretation of temporal trend data, *Science of the Total Environment 342*: 5-86.

Martin, S., D.J. Cavalieri (1989), Contributions of the Siberian shelf polynyas to the Arctic Ocean intermediate and deep water, *Journal of Geophysical Research 94*: 12,725-12,738.

Martin, S., R. Drucker, R. Kwok, B. Holt (2004), Estimation of the thin ice thickness and heat flux for the Chukchi Sea Alaskan coast polynya from Special Sensor Microwave/Imager data, 1990-2001, *Journal of Geophysical Research 109*: doi:10.1029/2004JC002428.

Martin, S., R. Drucker, R. Kwok, B. Holt. (2005), Improvements in the estimates of ice thickness and production in the Chukchi Sea polynyas derived from AMSR-E, *Geophysical Research Letters 32*: doi:10.1029/2004GL022013.

Mathis, J.T., R.S Pickart, D.A. Hansell, D. Kadko, N.R. Bates (2007), Eddy transport of organic carbon and nutrients from the Chukchi Shelf: Impact on the upper halocline of the western Arctic Ocean, *Journal of Geophysical Research 112*: doi:10.1029/2006JC003899.

McLaughlin, F.A., E. Carmack, R. Macdonald (1996), Physical and geochemical properties across the Atlantic/Pacific water mass front in the southern Canadian Basin, *Journal of Geophysical Research 101*: 1183-1197.

McLaughlin, F.A., E. Carmack, R. Macdonald (2002), The Canada Basin, 1989-1995: Upstream events and far-field effects of the Barents Sea, *Journal of Geophysical Research 107*: doi:10.1029/2001JC000904.

McLaughlin, F.A., E.C. Carmack, R.W. Macdonald, H. Melling, J.H. Swift, P.A. Wheeler, B.F. Sherr, E.B. Sherr (2004), The joint roles of Pacific and Atlantic-origin waters in the Canada Basin, 1997-1998, *Deep-Sea Research I 51*: 107-128.

Melling, H., T.A. Agnew, K.K. Falkner, D.A. Greenberg, C.M. Lee, A. Munchow, B. Petrie, S.J. Prinsenberg, R.M. Samelson, R.A. Woodgate (2008) in *Arctic-Subarctic Ocean Fluxes: Defining the Role of the Northern Seas in Climate*, eds. R.R. Dickson, J. Meincke, and P. Rhines, Springer, pp. 193-247.

Morison, J., R. Andersen, N. Larson, E. D'Asaro, T. Boyd (1994), The Correction for Thermal-Lag Effects in Sea-Bird CTD Data, *Journal of Atmosphere & Ocean Techology 11*: 1151-1164.

Morison, J., M. Steele, R. Andersen (1998), Hydrography of the upper Arctic Ocean measured from the nuclear submarine *U.S.S. Pargo*, *Deep-Sea Research I 45*: 15-38.

Morison, J., M. Steele, K. Falkner (2002, updated 2006), *North Pole Environmental Observatory aerial CTD survey.* Boulder, Colorado USA: National Snow and Ice Data Center. Digital media.

Morison, J., M. Steele, T. Kikuchi, K. Falkner, W. Smethie (2006), The relaxation of central Arctic Ocean hydrography to pre-1990s climatology, *Geophysical Research Letters 33*: doi:10.1029/2006GL026826.

Morison, J., J. Wahr, R. Kwok, C. Peralta-Ferriz (2007), Recent trends in Arctic Ocean mass distribution revealed by GRACE, *Geophysical Research Letters 34*: doi:10.1029/GL029016.

Muench, R.D. (1971), The physical oceanography of the northern Baffin Bay region, Ph.D. thesis: University of Washington, Seattle.

Munchow, A., K.K. Falkner, H. Melling (2007), Spatial continuity of measured seawater and tracer fluxes through Nares Strait, a dynamically wide channel bordering the Canadian Archipelago, *Journal of Marine Research 65*: 759-788.

Nitishinsky, M., L.G. Anderson, J.A. Holemann (2007), Inorganic carbon and nutrient fluxes on the Arctic Shelf, *Continental Shelf Research 27*: 1584-1599.

Nguyen, A.T., D. Menemenlis, R. Kwok (2009), Improved modeling of the Arctic halocline with a subgrid-scale brine rejection parameterization, Journal of Geophysical Research 114: doi:10.1029/2008JC005121.

Olsson, K., L. Anderson (1997), Input and biogeochemical transformation of dissolved carbon in the Siberian shelf seas, *Continental Shelf Research 17*: 819-833.

Ostlund, H.G., G. Hut (1984), Arctic Ocean Water Mass Balance From Isotope Data, *Journal of Geophysical Research 89*: 6373-6381.

Paren, J. G. and J. R. Potter (1984), Isotopic tracers in polar seas and glacier ice, *Journal of Geophysical Research 89*: 749-750.

Pfirman, S.L., R. Colony, D. Nurnberg, H. Eicken, I.G. Rigor (1997), Reconstructing the origin and trajectory of drifting sea ice, *Journal of Geophysical Research 102*: 12575-12586.

Pfirman, S., W. Haxby,, M. Jeffries, D. Bauch (2004), Drifting Arctic sea ice archives changes in ocean surface conditions, *Geophysical Research Letters 31*: doi:10.1029/2004GL020666.

Polyakov, I.V., G.V. Alekseev, L.A. Timokhov, U.S. Bhatt, R.L. Colony, H.L. Simmons, D. Walsh, J.E. Walsh, V.F. Zakharov (2004), Variability of the Intermediate Atlantic Water of the Arctic Ocean over the Last 100 Years, *Journal of Climate 17*: 4485-4497.

Polyakov, I.V., A. Beszczynska, E.C. Carmack, I.A. Dmitrenko, E. Fahrbach, I.E. Frolov, R. Gerdes, E. Hansen, J. Holfort, V.V. Ivanov, M.A. Johnson, M. Karcher, F. Kauker, J. Morison, K.A. Orvik, U. Schauer, H.L. Simmons, O. Skagseth, V.T. Sokolov, M. Steele, L.A. Timokhov, D. Walsh, J.E. Walsh (2005), One more step toward a warmer Arctic, *Geophysical Research Letters 32*: doi:10.1029/2005GL023740.

Proshutinsky, A.Y., M.A. Johnson (1997), Two circulation regimes of the wind-driven Arctic Ocean, *Journal of Geophysical Research 102*: 12493-12514.

Raymond, P.A., J.W. McClelland, R.M. Holmes, A.V. Zhulidov, K. Mull, B.J. Peterson, R.G. Striegl, G.R. Aiken, T.Y. Gurtovaya (2007), Flux and age of dissolved organic carbon exported to the Arctic Ocean: a carbon isotopic study of the five largest arctic rivers, *Global Biogeochemical Cycles 21*: doi:10.1029/2007GB002934.

Redfield, A.C. and I. Friedman (1969), The effect of meteoric water, melt water and brine on the composition of Polar Sea water and of the deep waters of the ocean, *Deep-Sea Research*: 197-224.

Rignot, E., J.E. Box, E. Burgess, E. Hanna (2008), Mass balance of the Greenland ice sheet from 1958-2007, *Geophysical Research Letters 35*: doi:10.1029/2008GL035417.

Rigor, I.G., J.M Wallace, R.L. Colony (2002), Response of Sea Ice to the Arctic Oscillation, *Journal of Climate 15*: 2648 – 2668.

Rigor, I.G., J.M. Wallace (2004), Variations in the age of Arctic sea-ice and summer sea-ice extent, *Geophysical Research Letters 31*: doi:10.1029/2004GL019492.

Rudels, B., L.G. Anderson, E.P. Jones (1996), Formation and evolution of the surface mixed layer and halocline of the Arctic Ocean, *Journal of Geophysical Research 101*: 8807-8821.

Rudels, B., E.P. Jones, U. Schauer, P. Eriksson (2004), Atlantic sources of the Arctic Ocean surface and halocline waters, *Polar Research 23*: 181-208.

Sakamoto, C.M., K.S Johnson, L.J. Coletti (2009), Improved algorithm for the computation of nitrate concentrations in seawater using an in situ ultraviolet spectrophotometer, *Limnology and Oceanography Methods 7*: 132-143.

Salmon, D.K. and C.P. McRoy (1994), Nutrient-based tracers in the Western Arctic: a new lower halocline water defined, in *The Polar Oceans and Their Role in Shaping the Global Environment: The Nansen Centennial Volume, Geophys., Monogr. Ser.*, vol 85, edited by O.M Johannessen, R.D. Muench, and J.E. Overland, pp. 47-61, AGU, Washington, D.C.

Schlitzer, R. (2001) Ocean Data View, http://www.awi-bremerhaven.de/GEO/ODV.

Schmidt, G.A., G.R. Bigg, E.J. Rohling (1999), "Global Seawater Oxygen-18 Database," http:data.giss.nasa.gov/o18data/

Seabird (2009), Application Note No. 64: SBE43 Dissolved Oxygen Sensor – Background Information, Deployment Recommendations, and Cleaning and Storage, http://www.seabird.com/application_notes/AN64.htm, last modified 06 Jul 2009.

Serreze, M.C., A.P. Barrett, A.G. Slater, R.A. Woodgate, K. Aagaard, R.B. Lammers, M. Steele, R. Moritz, M. Meredith, C.M. Lee (2006), The large-scale freshwater cycle of the Arctic, *Journal of Geophysical Research. 111*: doi:10.1029/2005JC003424.

Shimada, K., M. Itoh, S. Nishino, F. McLaughlin, E. Carmack, A. Proshutinsky (2005), Halocline structure in the Canada Basin of the Arctic Ocean, *Geophysical Research Letters 32*: doi:10.1029/2004GL021358.

Steele, M., J.H. Morison, T.B. Curtin (1995), Halocline water formation in the Barents Sea, *Journal of Geophysical Research 100*: 881-894.

Steele, M. and T. Boyd (1998), Retreat of the cold halocline layer in the Arctic Ocean, *Journal of Geophysical Research 103*: 10,419-10,435.

Steele, M., J. Morison, W. Ermold, I. Rigor, M. Ortmeyer, K. Shimada (2004), Circulation of summer Pacific halocline water in the Arctic Ocean, *Journal of Geophysical Research 109*: doi:10.1029/2003JC002009.

Strain, P.M. and F.C. Tan (1993), Seasonal evolution of oxygen isotope-salinity relationships in high-latitude surface waters, *Journal of Geophysical Research 98*: 14589-14598.

Swift, J.H., E.P. Jones, K. Aagaard, E.C. Carmack, M. Hingston, R.W. Macdonald, F.A. McLaughlin, R.G. Perkin (1997), Waters of the Makarov and Canada basins, *Deep-Sea Research II 44*: 1503-1529.

Swift, J.H., K. Aagaard, L. Timokhov, E.G. Nikiforov (2005), Long-Term Variability of Arctic Ocean Waters: Evidence From A Reanalysis of the EWG Data Set, *Journal of Geophysical Research 110*: doi:10.1029/2004JC002312.

Tan, F.C. and P.M. Strain (1980), The distribution of sea ice meltwater in the Eastern Canadian Arctic, *Journal of Geophysical Research 85*: 1925-1932.

Tan, F.C. and P.M. Strain (1996), Sea ice and oxygen isotopes in Foxe Basin, Hudson Bay, and Hudson Strait, Canada, *Journal of Geophysical Research 101*: 20869-20876.

Tang, C.C.L., C.K. Ross, T. Yao, B. Petrie, B.M. DeTracey, E. Dunlap (2004), The circulation, water masses and sea-ice of Baffin Bay, *Progress in Oceanography 63*: 183-228.

Taylor, J.R., K.K Falkner, U. Schauer, M. Meredith (2003), Quantitative considerations of dissolved barium as a tracer in the Arctic Ocean, *Journal of Geophysical Research 108*: doi:10.1029/2002JC001635.

Thompson, D.W.J., J.M. Wallace (1998), The Arctic Oscillation signature in the wintertime geopotential height and temperature fields, *Geophysical Research Letters 25*: 1297-1300.

Weeks, W. F. and S. F. Ackley (1986), The growth, structure and properties of sea ice, *The Geophysics of Sea Ice*. N. Untersteiner. New York, Plenum Press. 146**:** 9-164.

Weingartner, T.J., D.J. Cavalieri, K. Aagaard, Y. Sasaki (1998), Circulation, dense water formation, and outflow on the northeast Chukchi shelf, *JGR 103*, 7647-7661.
Wilson, C. and D.W.R. Wallace (1990), Using the nutrient ratio NO/PO as a tracer of continental shelf waters in the central Arctic Ocean, *Journal of Geophysical Research 95*: 22193-22208.

Weingartner, T., K. Aagaard, R. Woodgate, S. Danielson, Y. Sasaki, D. Cavalieri (2005), Circulation on the north central Chukchi Sea shelf, *Deep-Sea Research II 52*: 3150-3174.

Woodgate, R.A., K. Aagaard, J.H. Swift, K.K. Falkner, W.M. Smethie, Jr. (2005), Pacific ventilation of the Arctic Ocean's lower halocline by upwelling and diapycnal mixing over the continental margin, *Geophysical Research Letters 32*: doi:10.1029/2005GL023999.

Woodgate, R.A., K. Aagaard, T.J. Weingartner (2005b), A year in the physical oceanography of the Chukchi Sea: Moored measurements from autumn 1990-1991, *Deep-Sea Research II 52:* 3116-3149.

Yamamoto-Kawai, M., N. Tanaka, S. Pivovarov (2005). Freshwater and brine behaviors in the Arctic Ocean deduced from historical data of $\delta^{18}O$ and alkalinity (1929-2002 A.D.), *Journal of Geophysical Research 110*: doi:10.1029/2004JC002793.

Yamamoto-Kawai, M., F.A. McLaughlin, E.C. Carmack, S. Nishino, K. Shimada (2008), Freshwater budgets of the Canada Basin, Arctic Ocean, from salinity, $\delta^{18}O$, and nutrients, *Journal of Geophysical Research 113*: doi:10.1029/2006JC003858.

Yamamoto-Kawai, M., F.A. McLaughlin, E.C. Carmack, S. Nishino, K. Shimada, N. Kurita (2009), Surface freshening of the Canada Basin, 2003-2007: River runoff versus sea ice meltwater, *Journal of Geophysical Research 114*: doi:10.1029/2008JC005000.

Yamamoto-Kawaii, M., F.A. McLaughlin, E.C. Carmack, S. Nishino, K. Shimada (2009), Aragonite undersaturation in the Arctic Ocean: effects of ocean acidification and sea ice melt, *Science 326*: doi:10.1126/science.1174190.

APPENDICES

APPENDIX A: INTERNATIONAL ARCTIC BUOY PRORAM BACK-TRAJECTORIES FOR INDIVIDUAL STATIONS

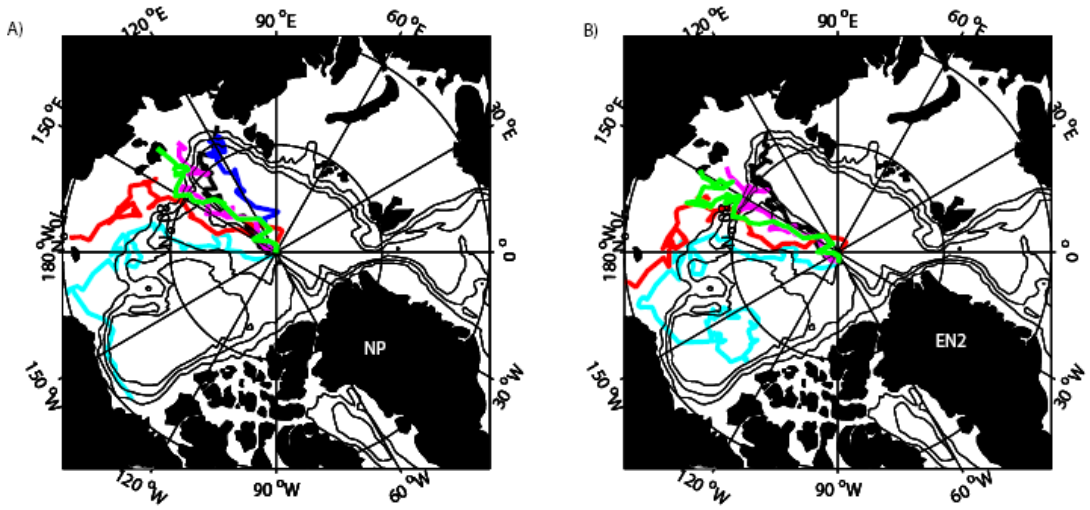

Figure A.1 Individual IABP back-trajectories for stations (A) NP and (B) EN2. The colors identify the year of station occupation: 2000 (black), 2001 (blue), 2003 (cyan), 2004 (red), 2005 (magenta), and 2006 (green).

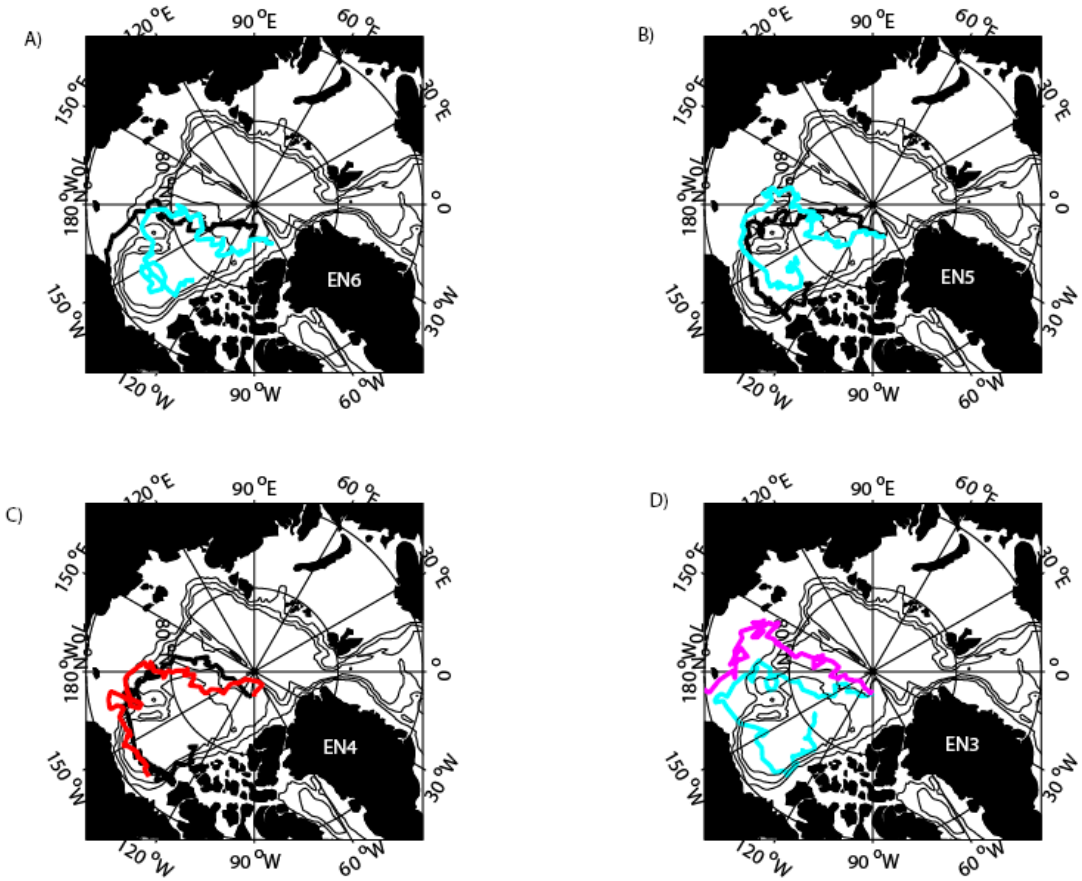

Figure A.2 Individual IABP back-trajectories for stations (A) EN6, (B) EN5, (C) EN4, and (D) EN3. The colors identify the year of station occupation: 2000 (black), 2001 (blue), 2003 (cyan), 2004 (red), 2005 (magenta), and 2006 (green).

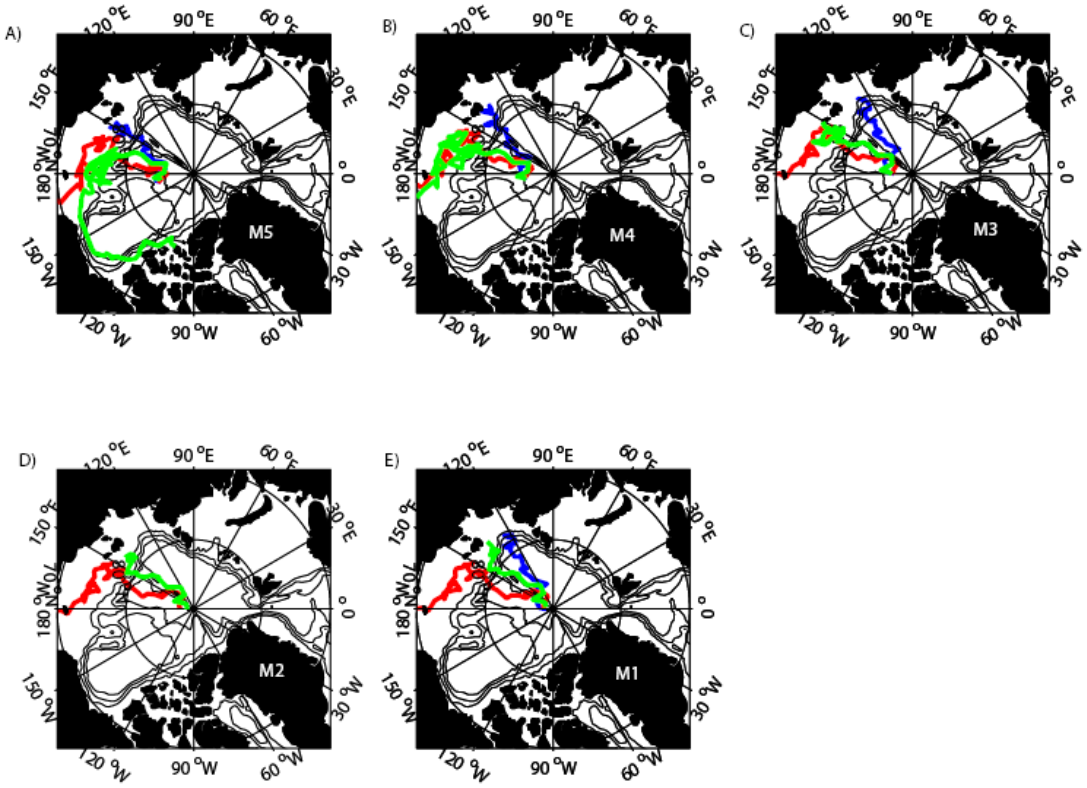

Figure A.3 Individual IABP back-trajectories for stations (A) M5, (B) M4, (C) M3, (D) M2, and (E) M1.. The colors identify the year of station occupation: 2000 (black), 2001 (blue), 2003 (cyan), 2004 (red), 2005 (magenta), and 2006 (green).

APPENDIX B. ISUS INSTRUMENTAL SIGNAL PROCESSING

B.1 CTD and SBE43 O_2 sensor processing

Temperature, conductivity, and SBE43 voltage data were smoothed using a 0.5 second low-pass filter, and the pressure data were smoothed using a 1.0 second low pass filter, in accordance with Seabird's recommendations for standard SBE19 *plus* data processing. Temperature records were advanced 0.55 seconds with respect to pressure to minimize salinity spiking (Roger Andersen, personal communication). This advance is slightly longer than that recommended by Seabird (0.5 seconds) presumably due to the increase in the response time of the temperature sensor when deployed in cold Arctic Ocean waters. The SBE43 oxygen voltage was advanced between 1.5 and 4.0 seconds relative to pressure on a cast by cast basis. The calculation method used to determine these advances is described in detail in section B.2.

A small standard thermal mass correction was then applied to the conductivity data (Morison et al., 1994). Using Seabird SBE Data Processing software (Version 7.12), final dissolved oxygen concentrations were calculated from the advanced voltages using the Murphy-Larson equation (Seabird, 2009), which incorporates a cubic temperature correction and includes a feature-sharpening term involving the time derivative of the SBE43 voltage. This latter term corrects signal broadening resulting from the response time of the oxygen sensor (~3-5 seconds in our deployment conditions).

Bottle samples collected for dissolved oxygen analysis were suspect and could not be used to check the calibration of the SBE43 O_2 sensor. Sensor calibrations performed by Seabird before and after each mission were instead used to validate the accuracy of the O_2 profiles. Of these four calibrations, three were very similar; the odd one was the 2007 post-mission calibration. Because the 2007 and 2008 pre-mission calibrations were almost identical (O_2 concentrations calculated using these different calibrations differed by ~0.9 mmol m^{-3} on average), and because the oxygen sensor was not used between the (odd) 2007 post-mission and 2008 pre-mission

calibrations, we used the 2007 pre-mission calibration to determine the final [O_2] values for the 2007 data. The calibrations performed before and after the 2008 mission suggested that the sensor readings remained accurate to $\leq$ 2.2 mmol O_2 m^{-3} during this mission.

The largest uncertainty associated with our calculations of [O_2] values from the raw sensor data stemmed from the unknown voltage advance(s) applied to the SBE43 signals to correct for the flow lag between the oxygen and TC sensors. A conservative estimate of this uncertainty was obtained by re-processing all of the profiles using the minimal (1.5 s) and maximal (4.0 s) calculated advances and differencing the resulting profiles. Deviations typically ranged between 0.0 and 0.5 mmol O_2 m^{-3} ($\leq$ 0.5%) although high gradient regions exhibited larger differences of between 1 and 4 mmol O_2 m^{-3} ($\leq$ 2%).

B.2 SBE43 voltage advance

The SBE43 O_2 sensor is located downstream of the temperature sensor. For this reason, the SBE43 O_2 sensor voltage must be advanced relative to pressure such that the voltage readings correspond with the temperature and conductivity recorded by the CTD for the same water volume. There are numerous ways to determine an appropriate advance, most of which assume that temperature and dissolved oxygen should be anti-correlated in high-gradient regions. We adopted an alternate approach that avoids this assumption.

Hysteresis in the temperature record when plotted versus pressure is commonly observed when comparing data acquired during the downcast and upcast. For our instrument configuration, the magnitude of the observed hysteresis in the oxygen record will be greater because it takes time for the pumped seawater sample volume to travel from the temperature sensor to the oxygen sensor. This time lag is equivalent to the advance necessary to line up the oxygen record with respect to the other CTD sensor records. Therefore, the desired advance can be calculated as the difference between the time advance required to superimpose the downcast/upcast oxygen records when plotted against pressure and the advance required to

superimpose the downcast/upcast temperature records when plotted against pressure. The calculations of these advances for each cast were implemented as follows.

After processing the conductivity, temperature, and pressure data as previously described, we applied a least-squares minimization procedure to determine the advance (relative to pressure) resulting in the coincidence of the downcast and upcast temperature records for each cast. We carried out a separate least-squares minimization procedure to determine the advance relative to pressure of the (0.5 second low-pass filtered) SBE43 O_2 voltage records resulting in the coincidence of the downcast and upcast dissolved oxygen concentrations for each cast. Note these trial oxygen concentrations were calculated using conductivity, temperature, and pressure data processed exactly as described in section A.1 incorporating the Murphy-Larson algorithms. The final correction times for each cast (advances of from 1.5 to 4.0 seconds) accounting for the downstream position of the O_2 sensor are equal to the differences between the least-squares advances computed for the trial O_2 concentrations and those for the temperature records.

B.3 ISUS NO3 signal processing

Our ISUS instrument measured the ultraviolet (217-240 nm) absorbance across its probe's 1-cm path length in seawater approximately once per second (0.9 Hz). A dark reading (light source shuttered) was taken after every ten measurements to track any drift in background signal level. Time-stamped spectral readings were logged internally for each station. Since the ISUS does not record pressure or external temperature, the separate ISUS and CTD casts were merged after collection using the time stamp information as follows.

A new time axis was calculated for the ISUS data by setting the origin ($t = 0$) to that of the start of the CTD downcast using the instruments' respective time stamp information (the CTD effectively timestamps the first data record of each of its casts). The uncertainty in the synchronization of the instrument clocks led to possible errors in this synchronization procedure (1-2 seconds) which are taken into account when estimating the uncertainties in the ISUS-CTD alignment (described at the end of this

section). The depths for the ISUS data points were then determined by interpolating the ISUS data point times into the CTD time record and subtracting 0.889 meters (the distance spanning the CTD thermistor and ISUS sample probe) from the resultant interpolated depths. The remaining CTD data (temperature, salinity, and oxygen processed as discussed in sections B.1 and B.2) were smoothed using a 1.0-second low-pass filter in order to better match the approximate sampling rate of the ISUS. These data were then interpolated onto the newly-calculated ISUS depth record so that each nitrate value was associated with a corresponding record of depth, temperature, salinity, and oxygen.

The ISUS spectra were corrected by subtraction of bromide absorbance spectra calculated from the *in-situ* temperature and salinity data (Sakamoto et al., unpubl. man.; Johnson and Needoba, 2008). Nitrate concentrations were then calculated by fitting the corrected spectra to a (temperature independent) nitrate spectrum and linear baseline. Each nitrate concentration calculated has an associated fit-error (RMS deviation of observed nitrate absorbance from modeled values). Any concentrations with fit-errors exceeding 0.002 were omitted from the final data files to accommodate known instrumental noise (Ken Johnson, personal communication).

Since the goal of this study was to combine nitrate and dissolved oxygen records to calculate the NO parameter ($9 \times NO_3 + O_2$), smooth nitrate profiles were desired as noise in the nitrate record will be greatly magnified in this calculation. Therefore, the nitrate concentration values were smoothed using a 5-point running mean, which, given the sampling frequency of the ISUS (0.9 Hz) and drop rate of the instruments (0.6-0.9 m s^{-1}), effectively averaged the data into overlapping 3-5 meter bins. The 5-point running mean was empirically determined to yield a suitably smooth nitrate profile while minimizing the unavoidable loss in vertical resolution.

Downcast data are reported as they should be minimally impacted by wake effects (though the positioning of the ISUS above the CTD likely resulted in the ISUS downcast data being somewhat affected). Downcast ISUS nitrate profiles were corrected individually using bottle-based nitrate concentrations measured at each

station. Assuming the oxidation of NH_4^+ to NO_3^- in collected seawater samples during storage did not occur, bottle nitrate concentrations are taken as true and disagreements between bottle and ISUS data were interpreted as resulting from changes in the instrument's calibration, whether due to long-term drift or short-term environmental effects. Such discrepancies were most likely a consequence of deviation from recommended deployment procedures. A pre-deployment "warm-up" period of at least 8-10 minutes with the ISUS operating at the ambient deployment temperature is recommended by the manufacturer in order to stabilize the output of the excitation source of the ISUS (deuterium lamp). It is also recommended that the instrument be tested daily in a solution free of nitrate to check for drift. Neither of these recommended procedures proved to be readily feasible under polar field conditions. We plan to include such procedures in future deployments. A simple linear regression was performed between the bottle nitrate concentrations and ISUS downcast concentrations determined at the same depths collected at each station. The coefficients obtained from the regression were used to correct the full ISUS nitrate profile. An example of raw, smoothed, and bottle-corrected ISUS profiles as well as bottle nitrate data is shown in Fig. B.1.

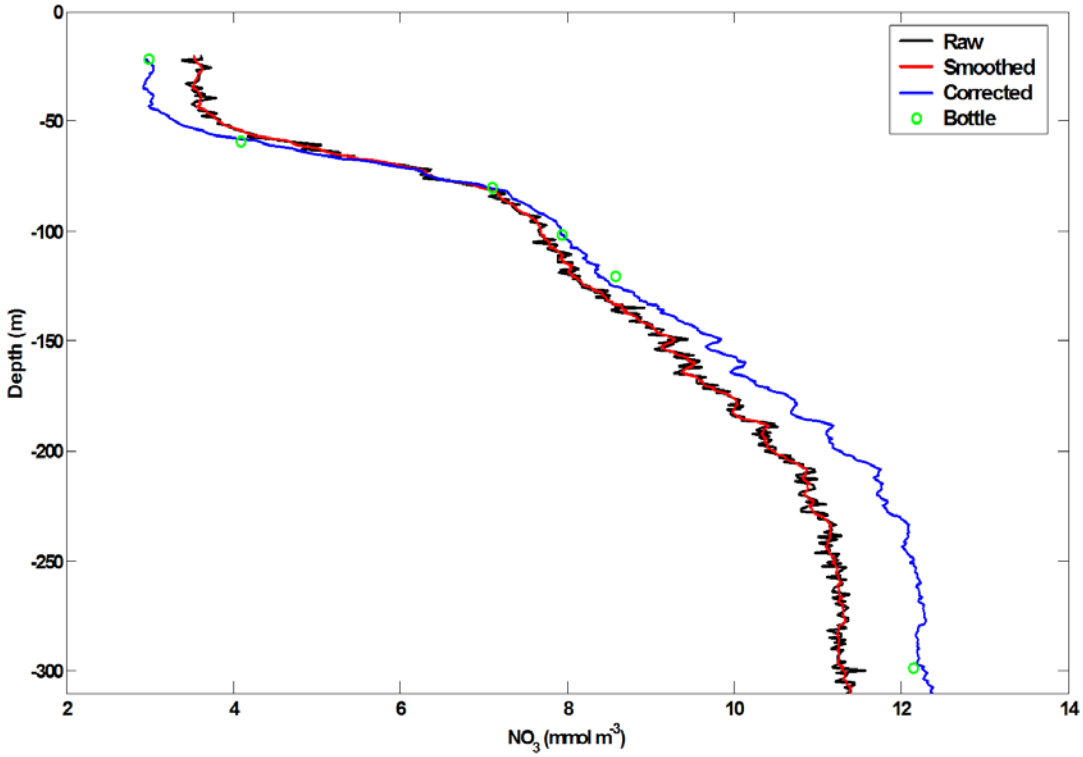

Figure B.1 Raw (black), smoothed (red), and bottle-corrected (blue) downcast ISUS nitrate data from station 5 occupied during spring 2007. Bottle nitrate concentrations are illustrated as green circles.

A sensitivity analysis similar to that for the O_2 sensor was conducted as an additional check on uncertainties. Casts were fully re-processed after adjusting the time synchronization ± 2 seconds and the resulting nitrate profiles (relative to pressure) differenced. Differences ranged between 0 and 0.5 mmol m^{-3} with larger differences (0.5-1.0 mmol m^{-3}) associated with high gradient regions.